2024

EVALUATION OF MICROGLIA'S STRUCTURAL VARIATIONS WITHIN AN ORGANOTYPIC HIPPOCAMPAL SLICE MODEL AFTER REGIONALIZED TOXIC INJURY

Jesus Antonio Trejos

EVALUATION OF MICROGLIA'S STRUCTURAL VARIATIONS WITHIN AN ORGANOTYPIC HIPPOCAMPAL SLICE MODEL AFTER REGIONALIZED TOXIC INJURY

A dissertation submitted in partial fulfillment
of the requirements for the degree of

DOCTOR OF PHILOSOPHY

to the faculty of the

DEPARTMENT OF PHARMACEUTICAL SCIENCES

of

COLLEGE OF PHARMACY AND HEALTH SCIENCES

at

ST. JOHN'S UNIVERSITY
New York
by
Jesus Antonio Trejos

Date Submitted 7/26/2023 Date Approved 8/10/2023

Jesus Antonio Trejos	Dr. Francis X. Schanne

ABSTRACT

EVALUATION OF MICROGLIA'S STRUCTURAL VARIATIONS WITHIN AN ORGANOTYPIC HIPPOCAMPAL SLICE MODEL AFTER REGIONALIZED TOXIC INJURY

Jesus Antonio Trejos

The dendritic cells of the CNS, the microglia (MG), are an initiation point of the immunological response within the post blood-brain barrier (BBB) compartment. Microglia morphology drastically changes in response to cell stress to a much different non-dendritic morphology. This investigation postulates that if the first MG responses to toxic injury are isolated and studied in greater morphological detail there is much to be learned about MG metamorphosis from a baseline (M2) to an activated (M1) state. The organotypic hippocampal slice was the experimental setting used to investigate microglial response to toxic injury. This isolates dendritic cellular responses and associated post-BBB cells dynamics from the impact of nonspecific of in-vivo blood-derived factors. Within the context of biochemically verified precise toxic cell injury/death (induced with mercury or cyanide in combination with 2-deoxy-glucose) to a specific region within a cultured hippocampal slice, MG's morphological response near and distal to the site of toxicological insult was evaluated. There was up to 35% increase in MG activation proximally to injury (CA3 region) and no changes distally (DG region) when compared to control slices treated with PBS. Maximum MG activation consisted of a 3 plus-fold increase in the distance between the nucleus membrane and the cell membrane, which underscores an extensive and quantifiable amount of membrane rearrangement. In

between baseline and activated MG morphologies, 5 intermediate morphologies (or morphological variations) are described as it relates to its cell body, nucleus, and dendrites. The result from this study reconciles details of MG's structure to its holistic characteristics in relation to parenchymal cell stress within a cultured CNS tissue sample.

DEDICATION

I would like to dedicate this to first and foremost my late mother, Luz Teresa Piedrahita, whom always carried her “PROUD PARENT. ST JOHN’S UNIVERSITY” keychain and provided me catholic upbringing whose values were imbued by the University. She had also told me that she hoped that one day I would get to do important science work, a motive that galvanized all the intention and effort I put into this research.

I would also like to dedicate this to my father, Luis Armando Trejos, whom clearly defined to me that a Doctor of Philosophy bumps out the uneven circumference of human knowledge, this too also galvanized the intentions of my research.

ACKNOWLEDGEMENTS

I would like to acknowledge and express profound gratitude to the Pharmaceutical Sciences Department of St John's University for all the financial and operational support provided to conduct this research.

I would also like to acknowledge Dr Francis X. Schanne, who's unwavering enthusiasm and patience carried me through many challenges of this work. His encouragement to follow my scientific instincts gave me the confidence that I needed to pursue the aims of my study and prove my hypotheses.

I would also like to acknowledge the committee members for intellectually digesting my work and giving me sage feedback as to how to make my research and research presentation better.

TABLE OF CONTENTS

LIST OF FIGURES

LIST OF ABBREVIATIONS

Adenosine Triphosphate (ATP)

Antibody (Ab)

Blood Brain Barrier (BBB)

Cell Counting Kit 8 (CCK-8)

Central Nervous System (CNS)

Cluster of Differentiation 11 (CD11)

Dentate Gyrus (DG)

4′,6-Diamidino-2-Phenylindole (dapi)

3-(4,5-Dimethylthiazol-2-yl)-2,5-Diphenyltetrazolium Bromide (MTT)

Disease Associated Microglia (DAM)

Fetal Bovine Serum (FBS)

Fluorescein Diacetate (FDA)

Immunohistochemistry (IHC)

Ionized Calcium-Binding Adaptor (IBA-1)

Lactate Dehydrogenase LDH

Messenger Ribonucleic Acid (mRNA)

Microglia (MG)

Modified Eagle Medium (MEM)

Phosphate Buffered Saline (PBS)

Propidium Iodide (PI)

CHAPTER 1: HISTORY OF MICROGLIA AND ITS EVALUATION IN AN ORGANOTYPIC HIPPOCAMPAL SLICE MODEL

1.1. INTRODUCTION

Microglia (MG) are the surveillance and maintenance immune cells of the central nervous system; and are also known as a type of dendritic cell. The baseline dendritic morphology of MG covers a large area of interstitial space and probes the highly exclusive compartment of the of the central nervous system ([1]; [2], [3], [4], [5] [6]). However, MG shape (the baseline dendritic shape) can drastically change in response to cell stress to a starkly different and compact and globular morphology. Therefore, this indicates MG can take on several roles that are related to their different opposing morphological states [7]; namely the M1 state (activated, globular shape) and its M2 state (inactivated, dendritic shape). Importantly, MG monitor an interstitium that is considered one the purest ultrafiltrates in the body (cerebrospinal fluid) as it surveys tissue for damaged, dying, or dead cells. As such, MG sensitivity to the CNS environment allows prompt reaction to homeostatic perturbations within the CNS tissue matrix through 3 main characteristics; MG are small, highly amorphous, and motile. In addition to its janitorial duties, MG are implicated in the pruning of synaptic connections that are important for neuronal networking [8]. Contemporaneously, much investigation has described some of portions of MG morphological characteristics; such as size, area, branching, hull ratio, podocyte status has been considered [10] [11]. Gene expression assays, mRNA profiling and single cell assessments have also been conducted to better understand MG genetics [12]. However, more detailed information on MG individual and

overall structural components is warranted to further characterize MG dynamic morphology, and potentially understand events antecedent to CNS cell death (loss of cell membrane integrity), modeled by toxic injury. This isolated tissue injury model can be harnessed to better establish intermediate microglial morphological states which could inform about roles of MG in homeostasis and disease within the isolated CNS post BBB compartment ([13]; Li, et al., 2018). Using MG morphology as an endpoint can add greater resolution as to how this cell behaves during injury within the CNS which could be harnessed as a form of proxy for determining adequacy for post BBB homeostasis. This postulates that the more MG are presented in its dendritic shape (M2 baseline state), the more adequate the BBB homeostasis is presented.

The differential shapes and sizes of MG have been previously characterized in cell culture when the full range of morphology was evaluated 2 hours after ATP exposure, which is a significant instigator of MG activation ([14]). The morphological profile is described in population of isolated MG cells. However, the morphological profile of MG has not yet been thoroughly evaluated when embedded within cultured tissue matrix. Therefore, a contextual way to evaluate the MG response is to utilize a model that represents not only the dendritic cell but also in the nascent cytostructural milieu, the adjoining tissue matrix. In addition, it would be ideal to home in on the responses and signaling directly related to MG and CNS tissue matrix by measuring responses away from significant blood-derived immune cell or factors and signaling outside the brain *in-vivo.* In evaluating this response there is a focus on the morphological aspects such as MG cell body, dendrites, and nucleus placement, independently as individual structural components of the MG and holistically as it pertains to MG cell metamorphosis from M2

to M1 state. These details can be potentially used to define intermediate forms of MG as it relates to different levels of CNS cells stress. As such, these different morphologies between M1 and M2 can be designated to define the MG's "structural variation," which could be an important aspect of MG characterization as is found in and around injured tissue [7]. Besides contextually displaying MG morphological information, this paradigm also concurrently isolates immune cell (represented by MG)-parenchymal cell (represented by neurons and other glia) dynamics under the influence of cell stress with multiple controls. This is the first time it has been characterized in an ex-vivo tissue model. Not only does the model confirm many of the known aspects of MG studied in-vivo and in-vitro, but also it allows visualization of MG inherent properties such as its sensitivity to fluid turbidity and motility. Overall, all this study will define in in-depth morphological detail, qualitative and quantitative aspects of MG metamorphosis from baseline (M2) to its activated state (M1) propagated by chemical toxicity within an isolated tissue context.

1.1.1. Hippocampal slice

The organotypic hippocampal slice has well-defined regions and has been validated for evaluating neuronal activity using electrophysiologic methods. Therefore, this model is considered well-characterized live and functional tissue for a considerable period after excision ([15], [16], Raghuraman et al., 2019; [17]. One important characteristic about hippocampal slices is its innate ability to suffuse itself with media when placed on a semiporous membrane and therefore maintains, in some context, the conditions of extracellular fluid flow. This suffusion is indicative that the intercellular space needed for extracellular fluid flow and motile cell passage is preserved. This was described by

Stoppini (1991 [15]), a film of fluid sheathes the tissue and likely reflects innate ability of the slice to stay covered in media. Tracking microglial morphology in response to different types of toxicity in this isolated tissue sample can give insights to the versatility and sensitivity of MG to a regionalized toxic injury. This model has been used previously to evaluate MG response [18]; [19]. However, this study investigated the morphologic changes in cluster of differentiation 11 positive (CD11+) MG in the presence of biochemically verified toxic cellular injury and death within a subset of cells within the CA3 region.

Also, this model has multiple independent controls; an intra-slice control (the untreated DG region, which is distant from the CA3 region) and control slice CA3 region that are exposed to vehicle control. Cell injury and death due to toxic injury were biochemically defined in this study by simultaneously probing the activity of a mitochondrial reductase enzyme using 3-(4,5-Dimethylthiazol-2-yl)-2,5-Diphenyltetrazolium Bromide (MTT) and membrane integrity using propidium iodide (PI). Leveraging the well-established mechanistic knowledge of two classic toxicants, mercury, and cyanide (the latter in combination with 2-deoxy-glucose attempt to fully abrogate of ATP availability), cell death was elicited in 2 distinct modes of chemical toxicity.

1.1.2. Evaluation of MG

The evaluation of MG was predicated on using one a signature membrane protein to determine its morphology. CD11 protein is an important component of MG migratory capacity and, therefore, relates to one of its defining functions of surveillance of CNS [20] [21]. Furthermore, considering that CD11 is a membrane protein expressed on the extracellular surface of MG, a more detailed and representative depiction of MG dynamic

morphology could be appraised better than an intracellular protein, such as Iba-1. The definition of MG can vary across the literature; here MG were categorized by 2 criteria, the expression of CD11 and the morphological presentation as a cell with several dendrites emanating out of a nucleated cell body. Based on the immunocytohistochemical CD11 detection, the CD11+ cells evaluated in this study have a morphology consistent with the MG dendritic motif and, thereby, under the purview of dendritic cell, that is a cell with dendritic processes that migrate through the post-BBB parenchyma([22]; [14]; [10]).

This study aims to investigate whether MG have a definable gradient morphological response to regionalized, biochemically-verified toxic cell injury and/or CNS cell death (2 hours after inducing a toxic insult) in the context of an *ex-vivo* model, the organotypic hippocampal slice. Furthermore, the untreated area of the hippocampal slice can serve as an internal control to compare baseline MG near non-injured cells within tissue to activated MG near injured/dead cells within tissue, and the intermediate morphologies in between. Nonetheless, within this response there is a focus on the morphological aspects such as MG cell body, dendrites, and nucleus placement, independently as individual structural components of the MG and holistically as it pertains to MG cell metamorphosis from M2 to M1 state. These details can be potentially used to define intermediate forms of MG as it relates to different levels of CNS cells stress. As such, these different morphologies between M1 and M2 can be designated to define the MG's "structural variation," which could be an important aspect of MG characterization as is found in and around injured tissue [7]. Besides contextually displaying MG morphological information, this paradigm also concurrently isolates immune cell (represented by MG)-

parenchymal cell (represented by neurons and other glia) dynamics under the influence of cell stress with multiple controls. This is the first time it has been characterized in an *ex-vivo* tissue model. Not only does the model confirm many of the known aspects of MG studied *in-vivo* and *in-vitro*, but also it allows visualization of MG inherent properties such as its sensitivity to fluid turbidity and motility. Overall, all this study will define in in-depth morphological detail, qualitative and quantitative aspects of MG metamorphosis from baseline (M2) to its activated state (M1) propagated by chemical toxicity within an isolated tissue context.

1.2. METHODS

1.2.1. Organotypic hippocampal slices

Animal work in this study was performed under a IACUC (Institutional Animal Care and Use Committee) approved protocol in a facility accredited by the Association for Assessment and Accreditation of Laboratory Animal Care International. This facility also follows The Guide for the Care and Use of Animals, AVMA Guidelines on Euthanasia, PHS Policy on Humane Care and Use of Lab Animals, and USDA Animal Welfare Act regulations. All Sprague-Dawley rats were provided ad lib food; temperatures and humidity kept within recommended ranges; 12-hour light/dark cycles were maintained. Neonates were obtained from in-house IACUC- approved breeding protocol (protocol #1912) with breeder males and dams obtained from Taconic Farms.

The best visualization of MG (CD11+ cells) is in the neonate rat 10-21 day old (usually 1 neonate male or female per experiment), due to the relative translucency of the tissue matrix. Older animals have more opaque tissue and therefore CD11+ cells cannot be visualized in fine detail beyond 10x magnification. Animals were sacrificed via decapitation and brain was immediately excised from cranium, the whole hippocampi

were carefully dissected out and placed in ice cold calcium and magnesium free Hanks balanced salt solution. Hippocampi were then placed on top of a 1.5% agar (Acros Organics Cat#: 400402500) block to slice tissue in a sagittal orientation at a thickness of 200 microns using a Syskiyou Tissue Slicer (Cat#: SKU 14240000E). Slices are then manually separated out individually by using a micro spatula immersed in ice cold calcium and magnesium free Hanks balanced salt solution. One rat (2 hippocampi) can yield 26-40 hippocampal slices.

1.2.2. Tissue incubation

Using a trimmed transfer pipette slices were removed from ice cold media and placed into Millipore filter (Cat#: PICM0RG50) within a well of a 6-well plate with preincubated culture media as described in previous papers this media consists of 50% Minimum Essential Media (MEM), 25% Hanks Balanced Salt Solution (with calcium and magnesium) and 25% Horse serum [18]; [15]);. Excess calcium free and magnesium free media on the top of the filter should be removed prior to equilibration. Before any treatment with toxicants, the tissue was equilibrated in a cell culture incubator for 1 hour.

1.2.3. Tissue treatment

Treatment with Mercury (HgCl, Merck Cat#: 7290) or cyanide (KCN Alfa Aesar, Cat#: L13273) /2-deoxy-glucose (2-DG) (Cat#: NC9864731), diluted in PBS, consisted of a "spot tox" (a small and specific region of the tissue that will be exposed to toxicant) within the CA3 region of the hippocampal slice. The spot tox was delivered as an aliquot of 180 nL (using a micropipette calibrated to go down to 100 nL). After a concentration that elicited biochemically-confirmed toxicity was established lower concentrations were evaluated. Control slices were exposed to vehicle solvent used for both toxicants (PBS).

Dispensing the 180 nL droplet allowed placement of the droplet on top of the CA3 region of the hippocampus slice (Figure 1), eventually (after a few minutes) this dollop will be absorbed into the tissue. The DG region was not treated in order to have a healthy tissue control within the slice. The regionalized injury allows an effective contrast of the appearance of CD11+ MG cells look like within untreated DG region and, thus healthier regions versus what MG appearance in regions in and around the area of spot tox. This method enables not just healthy and toxic-injury contrast but also a gradation of changes in the space in between healthy and injured cells. In all experiments, MG cells morphology within healthy and injury regions were evaluated 2 hours after spot tox.

1.2.4. Biochemical Confirmation of Toxicity

To ascertain that toxicity was elicited within the spot tox MTT (Millipore Cat#: CT02) and PI (Millipore Cat#: 537059-50mg) were used as viability indicators. The appropriate volume of 0.5 mg/ml MTT stock (100 µL) was added to the 1 mL media pool within the well immediately after the 2-hour incubation period was finished [23]. Propidium Iodide was added 30 minutes later [24]. After a 1 hour of incubation the entire slice turns dark blue; longer incubation time will lead to drying out and crystallization of the formazan salt. Within the slice some of the cells do take up PI however the slice is mostly dark and thereby most cells are excluding PI. To confirm the aforementioned two probes, viability testing was also done with FDA (Cat #: F1303), CCK-8 (Cat #: NC9864731) and rhodamine 125 (Cat #: 62669-70-9); however, the most clear and affirmative results based on color contrast was with MTT and PI. In addition, slices fully immersed in media with several concentrations of toxicants (also for 2 hours) was done to better understand the tissue slice's holistic toxic dose response and MG morphology in liquid.

1.2.5. Microglia Visualization

After isolation and/or treatments hippocampal slices were placed in 4% paraformaldehyde in PBS for 15 minutes. Then slices were blocked with 10% FBS in PBS for 30 minutes. Primary Anti-CD11 Antibody (mouse anti-rat mAb Cat#: MA-9u29) was added to slice with 1.5% FBS and 1.5% goat serum for 1 hr under slight shaking. Secondary Ab conjugated with phycoerythrin (goat anti-mouse Cat #: Fb106) was added to slices with 1.5% FBS and 1.5% goat serum for 30-60 minutes. Slices were visualized from directly semiporous filter top appraise morphology. Slice could also be visualized after being placed into a glass slide and mounting media (Cat #: P36983 -) and gently capped with cover slip. An EVOS fluorescence microscope (Cat#: AMF7000) was utilized to capture all MG imagery after mounting media sets, preferably on the same day. Images were surveyed for CD11 cells (in between the central portion of slice and the CA3 or DG row of cells) and their morphological categorization; baseline shaped (stellate with fine processes) or activated (enlarged cell body with thickened processes). Greater than 3 activated MG adjacent to each other are rarely observed in baseline untreated slices and therefore when this was observed they were indicative of site of toxicant-related injury.

1.3. RESULTS

1.3.1. Characterizing MG layout within the hippocampal slice

Represen*t*ative low magnification images (Figure 2) demonstrated the labelling profile of MG wit*h*in several slices. MG within th*e* cultu*r*ed 200-micron hippocampal slic*e* tagged w*i*th a*n* anti CD11 antibody demonstrated the same morpholog*i*cal featured reported in other *in-vivo* and *in-vitro* investigation*s* [9] [10];[11]; [25]. Microglia are henceforth defined visually as CD11+ continuous red staining enveloping a blue DAPI-stained

nucleus. Baseline MG were similar w*h*ether slic*e* wa*s* evaluated immediately after isolation or after a 2-hour incubation, indicating stability of baseline MG 2 hours after excision. Within the confines of the hi*pp*ocampal t*i*ssue slice, MG we*r*e ub*i*quitously observed *t*hroughout. MG consist of a significant proportion of the overall cell population and were evenly distributed (Figure 2A, B, C). Within the isolated tissue context MG demonstrate a homogeneous distribution and seldom overlap. Unlike the close nuclei placement of the CA3 tract, MG cells are generally evenly spaced according to their spatial size, 30-40 ums, (35.7 ±7 um average of 60 cells across 5 slices) which generally correspond to the previously reported MG size at its baseline non-activated state (Figure 3). A cell population analysis of MG contrasted with non-CD11 staining nuclei demonstrated that CD11+ MG constitute 10-18% of the overall cell population (counting total dapi-stained nuclei vs those that stained with anti-CD11 Ab tag) within the slice. In between the center of the slice and the neuronal tracts that demarcate the CA3-CA1 regions (where predominantly more neurons are lined up); this percentage of MG was decreased in the CA3-CA1, DG areas of highly dense nuclei, thereby indicating that MG distribution is area based, rather than cell population based. Thus, this indicates that MG are distributed based on space, not number of cells. The central portion of the hippocampal slice (yellow circle in Figure 2- A, B, C) contains slightly more condensed MG staining. It is also worth noting that there were more activated ameboid-shaped MG present within this central region. This central area, near the hippocampal sulcus has been also characterized as a source of blood vessel passage and protrusion , which has also been reported previously [26]. After surveying MG beyond the central portion (yellow circle in Figure 2A, B, C) reveals that they have more spacing in between them and there

are 5-7 cell rows of MG out before reaching the CA3 track of nuclei. The density of nuclei of the CA3 track interfere with clear MG visualization, and thus optimal region of MG morphological evaluation is the region in between the central MG-dense portion and the CA3 track (Where MG were circled with blue circles Figure 2B). Therefore, after an appraisal of MG's distribution and appearance throughout the hippocampal slice, MG's morphology can be most effectively evaluated within the proposed tissue context in between the CA3 region and the central portion.

Consistent with the reported functional characteristics of MG, MG motility and extreme morphological changes were observed when the slice was put through certain experimental conditions. After 5-7 days (with at least 1 media change) MG in its ameboid morphology start to evacuate the organotypic tissue mass onto the semiporous membrane in a matter consistent with cellular motility and migration ([4]; [19] (Figure 5). Upon staining, many of these cells stained positive for CD11, further corroborating CD11 protein's functionality (along with CD18 [20]) as an instrument of cellular motility. Thus, MG exhibits its motility capacities within the hippocampal slice.

In conditions where the hippocampal slice was immersed in media, instead of resting on a semiporous membrane (as historically used in electrophysiology experiments), several MG cells exhibited a highly ameboid shape (Figure 6), insofar as suggesting that the lack of stability brought about how the fluid destabilizes the cell body and thus MG lose its fine structured dendritic motif. The stark change in morphology is consistent with the notion that this cell can readily be prompted to change shape from its originally observed fine-processed structured motif. Also, this suggests that a MGs baseline state (and ergo

shape) is predicated upon attachment points [27] [28]within the tissue. Therefore, MG can be prompted to change shape within the hippocampus slice.

1.3.2. Confirmation of cellular toxicity using biochemical probes yielding a "tox-spot" and evidence of eliciting biochemically verified toxicity

The mechanisms of the selected toxicants mercury and cyanide (in combination with 2-deoxy-glucose) to induce cellular toxicity are well understood. Mercury will induce cell death by cross-linking protein sulfhydryl groups and thereby arresting proteomic function [29]. Cyanide will elicit cellular death by inhibiting complex 4 in the mitochondria [30], this, in combination with 2-deoxy-glucose- a glycolysis inhibitor- [31] will impair much ATP generation and thereby depleting the cell of the capacity to conduct ATP-related metabolic processes.

All viability testing with toxicants was contrasted with a positive control, 10x Lysis solution from an LDH kit. Biochemical confirmation of toxicity resulted in clearly distinguishable areas of induced toxicity. Adding MTT to the cell media resulted in conversion into formazan salt that resulted in hippocampal tissue pigment changing from beige to its characteristic dark blue (control in Figure 7). Adding PI resulted in individual cell's uptake; however, the majority of the slice was dark suggesting PI exclusion and thus intact cell membranes (Figure 8, Figure 10, Figure 12). MTT and PI biochemical probes simultaneously verified that a significant portion of the slice was still viable (control in Figure 1, Figure 8) consistent with the notion that the slice remains viable after excision as previously demonstrated in electrophysiology studies [15], [16], [32]. For example, light microscopy reveals that the absence of MTT conversion was defined as an area of toxicity by the appearance of white amidst the formazan blue staining within

the tissue sample, which corresponds to cell injury and death (Figure 7). After PI exposure, toxicity was defined as a spot tox area of saturated red fluorescence amidst the black within the tissue sample (Figure 8), which indicates that PI was not excluded, or that there was extensive nucleic acid leakage in that region, which corresponds to damaged membranes and hence cell death (Figure 8)

It is worth noting that part of the workup of this slice model was to use a positive control, which consisted of a 10x lysis solution from an LDH kit. Placing a 180 nL aliquot of this lysis solution consistently elicited a spot. To induce a more mechanistic form of toxicity a 180nL aliquot of 12 mM mercury was used to produce a spot. At first lower concentrations of known toxicants did not produce spot after 2 hrs; these toxicants consisted of 100 mM of an ionophore (A23187), 50 mM of a chemotherapy agent (gemcitabine), 2% triton, 4 mM of cyanide, 100 mM Rotenone, 100 mM of 2-deoxy glucose, 10 mM lead (Pb), 10 mM ATP. Based on the nuanced of bioavailability toxicity in the form of a spot tox could only be elicited by using vey high concentrations of toxicants. Eventually spot tox was produced using very high concentrations of cyanide (1000 mM for 2 hrs), Pb (300 mM for 2 hrs), ATP (300 mM for 2 hrs) and gemcitabine (1000 mM for 24 hrs, MTT only spot). Interestingly the delayed effect of gemcitabine reflects a delayed toxicity that only resulted in mitochondrial damage, but cell membranes were still intact. Noteworthy, a hot needle was used to benchmark mechanical damage and interestingly no spot was produced with either MTT or PI. After conducting a dose response assessment on what concentration levels of Hg and CN2-DG are needed to elicit toxicity via the observation of a spot tox, it was determined that at a volume of 180 nL 12-1 mM (added once) of mercury (Figure 9 A) and 125-

500mM (dosed 3X to the same region) of both CN/2-DG (Figure 9 B), are the concentrations are needed to induce biochemically verifiable cell death within the CA3 region and throughout the thickness of the 200-um hippocampal slice (Figure 13). The disparate concentration ranges used to generate toxicity are consistent with the notion that the more non-polar toxicant (mercury) can elicit cell death at much lower concentrations that the polar toxicants (CN/2-DG). Considering the intracellular bioavailability issues with CN/2-DG, three doses of CN/2-DG were administered to the same region ensure that toxicity was achieved at lower concentrations levels where more physiologically relevant pH is approximated, specific CN/2-DG mechanistic toxicity will deplete ATP levels within the cell. High concentrations of cyanide that reliably yielded a white or/and red spot in a single spot (1 molar) dose brought the pH to higher levels and thereby introduced non-specific toxicity by pH stress. Thus, cyanide concentrations were lowered to 250 mM (added 3 times to same region) elicit the sought mechanistic toxicity related to ATP depletion. The toxicity of mercury and CN/2-DG regions injured with the 180 nL aliquot spot tox does not turn blue (and hence no formazan formation). In addition, at the most toxic doses a bright spot of red fluorescence appeared in the same region confirming the toxicity with PI not being able to be excluded from nucleic acid interaction; this change in PI uptake could be measured quantitatively using image analysis of red color area (Figure 10). Therefore, biochemically verified cell injury and death can be simultaneously visualized using 2 distinct probes yielding a "spot-tox,".

An anecdotal, yet reproducible, characteristic of the functionality of the hippocampal slice is the observation of blood blue vessel macrostructures (viable capillary cells that convert MTT into formazan salt) within injured white areas of the hippocampus (Figure

4); which underscores the fidelity of the blood brain barrier (excluding out toxicants from vascular compartments), and ergo some further evidence of maintained known *in-vivo* functionality of this *ex-vivo* sampling.

1.3.3. Disparate sensitivity to cellular injury and death between 2 probes

Another noteworthy observation is that albeit toxicity can lead to changes in MTT and PI signals within the area of injury, the appearance of these signals in a concentration response effect is disparate. An MTT-white spot appears first in the dose response assessments than the PI-red spot. This assay indicates that, at a lower, mildly toxic dose level, whilst the cells within that region are metabolically debilitated and declining, the injured cells are still excluding PI. This suggests that these lower intermediate toxicity dose levels (Figure 9 A, B) (1 mM for mercury and 250 mM 3X, for CN/2-DG) are cell stress/injury doses; that is that the cell is damaged to the point that it does not adequately maintain a functioning mitochondrial reductase enzyme but is still viable enough for these cell's membranes to still exclude PI out of the nucleus' compartment. This discrepancy was manifested in the outer regions of the spot tox, and where the majority of activated ameboid MG were found.

Examining the MG response within the hippocampal slice using biochemically verified toxic doses resulted in stark morphological changes to MG. Upon toxicant exposure within a specific region of slice (on CA3 side) a crater forms and at high doses it is characterized by an intense core of nonspecific red fluorophore staining with a rim of activated MG (Figure 11). MG morphology evaluation was done on 40X field in the circled regions of Figure 11; MG too close to the red rim were not evaluated for morphology because they are presumed dead (based on MTT and PI results). Activated

MG exhibit more intense fluorophore intense staining, have shorter and thicker dendritic processes and have enlarged cell bodies around the nucleus that make MG easier to visualize in the magnification plane than when MG are in their baseline state (Figure 12). The dentate gyrus region was not treated with toxicant and thus baseline MG remained in its non-activated fine-processed structured motif with a small cell body around the nucleus. Cell counting analysis on all the MG in 40x images indicated that not all MG become activated with greater distance you get from the site of injury the less activated the MG (Graph 2 A, B). Areas of tissue injury were characterized by the appearance of different MG morphologies that were different from its baseline shape. The spot-tox demonstrated a gradation of MG profile related to injury distance. The closer the MG were to the area of injury, the more activated and condensed they appeared. Therefore, MG can exhibit morphologies that indicate it is in its activated state (M1, ameboid) after being treated with biochemically verified toxic doses of mercury and cyanide in combination with 2-deoxy-glucose.

It is noteworthy that MG were activated at toxicant dose levels much lower than the appearance of the white MTT spot and red PI biochemically verified spot tox, 500 mM and 12 mM for cyanide and mercury, respectively. MG were activated at concentration levels as low as 5mM and 0.04 mM for cyanide/2DG (both same concentration 5 mM) and mercury, respectively (Graph 2). This suggests that the cellular structural changes of MG are more sensitive to injury assessment more so than the stark visualization of a white MTT and red PI biochemically verified spot within the 200-micron thick hippocampal slice. This is likely due to the thickness of the hippocampal slice; the propagation of regionalized toxicity required the utilization of a very small dose volume,

180 nanoliters, as this volume was the smallest technically possible way to only injury a specific region within the hippocampal slice (and maintain enough healthy slice tissue regions for comparison); however, this volume does not affect cells throughout the entire thickness of the slice at lower concentrations. Based on the results from Jeong et al. [33] [34] where brain tissue was treated with 50 mM or 500mM of ATP concentrations, it was noted that toxicants' concentrations can impact the size of the area of injury [35]. To probe this possibility, the slice thickness was assessed for biochemically verified injury and indeed lower doses affect the topmost portion of the slice, but do not reach the bo*t*tom portion of slice (Figure 13). During method development it was noted that at concentrations of 250-500 mM of CN/2-DG treatments in thicker 300-micorn slices would not result in areas of verified toxicity, when the slice thickness was lowered to 200-microns verified toxicity was verified at the same concentration; this suggests that *t*hickness of slice drives t*h*e s*e*nsitivity of the dose-*r*esponse in this mod*e*l. It *i*s also *n*oteworthy that the number of MG cells w*i*thin the 40x micro*s*copic image evalua*t*ed did not drastically c*h*ange (Graph 5), from control and untr*e*ated area*s* indicating that, albeit, there is injury, more MG cells do not migrate (from other regions of the slice) to that region within 2 hours of the toxic insult.

1.3.4. Microglia's different shapes and sizes from injured to non-injured tissue.

After *s*urveying the IHC (labelled for CD11) slice for MG in treated slices, MG changes in sha*p*e were observed near and around the area of tox*i*cant exposu*r*e (spot-tox). Areas d*i*stant (denta*t*e gyrus) from spot-tox site exhibited mostly MG that resembled baseline shapes and were corroborated with control slices; that is, with fine dendrites and stellate

form with a small cell body. In between these two regions there was a variation of shapes noted mostly in changes in overall shape and size. The size of a baseline shaped MG distal to the injury site is 30-40 microns and mostly exhibits fine-stellate processes that were 1 micron thick. MG near the nearest surviving area of the spot tox were much more condensed, globular and smaller in size (10-15 microns), however in certain instances stellate MG were also noted but with thicker processes of 3-4 microns thick. The MG in between these 2 shapes may represent a gradation of activation that is being predicated by differential toxicant concentration from the core of the placement of the 180 nL aliquot. Whereas the toxicant concentrations were highest at the central site where the 180nL drop landed on the tissue, the surrounding areas were diluted with the media already within the slice tissue matrix and thus the portions further from that area represent places where toxicant concentration was decreased. This is corroborated in the MTT studies, where a gradation in the shade of formazan blue was decreased, but PI was still being excluded; indicating areas of injured but still viable cells (defined as cells with membranes still excluding PI) toxicant concentrations. In these sublethal regions, MG were more mixed in morphology and varied between shapes that resembled baseline fine dendritic stellate motif, stellate with thicker dendrites and ameboid with little to no dendritic processes (Figure 12). Another way to consider the changes of MG from injured to healthy tissue is the rearrangement of its cell membrane; insofar as there is an appreciable accretion of the membrane (and hence IHC CD11+ mediated staining) that thickened as it becomes more activated, and importantly, it becomes a denser cellular particle; this shape is contrary to a delicate fine structured web of stellate branching emanating from a small cell body when MG is in its baseline state. Ergo upon surveying

these MG, the progression from baseline stellate structure in uninjured tissue to that of an activated ameboid around most injured viable tissue one may correspond a measurable change to the membrane, which accretes and thickens around the nucleus based on the severity of injury.

1.3.5. Quantifying microglia's structural aspects in different morphological state

After 12mM Hg injury within a small region of a cultured slice, comparing baseline MG with activated MG results elucidation of quantifiable structural data as it pertains to its cell body/soma and rearrangement of cell membrane. As previously mentioned, baseline MG's shape characteristics relates to not just size of the entire cell, but the presentation of membrane distribution. The membrane encapsulates the nucleus and emanates from this centrality via the protrusion of fine filaments that are typically no wider than 1 micron thick; taken together, resembles the shape of a star and hence stellate in appearance (Figure 3, Figure 12). The opposite extreme of MG's membrane distribution is the ameboid shape of MG that is the morphologically characterizes it as this it being in its activated form (Figure 15). In this opposite motif, the membrane also encapsulates the nucleus, however two main distinctions are obvious; that is that most, if not all, processes are no longer present (and those that remain are shorter), and the cell body that surrounds the nucleus is much thicker and stains more intensely. The stark changes in cell body can be quantified by measuring the greatest lateral distance (after an initial polarization of MG's soma) of the cell membrane to that of the nucleus' membrane within an individual MG. During surveying of control slices MG's baseline state this distance is typically 0.8-1.5 micron thick, as demonstrated in Figure 15. During surveying of spot-tox treated

slices MG opposite activated state this distance is greater than 3 microns as demonstrated in Figure 15. This structural demarcation was compared in the spot-tox injury model 20x images, and upon comparisons of different MG's within, statistically significant (student t-test) quantitative changes in distance between the nucleus membrane and cell membrane resulted. When all the MG in the control slices were compared to all the MG in spot-tox treated slices a statistically significant change was observed; control slice MGs had distance from nucleus to cell membrane was 1.49 microns, while treated slices had distances of 2.93 microns (Graph 3). Within Hg-treated slices that had activated MG around the injury area of spot-tox were compared to MG in regions proximal (non-treated area) and distal (DG area) to injury and thus within healthy portions of the tissue and statistically significant quantitative changes in structure were also found. A spot's borders were set by the appearance of 2-3 MG next to each other within the region between center of slice and the CA3 track of nuclei. These MG has a nucleus to cell membrane distance of 3.46 microns (Graph 4). Any other MG outside this border in between the CA3 nuclei track and the center of the slice was considered a proximal non-treated area; this area had average distance of 2.40 (Figure 16). To ensure that the slice had enough baseline MG present, the dentate gyrus region was evaluated as a healthier portion of the slice that was distal to the spot-tox; these MG have a distance that was similar to control slices at 1.56 microns (Graph 3). Therefore, MG structural changes can be quantified by measuring the distance of the nucleus membrane to that of the cell membrane.

This quantitative data is indicative of the amount of cell membrane rearrangement that occurs when a MG goes from one extreme state (baseline) to the other (activated).

Collated images of MG's distinct morphologies (Figure 18) exemplifies many of the different shapes and forms captured in between the baseline form of MG and the activated form of MG. Within his study, there are intermediate forms of MG that were also captured; this metamorphosis indicates that as the MG gets activated and accretion of the cell membrane occurs, and thus the area that the cell membrane spreads throughout shrinks and the fine filaments (characteristic of the baseline state) thicken as they shorten into the cell body. Also, there is a polarity of the MG soma that is exhibited as it accretes more intensely at polar opposite ends of the cell body, which is indicative of a pattern of membrane compression. This significant rearrangement of cell mass is an important consideration to bear in mind within the context of the tissue matrix; this will be elaborated upon in follow up chapters 2 and 3 that endeavors in describing intercellular spacing within this tissue.

Another important consideration with regards to the changes in membrane rearrangement that MG undergo is the location of the nucleus within the enlarged cell body (Figure 17). Since MG generally have an asymmetric layout the placement of the nucleus can be an important consideration as it can serve as a point of morphological distinction. This is mostly appreciable when MG cell body is greater than 10 microns in length, which is twice the size of its nucleus' diameter (consistently measured at 5 microns in this study). At baseline although the nucleus is clearly present there is very minimal cell body present to appraise the nucleus' placement within. However, when the cell body is big enough, the placement of the nucleus can be categorized as central, or it can be located closer to one of the extremities of the elongated/enlarged cell body.

1.3.6. In between baseline and activated morphologies MG exhibit many characteristics and different forms

One of the most important visual characteristics of baseline MG is the preponderance of dendritic branching (1 micron in thickness) emanating from a small cell body that contains the nucleus. Notably, that MG cell bodies are somewhat more difficult to see when in their baseline morphology as MG are not only thinly dispersed, but they are also well-ensconced within the tissue matrix and hence visually blocked within the image fields (40x). At the other extreme, MG have very little to no branching and it is very globular in shape and very stark in appearance; activated MG morphologies are more readily visible than the baseline MG morphologies. In between these 2 extremes, other morphologies were observed (Figure 18), which are likely intermediate shapes that represent the membrane rearrangement described in the previous section. Also, it is important to note that these intermediate MG morphologies are present 2 hours after initial injury. As baseline MG accretes, the cell body in and around the nucleus begins to gain form in a polar manner; that is, the membrane is closing in from 2 opposing ends. Concurrent to this cell body rearrangement, the dendritic processes become shorter and thicken to greater than 1 micron. This thickening helps improve the resolution of MG seemingly amorphous cell body appearance as it gives the cell body and dendrites more structural definition, which assists in the delineation of structural landmark dendritic protrusions as they thicken as the membrane is rearranging into the cell soma. The plasmalemma from distal dendrites involute towards the nucleus which is considered a central position of this cell's baseline layout. A simplified perspective, from a cell structural standpoint, this metamorphosis is a complete redistribution of MG

plasmalemma. Membrane that was once 20+ microns away from the nucleus is now proximal to the nucleus and yielding a more prominent dense cellular particle with its plasmalemma concentrated in and around the nucleus. Therefore, within this controlled tissue sample matrix different iterations of CD11+ MG's morphology and details of its structural constituents (soma, nucleus, dendrites) are visualized.

1.3.7. Visualizing the number of microglia's processes/dendrites

A range of 6-10 dendritic processes were usually counted in an assessment of 26 baseline-shaped MG cells (in 16 different 40 x images across different experiments Figure 21); the dendritic counts were corroborated with several other published studies [25] [9] [18] that looked at MG morphology and thereby displayed detailed MG images (Figure 21). A dendrite was characterized as a track of red fluorescence (CD11-labelling) emanating out of MG main cell body's membrane in a perpendicular trajectory. There are several presentations of how dendrites protrude out to resemble distinct motifs. A common MG motif is where one end has a major off-center dendrite that bifurcates into 2 large branches, the other major dendrite, seemingly a tail, that emanates directly from the soma end that spits into 2 tapering ends, similar to a maimed lobster (guide bars run parallel to dendrites in pictures of Figure 20 A, B, C). Usually two of these three major (thicker) branches have 2-3 major sub-branches that keep bifurcating out to other smaller branches when MG is in a baseline (M2) state. The other 3-6 branches are not as thick and long but can also bifurcate out to create smaller dendritic processes. Taken together, MG in its baseline M2 state presents with several dendritic processes that can be quantitated to a number of 6-10 in any given individual MG cell.

1.4. DISCUSSION

Microglia cells have a unique position in the immune response in the post BBB interstitium as they are usually the first motile responders during perturbations within the extracellular biological matrix. This cell is mobile and highly amorphous and as such its characteristics can potentially be visually read by evaluating its shape and the sum of its three main structural components: the soma, the nucleus, and the dendrites. Much investigation has gone into studying its behavior and signaling during activation ([25] [9, 10]; [11], this is the first reported evaluation within a cultured organotypic tissue model that activated a subset of MG within the tissue model with a toxic injury but left the rest of the MG in its inactivated baseline state. Thus, one of the enticing aspects of observing MG embedded within a viable tissue matrix is observing MG response events in-situ; by modifying (via toxicity) the immediate interstitium amid a viable biologically active sample (as demonstrated in electrophysiology studies). Also, important to note that maintains the microscopic structural layout of a mammalian brain is preserve in this tissue slice. The benefit of this condition is that it allows for evaluation of a spectrum of MG morphological changes that occur from being in a baseline state to that of being fully activated within the tissue context. Also, equally important, the organotypic hippocampal tissue slice model evaluates MG's versatile characteristics (shape shifting and motility) *in-situ*; thereby, putting the slice through certain experimental conditions (immersion in media, and observing MG migration after several days in culture) allows affirmation of its versatility by being able to take a closer look at MG 's defining characteristics. This is the first time it has been characterized in an *ex-vivo* tissue model, not only does it confirm many of the known aspects of MG studied *in-vivo* and *in-vitro*, but also it allows

visualization of MG's inherent properties such as its sensitivity to fluid turbidity and MG's motility. Further, evaluating this tissue outside the animal in an *ex-vivo* manner not only corroborates many of the *in-vivo* findings but also isolates the genetic and resultant biochemical responses that arise from precise toxic insult with multiple controls. However, prior to delving into these deep queries on how MG (and CNS cells) ascribes a genetic commitment that leads to stress related biochemical, proteomic changes, a reproducible cellular response must first be ascertained, in this study such cellular response is morphology and thus how MG cell rearranges its cell membrane. Such is that this investigation into MG's morphology after precise toxic insult elucidates a nuanced cellular response, and in turn also revealed many details of MGs' structural variations within its nascent CNS surroundings.

To confirm the advantage of using a hippocampal slice to isolate and evaluate tissue injury and MG response we selected the organotypic hippocampal slice model as the experimental stage based on its rich history in elucidating neuronal activity, leveraging the ability of this sample to maintain viability well after it has been isolated from the whole brain. The likely reason for this is because of the nature of cerebrospinal fluid (CSF). Some of the main distinctions of CSF (from blood plasma) is the concentration of protein, for which there is 223 time less protein, half as much potassium and calcium in the interstitium than CSF [36]; and therefore, the cationic and anionic fluid dynamics differ from outside aqueous compartments. Cerebrospinal fluid is considered to move about the CNS compartment in a unidirectional and (apparently) diffuses through parenchymal openings ([37]; [38]), and this process is likely the contributing nature of a hippocampal slice that can naturally keep itself covered in fluid even though it is resting

on a semi-porous membrane, separate from media and thus in open air. As such this tissue exhibits a characteristic of being able to suffuse itself when isolated from the greater brain mass and circulation. In this model (tissue slice resting on a semiporous membrane) reagents added to the media are taken up by the tissue and exposes the cells within, and thereby indicates that there is an appreciable fluid dynamic that resembles interstitial flow.

Cluster of differentiation 11 (CD11) IHC stain was selected to detect MG since it is a protein that assists its movement and is an important characteristic of MG as a categorical dendritic cell; furthermore, this protein is abundantly expressed in the extracellular side of the cell membrane thereby outlines MG's shape from the outside as it relates to its extracellular layout [20] [27] [28]. This form detection scheme labels MG based in its motile identity to and relates it to it presented morphology. Evaluating of MG morphologies in this study was crossed referenced with other reported morphologies (using different IHC targets such as Iba-1) and therefore confirmed that the cell being evaluated was indeed a CD11+ MG [10]; [11].

To further describe MG characteristics within slice model we evaluated the morphology of these cells in the above-described experiments, considering that MG are generally evenly spaced, and each is endowed with covering a certain tissue region and they seldomly overlap; the placement of MG can in fact resemble a pixilation and have the potential to be grided in certain areas. The area between the center of the slice and the CA3 track of neurons was the region used to probe MG changes. This sub region of the hippocampal slice was selected as the location to expose to toxicants not only because it had the most visually defined baseline MG, but the tissue was spaced out enough to take

detailed images of MG. Thus, this consistent layout is also indicative of MG ability to survey extracellular terrains using its dendritic properties. And albeit there were minimal overlaps during baseline state it seems to have an appreciable level of spacing in between cells, when the tissue was injured with toxicants, the spacing in between them was decreased as this represents the shrinkage in the overall size of the MG cell as it changes into its activated state. It appears like MGs dendrites play a role in this spacing. Therefore, the nature of MGs shape seems to be dictated by being in a certain region of the tissue slice. Nonetheless, the notion that MG can be in different forms because of a specific location is noteworthy, a particularly interesting observation because they appear mostly activated near blood vessels, which is consistent with other literature findings [39]. Considering the observations made when the slice was immersed in media, that is, a preponderance of activated-shaped MG across the whole slice, this is indicative that MG must have attachment points to the matrix to define its morphology. When the tissue is immersed in media the turbidity of media's fluid destabilizes the fine structure of the MG and renders it an amorphous ameboid shape; thus, we are likely observing the MG evacuating the tissue compartments within the slice as it is interacting with media fluid. Such is probably why MG are mostly activated near blood vessels because they were just within the turbid compartment of the inside of a blood vessel, where all cells within the intravascular compartment are almost exclusively ameboid shaped.

To obtain biochemical evidence of *ex-vivo* toxicity we selected agents that induce cell injury and hence MG activation. These are known toxicological agents that have been studied for decades, and therefore their mechanisms of toxicity are very well understood. Leveraging the knowledge of their mechanisms of toxicity as it pertains to cell function, a

toxicant such as mercury could be used to arrest proteomic function and induce a very specific type of cell death [29]. Another set of very different toxicological agents that also induces cell death, but in a very different manner, is cyanide combined with 2-deoxy-glucose, as this combination will deplete ATP levels and lead to cell death by its inability to maintain adequate ATP levels (Way et al., 1988). Both these injury types were confirmed biochemically, by evaluating the activity of a reductase enzyme within mitochondria (a proxy for metabolic adequacy) using MTT-formazan conversion; and confirming this endpoint with an exclusion dye, propidium iodide, that can only permeate the nucleus of dead cells thereby indicating a damaged cell membrane. MTT was more sensitive to characterizing a stressed cell as it elicits a signal prior to more severe cell membrane damage. Sites of exposure to toxicants resulted in the appearance of a white spot (when viewed under light microscopy) amid blue formazan pigment that was converted from MTT by healthy cells; also considering that PI was added to the same media, a red spot (under red fluorescence lighting) would appear that overlayed the white spot that indicated that cells has not converted the MTT had damaged membranes thereby confirming the MTT results (Figure 14).

During biochemical verification of toxicity using MTT and PI simultaneously, there was a suggestion that MTT is a more sensitive indicator of cell stress as an MTT signal appears prior to a PI signal. In this study whether it was on the dose-response assessment, or temporal assessment of spot onset, or spot radius the white spot always appeared prior to the red spot. This suggests that stressed cells did not convert the MTT, signifying metabolic deficiency, but their membranes were still intact and able to still perform their prime directive, that is, to exclude indiscriminate aqueous extracellular molecules (such

as PI) out of the nucleus' compartment. It took extremely high doses of toxicants to induce verifiable cell death as the biomechanics of toxicity within a tissue model is that concentration of toxicant within a very small volume also drives the area of injury, that is, under a limited volume the higher the concentration, the larger area of injury. This is consistent with the results of other published studies [33] where a 10-fold difference in ATP concentration yielded a dose dependent change in the area of injury.

MG motility was evaluated within the hippocampal slice. Albeit MG motility was demonstrated when the tissue was cultured for multiple days, within the 2-hour timeframe there was no indication of MG motility towards the sites with the most injury; possibly because 2 hours is not enough time for MG to migrate within this *ex-vivo* model. *In-vivo* experiments indicate that 2 hours is enough time for appreciable migration [19] [4] and MG accumulation in an injury site The motility speed and direction of MG in vivo might be dictated by the flow of CSF into the tissue, which is not a factor in this hippocampal slice model when observed for 2 hours and, thus, may account for the lack of migration observed in this study. Irrespective of this limitation, the fact that MG do not move does lend some appreciation that the cells affected are static within the 2-hour window after treatment with toxicant and representative of a direct response to treatment in-situ and not a manifestation of MGs of different morphology migrating to the site.

Additionally, further MG structure was expansively characterized. Microglia's structure has been described in many other previous articles as several main morphological motifs, that bear different nomenclatures as deemed by the publishing authors [40] [9]. In this study MG was also categorized but by different criteria and holistic intermediate shapes between baseline and activated are being reported. To understand these intermediate

shapes, MG's main most discernible structural elements must be described in greater detail. If the massing of a baseline MG is broken down by categories it can be described by 3 main visual elements, as demonstrated in the IHC imagery that was generated. First, the clear appearance of a nucleus enveloped within a cell body (as dapi stained with an anti-CD11 Ab). Second, a cell body whose size is defined by a cell membrane that extends to a greater area beyond the nucleus compartment. Third, is the thickness and length of dendrites. In fact, upon closer examination MG can have 6-10 dendrites that emanate out of the cell body. This massing and its details are challenging to discern when MG are in a baseline state since the membrane is so thinly spread out and thus faint in appearance when labelled. However, as a faintly visible MG metamorphize into its activated extreme, some structural features do become more prominent; first the cell body becomes more well defined, as well as the dendrites' structures.

The first two characteristics, nucleus and cell body of the MG are intimately related as they are both stark visual landmarks whether MG is in its baseline state or its activated state. Albeit there are appreciable changes in size of MG when activated versus in baseline, the most consistent quantifiable change is the space between the nucleus membrane and the cell membrane, as mentioned in Graph 3, Caption: Comparing control slice CA3 region 2 hours after vehicle control exposure resulted in the membranes' distance of 1.49 compared to Hg treated slices CA3 region which resulted in a distance of 2.93 microns.. This is an important marker not just of size, but more so the rearrangement of MGs cell membrane borders. The amorphous nature of MG is one of its important characteristics and these stark changes to cell structure enable functions as it relates to MG's baseline state or activated state. Thus, when MG is in its baseline state

the cell membrane's distance (the wider of the lateral 2 distances) from the nucleus is around 1 micron thick, thus it is presupposed that the rest of the membrane is thinly spread out covering a designated surface area as it conducts its baseline activities. Conversely when MG is activated the nucleus' membrane distance from cell membrane is greater than 3 microns on average (up to 6 microns individually), which is a substantial change. This quantitative change can serve as an indicator of level of activation of MG. As such this distance can serve as a point of distinction by characterizing intermediate forms of MG, along with other ancillary visual characteristics: dendrites size, shape and nucleus placement. Irrespective of the two distinct mechanisms of cell death and injury, MG morphologically behaved in the same way at least in this rudimentary qualitative assessment of MG shape. These 2 models of toxicological insult (mercury and cyanide combined with 2-deoxy-glucose) leveraged the knowledge of toxicological agents' mechanism of toxicity to induce a cellular response, activating MG from an M2 to an M1 state.

Understanding the meaning/functionality MG dendrites is paramount in the understating of MG's inherent biology and response to toxic insult**.** One of the most defining characteristics of MG is the presentation of their dendrites [25]; [9] [18]et al., 2016). As described in the results, there are usually 3 major dendrites and one of them bifurcates into 2-3 branches of similar width, which resembles a claw (Figure 20). This dendrite is usually off center and therefore lateral, which indicates that these cells are asymmetrical. This asymmetry can be useful in determining the orientation of the cell and thus have a greater appreciation of its layout within the tissue matrix. Furthermore, the other dendrites serve some sort of functional weight, potentially distinguishing the functions of

all these variety of dendrites and providing important information about these morphological variations. These structural variations can offer information about how these dendrites are protruding and assist in several different functions, for example: the adhesion or anchoring to the extracellular matrix, reach out to neighboring MG to maintain adequate spacing (since they seldomly overlap), probe the extracellular fluid (for either signaling or indications of cell damage), or directly probe neurons, astrocytes (and other CNS cells), cellular address probes, etc. and other undiscovered functions. Conversely these dendrites involute during MG's most activated states, however often dendritic stumps remain, what role do these dendritic remnants emanating from the ameboid MG cell body play when MG is conducting its activation duties? Taken together, the nature of the MG cell is one that is highly animated and has several different opportunities for scientific endeavors on how these cells can serve as biomarkers of extracellular adequacy.

Morphology and placement of nucleus are important for MG characterization. Considering the asymmetry of MG, placement of the nucleus within the cell body can also be a point of MG structural variation distinction. In one of the intermediate forms of MG, the cell body elongates and has a polarized motif. Taking into consideration the asymmetry of MG, that is the 2 of the major dendrites are usually on the opposite end of the claw dendrite, the nucleus has been found to be closer to one of these extreme ends in certain intermediate structures (Figure 17). These features can serve as further characterization of MG's intermediate morphology as well. To gain a full appraisal of proximity of nucleus, the cell body must be long enough to appreciate that the nucleus is in a position more towards one extreme of the MG. The positioning of the nucleus is not

useful during the extremes of structural variation, that is when it is in its baseline state the cell body is too small; or when it is in its activated state the cell body's circular shape offers no definitive orientation. However, in between these extremes the body does elongate up to 15 microns (3 nucleus lengths, or rod and ameboid shape as described in this study and by Fernandes (2019), and thus whether it could be determined if the nucleus is closer to the end of MG motif that has the claw or the end of the MG that has the 2 other major tail dendrites; in Figure 17 the MG bracketed is opposite the tail end that splits into 2. In addition, the shape of the nucleus itself can lend some information about the state of the MG, insofar as if it deviated from its typical evenly spherical shape it can suggest an activity, such as in Figure 17 label P, the non-spherical shape of this nucleus indicates that the nucleus is being pinched as if it were trying to squeeze through a narrow opening, consistent with its motility characteristics.

The morphological plasticity of MG is intrinsically connected to its response to toxic injury. The main tenet of this study was to examine a controlled signal to noise of MG according to its morphology presentation within a sample that had simultaneously healthy and injured tissue, such is why the toxicity was localized to only injure a portion of the hippocampus tissue sample. As such as there was an appreciable layout of baseline MG in the non-treated regions of the slice, the treated region demonstrated an increase in activated MG; but most importantly the intermediate forms of MG, in between its baseline and activated morphological variation were carefully evaluated. This paradigm addresses one of the main questions about MG, what are its intermediate forms and what can they tell us about the state of the tissue in terms of stress related to toxic injury. After toxicant injury was induced, MG were not evaluated until 2 hours later, to allow

sufficient time for morphological changes to take place. What resulted was a circular injury crater that resembled the 180nL drop of toxicant (Figure 11). The epicenter of this circle contained baseline appearing MG that were dead (based on MTT and PI results). The dead cells within the core of the spot still were in their M2 baseline morphology, thereby indicating that MG has to be alive and functional before it can reach an M1 state. Nonetheless, around this core of dead baseline-shaped MG cells fully activated MG were observed (condensed MG with some dendritic stumps protruding or just predominantly globular in its overall shape). Albeit when the hypothesis was generated, it was expected that activated MG would appear consistently within a zonation of a certain length. Such was not the case, albeit most MG were activated within stress zone, there were also some non-fully activated MG observed in the most central portion of the crater. It is uncertain why all the first layer of MG cells did not all appear activated and create a clear zonation of just activated cells, but it is suspected that they dynamics of fluid flow played a role in this heterogenous structural variations. Or perhaps globular MG on top of deeper unaffected baseline shaped MG were not as well ensconced into the tissue and thus flaked off during IHC processing (which involves many steps of sheer liquid turbidity). There might also be a heterogeneity of responses within the population of MG. Nevertheless, in certain instances, up to 8 fully activated MG appeared sequentially, notably with much less spacing in between MG, indicative of the importance of dendritic presence which is at a minimal during MG activated globular state. Amidst these fully activated MG the morphology was heterogenous however, they were clearly no longer in the baseline fine stellate morphology, as presented in the untreated DG region and analogous region of control slices exposed to PBS.

Prinz et al., [13] describe that establishing microglial states can be essential to their roles in homeostasis and disease, such example was postulated as the disease associated MG (DAM) that was genetically characterized by [12]. This study ascribes the morphological state as a determinant of its behavior, ergo "structural variation". Structural variation alludes to the benefit of a cell's structure to a role it is executing in response to its surroundings. Structure is an important demarcation of cellular activity because of the cells biochemical, metabolic, proteomic, genetic, and adaptive commitment of maintaining a specific macro shape. Many of the descriptions of baseline MG in the literature default this structural motif to that of it being in a state of "sensing" the extracellular environment. Taking into account the known roles of MG it is understood that this state is within its purview of its characteristic activities, a sentinel of extracellular medium's adequacy. In a baseline state they are spread out evenly throughout the hippocampus tissue matrix and seldom overlap; this fine stellate form is suggestive of a behavior such as sensing and probing the interstitium's integrity as well as the somatic cells they mount as they migrate through an extracellular region. Baseline MG size ranges from 30 to 40 microns, and the filaments that emanate from the cell body that is just 1 micron thicker than the nucleus compartment, and the filaments themselves are barely thicker than a micron in width. This is logical considering the generally accepted phenotypic job description of dendritic cells, it is virtually a cellular detector of extracellular conditions. Upon its activation, MG changes into a much different shape and therefore it is no longer optimized for detection, it metamorphizes into a compact globular circular shape in its most extreme form of activation. The activated shape is likely more amenable for endocytosis of cellular debris that occurs during injury,

accelerated motility and/or cordoning off a space withing the interstitium as this enlarged shape decreases the space available through micro-openings in the interstitium from which motile cells lay their trails. Spatial obstruction by activated MG could decrease the flow of non-optimal extracellular fluid contaminated with potentially harmful intracellular contents from cells with compromised membranes.

It is also important to note that MG activation does not seem to be a binary outcome, that is, there are other intermediate forms that can arise and participate in the recovery or pathologic process. The most compelling piece of evidence of this is simply the appearance of these intermediate forms near regions of cellular stress. This region was aforementioned as regions that do not convert MTT to formazan salt but are still excluding PI; which is found right outside the most central part of the spot, where all cells are presumed dead (Figure 11). Further, these changes can be characterized by membrane rearrangement, the appearance and morphologies of dendrites and nucleus placement within the MG. Had MG morphology been a binary outcome only baseline and activated forms would have been found in these areas. Therefore, considering that MG activation fall into some sort of spectrum, these forms can signify the state of the immediate matrix they are surrounded by, and thus have a better understanding of the initial stages of cellular perturbation as recognized by this primary sentinel immune cell's morphological presentation.

As described in the results section (Graph 4) one of the most quantitative way to assign this morphological spectrum is to measure the distance of the nucleus membrane to the cell membrane as that underlines the extensive amount of membrane rearrangement MG undergo that happened after the cell polarizes. In between these 2 extremes 5 different

morphologies were identified using cues from the size and shape of the soma and dendrites as well as the overall length of MG (Figure 22). These are postulated to be stable morphologies since they are present even 2 hours after the initial toxicological insult and since there is no migration of MG observed these are not interloper MG cells that migrated from other region (or from nearby blood vessel). Had there been migration it could have been postulated that these were migrant MG from other areas that were just arriving at the sites of injury and thus in the middle of the M2 to M1 metamorphosis. Therefore, these intermediate morphologies can be ascribed to roles that have not yet been elucidated. Activation has been brough about in many ways in this model; by inducing toxic injury to a segment of the tissue matrix, by observing them as the tissue slice biodegrades over the course of several days, and by immersing cultured hippocampus tissue slice into media. The focus of this investigation is on these nuanced MG changes based on biochemically verified toxic injury.

1.4.1. MG's structural (morphological) variations

Collating the visual empirical data gathered in this study together, that is MG overall size, shape/size of soma and appearance of dendrites a pattern of other structural variation intermediates emerges. Namely 5 different intermediate structural variations become apparent (Table 9T). These qualitative categorizations are subjected to the appearance of the soma, nucleus, and dendrites in a 2-dimentional plane that captures all three. The 2 extremes of structural variation are M1 (activated MG) and M2 (baseline MG); the former is a dense cellular particle that is globular and has no dendritic processes, the latter is the appearance of a nucleus enveloped by a thin cell body with several thin dendrites emanating out of it. Since based on the quantitative assessment, the membrane

of the soma gains greater distance from the membrane of the nucleus, a qualitative assessment as to the orientation of the membrane is applied; that is, when and where this separation starts to happen. Also, how this qualitative characterization change in membranes' distance relates to the thickness and length of the dendrites is appraised. In between the two extremes five distinct structural variations are described:

Structural Variation 1- The first indication of morphological/structural changes after the baselines state is the widening of the soma as the space between the nucleus membrane and the cell membrane start to gain some distance, this distance improves the visualization of MG as membrane stain is more intense.

Structural Variation 2- Is demarcated after the first separation of the nucleus and cell membranes, the soma begins to polarize, that is, the slightly thicker membrane begins to accrete at opposite ends which results in an uneven encirclement of the nucleus which renders the soma more oval than circular in shape, in addition the soma is elongated to the point that the nucleus can be regionalized within, usually there is 10 microns (or 2 nucleus lengths) between the 2 polar ends of the soma. After the polarization/elongation the soma begins to widen and the measurement of the lateral distance of the soma's membrane to the nucleus' membrane could be objectively measured (as was demonstrated in Graph 3, Graph 4).

Structural Variation 3- Is the further elongation of the soma to the point that it reaches 3 nucleus lengths, but its width starts to be greater than 7-8 microns wide and thereby lateral separation from nucleus membrane begins; another very important distinction is the widening and shortening of the dendrites. An important structural consideration to structural variation 3 is that the accretion of soma is beginning to yield a denser cellular

particle, which means it is becoming a more obstructive presence within the space it occupies, an important spatial consideration. The immediate consequence of this size and shape change is the alteration of interstitial fluid flow and the passage of motile cells.

Structural Variation 4- After max elongation is reached (usually 3-4 nucleus lengths) presents as a highly visible MG that has a much bigger and thickened soma but still stellate as all the dendrites are also thickened. Notably its dendrites are shortening into the soma, also, the nucleus membrane will gain greater distance from the cell membrane.

Structural Variation 5- the last step before full activation, the soma is even more globular, rotund, but most notably there are fewer dendrites and the ones left over appear as stumps, compared to how they looked previously. This metamorphosis does appear to bear some impact on the conditions of the unique interstitium of the CNS, namely in the redistribution of the area of this cell's soma and the impact of this on the availability of interstitial space, which will be discussed at greater length in Chapter 2 and Chapter 3.

Taken together, breaking apart the main characteristics of MG (soma, dendrites, nucleus) their intermediate forms suggest that they could be objectively discerned as having distinct visually definable morphological variation; this is important because they can be associated with states of cellular stress prior to cell death as many of these intermediate shapes appear within the injury region of the spot tox adjacent to the epicenter (no MTT conversion to formazan salt, but still excluding PI); as demonstrated in Figure 9 A, B; Figure 14.

Microglia characterization within the tissue suggest a cell that undergoes dynamic change and structurally acquiesces to its extracellular environment, likely why MG evacuating the tissue matrix exhibit differences from MG embedded within tissue (Figure 5, Figure

6). Utilizing this structural variation criterion can inform the relative response of a MG with regards to its response to a cellular event that indicates cell damage is occurring. In Figure 23 the higher gradations of morphological variation surround the activated state whereas conversely the lower gradations surround the baseline state. Having this response layout can add resolution to the level of cell injury and how the structural variation of MG can be utilized as a proxy for perturbations in cellular or interstitial homeostasis. In this assessment it is critical to take into consideration the characteristics of MG's individual components change as MG changes shape (Figure 19), that is, how their dendrites shorten and thicken and cell body size increases in overall circumference, all the while the nucleus is still the same shape which serves as a relative control of these stark changes in MG's structural components. The offered resolution to cellular metamorphosis of MG should serve as important distinction points of its activity as it relates to its morphology that can suggest an anomalous interstitial condition (which arises from an injured cell that is about to lose viability) ergo a precursor pathological event that eventually leads to some CNS pathology (in this case pathology that arises from chemical toxicity). Importantly, this detectable/measurable precursor event, microglial metamorphosis, may offer better opportunity for understanding how dendritic/MG cells respond to post BBB CNS cell stress; that is, if we confide in the ability of these cells to detect CNS cell injury prior to than the current most sensitive determinants (intracellular enzyme levels increases in extracellular fluids which suggests their leakage from damaged cells). From a toxicological standpoint this effort represents an attempt to further refine cell injury related to toxic injury; whereas at the turn of the century toxicologists relied on the lethal dose at 50% these assessments evolved into

gross examinations of organs and organ weights, and then into a histopathological assessment of cells within tissue using histological techniques. In this research the changes that first responder cell, the MG (and liaison to the immune response), is carefully examined to further refine and contextualized its response to biochemically verified toxic injury within a tissue model that isolates many of important biochemical events during cell stress. The cellular events captured (MG's morphological change) are likely antecedent to mass enzyme leakage which represent cell membrane rupture and thus can further refine the understanding of the immune cell's role in detecting toxic injury.

In summary, *t*his investigation attempted to c*h*aracterize MG by *e*valuating its mo*r*phological variation within th*e* h*i*ppocampus tissue matrix as it reacts to cell stress related to a regio*n*alized prec*i*se toxic injury. The nature of chemical injury induced led to either proteomic deficiency (mercury) or ATP depletion (cyanide and 2-deoxy-glucos*e*), irrespec*t*ive of type of c*h*emical injury MG b*e*haved *s*imilarly. To characterize MG's structural variation s*p*ecific deta*i*ls about its mo*r*phology were descr*i*bed in de*t*ail as they appeared in the pictorial raw data generated in this study, which was also reconciled with analogous MG imagery from the literature (Fernández-Arjona et al., Filipo et al., 2019; [10]; [11]. As such it is expected that when these landmarks are explored in other MG images from other studies similar trends, layouts and characteristics will be made and role designations for these intermediate forms between baseline and activa*t*ed MG will be elucidated. However, this study *h*oned in on sp*e*cific st*r*uctural asp*e*cts such as: *i*ts se*n*sitivity to flu*i*d perturbation*s* when *t*issue wit*h* r*e*sident MG are immer*s*ed in media, how MG baseline sha*p*e is determ*i*ned by attachment points

within the tissue mat*r*ix and *i*ts abili*t*y to migrate and how it ability to migrate seems to be slower *ex-vivo* than *in-vivo* (as demonstrated by [19], likely due to lack of extracellular fluid pressure). Also, the number of dendrites it has and what the main dendrites look like, and a quantifiable appraisal of the amount of membrane rearrangement as it goes from baseline (M2) to activated (M1).

1.5. CONCLUSION

In conclusion, CD11+ MG is a unique cell within the most exclusive extracellular matrix in the body, its 3 main characteristics, that is: size and amorphous nature, shapes allows the assignment of distinct morphological structures. Affirmations of cell stress that is biochemically verifiable and confirmations of MG shape shifting characteristics could mos*t* effectively be done in this culture model; furt*h*er and probably most importantly, th*e* initial events of cellula*r* str*e*ss w*i*thin the co*n*text of cellular arch*i*tectural ti*s*sue ma*t*rix are isolated. Downstream bioc*h*emistries can b*e s*tudied that ascribe certain genetic (as demonstrated by Keren- Shaul et al. [12]) or *p*roteomic changes that can relate to MG's morphology can be further character*i*zed and studies in g*r*eater deta*i*l in *t*his isolated sample without the noise presented by extra-matrix influences of blood derived cells and chemokine signaling outside the interstitium; and conversely, much more contextually than in cell suspension culture isolation. And, albeit MG appears as an amorphous construct, it follows a certain structure pattern as it metamorphosizes and thus leads to 5 distinct intermediate definable morphological variation between baseline (M2) and activated (M1) forms. Furthermore, detailed, and definable aspects of its cell body structure (and quantitative changes), nucleus placement and number of dendrites indicate that perhaps MG's shape isn't as vague as it appears. Also, it is important to note that as

MG reach the M1 state (morphological variation 3+) they become a denser cellular particle that can impact interstitial spacing and thus glymphatics [41]; Chapter 3). Such is that the data generated from this isolation indicated that the hippocampal tissue slice is a relevant biological quantum of contextualized cells that maintains initial immune cell activity, confirmable survival, and spacing profile of CNS tissue matrix after excision. The biochemical confirmation of a cellular stress and death using MTT and PI, and then evaluating the individual properties of the MG cell response as a dendritic cell represents a fortified rational biological sequence of events that can be isolated and explored further. This isolation can shed some further depth of biochemical, proteomic, and genetic understanding as to what happens when tissue is injured and how it concerts with immune cells' morphological response. Nevertheless, the structural resolution offered describes how MG behave morphologically and can be used to potentially attribute events antecedent to cell death within the post BBB CNS and adds greater depth of knowledge to MG's role in this highly exclusive parenchymal compartment.

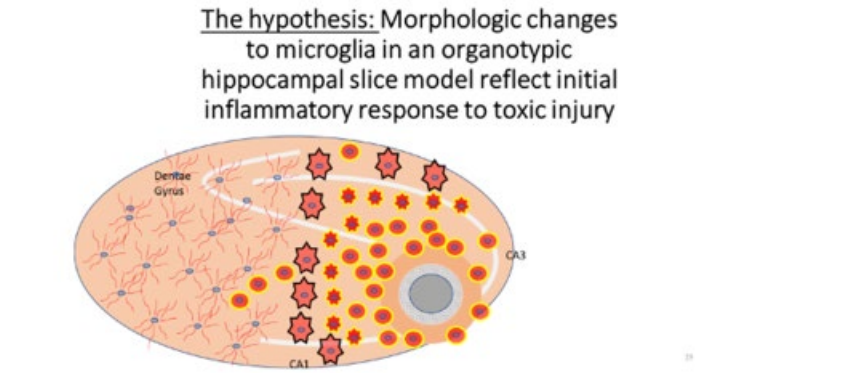

Figure 1: Visual demonstration of experimental design and anticipated microglia morphology outcome

A regionalized toxicant exposure to the CA3 area of a hippocampal slice will result to a graded microglia structural variation (or morphological behavior) based on the extent of cell injury. Surviving microglia near spot epicenter will be more M1 state, whereas microglia distal from spot epicenter will be more M2 state.

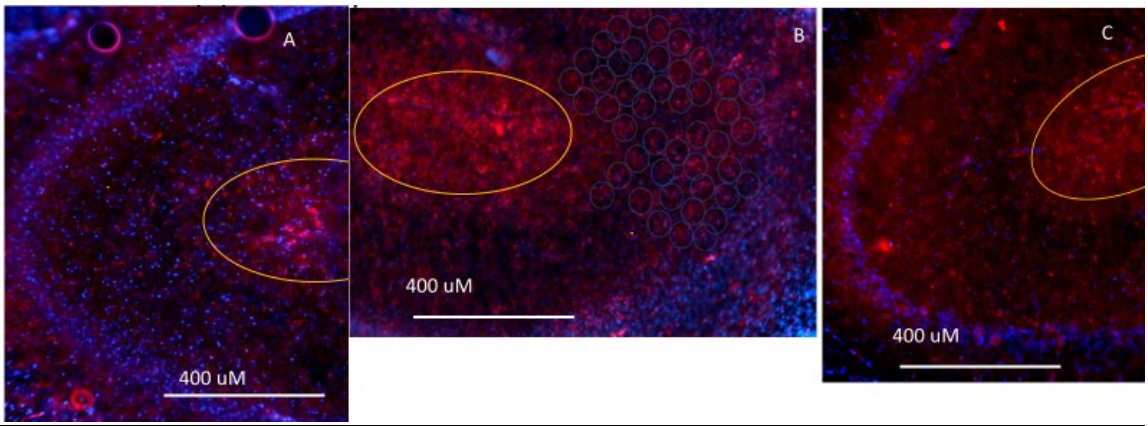

Figure 2: Typical MG IHC (tagged with an anti-CD11 antibody)

Typical field layout within cultured hippocampal slice (examples in figures A, B, C). Field layout consisted of 3 main visual landmarks, the track of dapi-stained nuclei that constitute CA3 (blue pixelated semicircle), a central core with increased red fluorescence staining (enclosed in yellow circle) and the space in between these 2 regions. This region is where the most clearly visualized MG (a sole MG is within small blue circles in figure 2B) are found due to minimal background, adequate spacing and preponderance of baseline MG this subregion within the hippocampal slice used to survey and conduct MG morphology analysis.

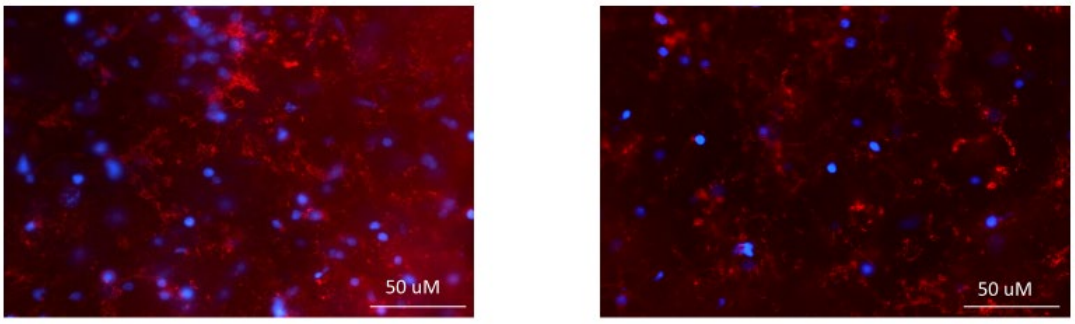

Figure 3: Typical MG layout through a 40x field area of analysis

MG have thin cell bodies that enclose the nucleus, thin processes also emanate out of the soma-nuclei structure. Also, MG are always covering a specific area and generally do not overlap with other MG.

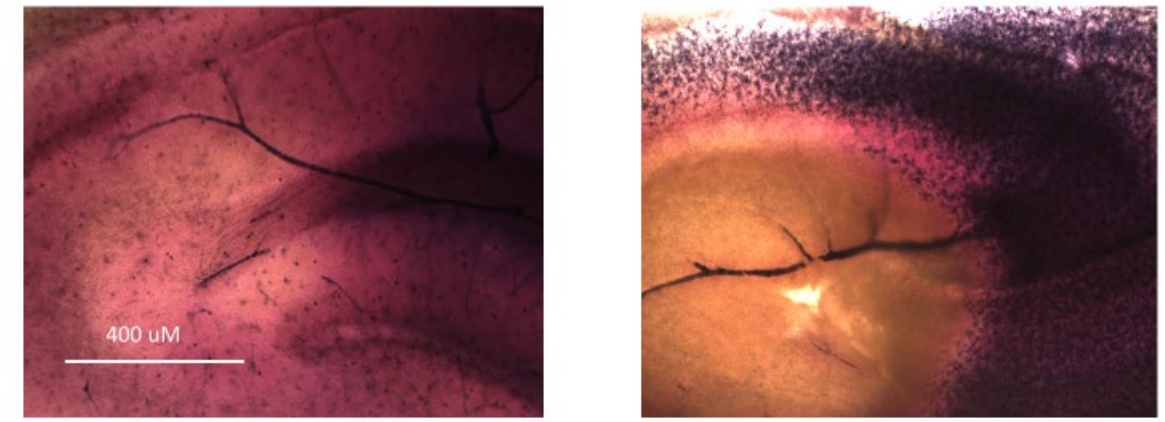

Figure 4: Hippocampal slices viability probing with MTT

After exposing hippocampal slices to MTT, healthy matrix stains dark blue, which represents formazan salt conversion. The staining was more intense with macro structures that resembled blood vessels. In addition, areas exposed to toxicants, where little to no formazan salt formation is expected (due to cell damage/death); interestingly, in some instances vascular structures still maintain viability, underscoring the fidelity of the blood brain barrier. This indicates that CNS cytostructure and function is preserved in some form, demonstrated previously in electrophysiology studies.

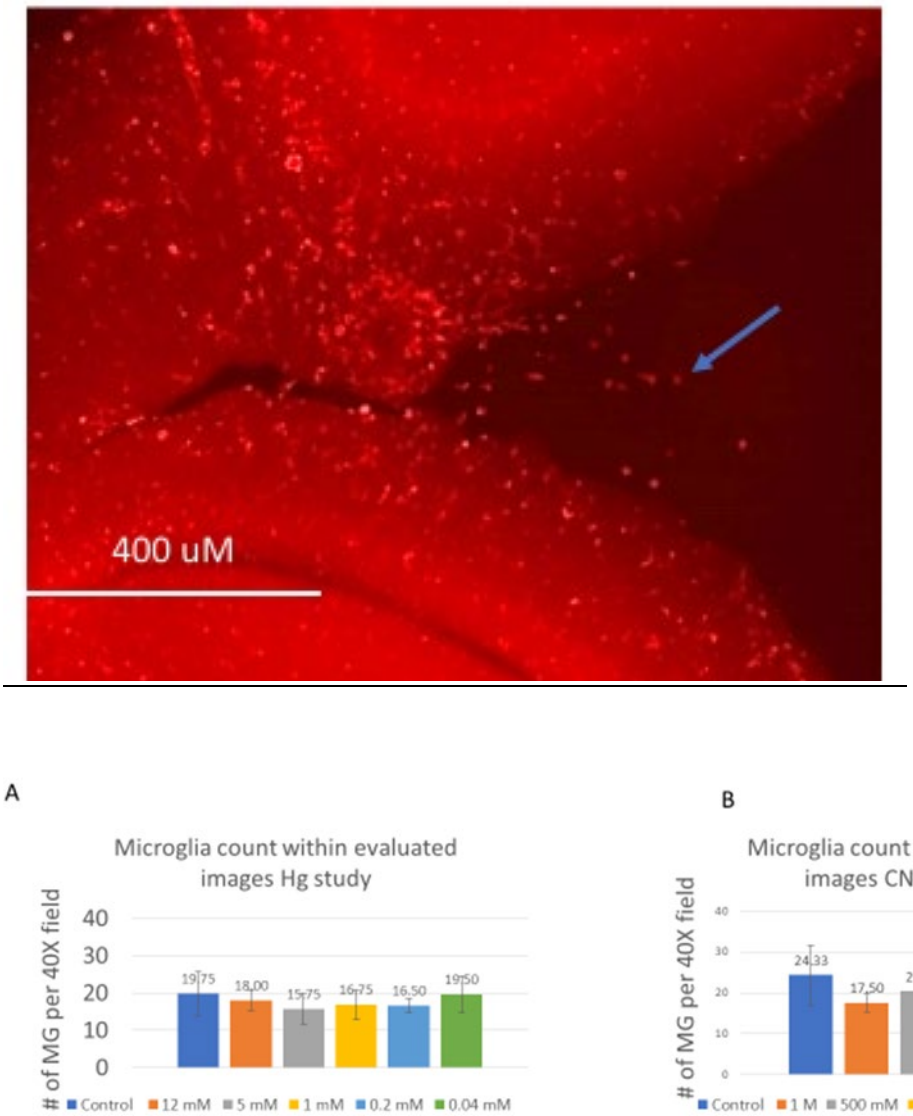

Figure 5: MG motility

After several days of culturing cells begin to dissociate from tissue mass, several of these stained for CD11 indicating that MG starts to evacuate out.

However, analysis in number of microglia within a 40x field indicate that number microglia do not increase as a result of 2 distinct forms of toxic injury (A, B). In vivo studies have demonstrated microglia migration toward sites of cell injury (indicated by an increased number of microglia cells); however, in this tissue model migration is not exhibited likely due to a lack of extracellular fluid pressure that is present in the in-vivo conditions. Albeit fluid flow is present in the cultured hippocampal slice, flow is not strong enough to assist in a motile cells' migration within a 2-hour window.

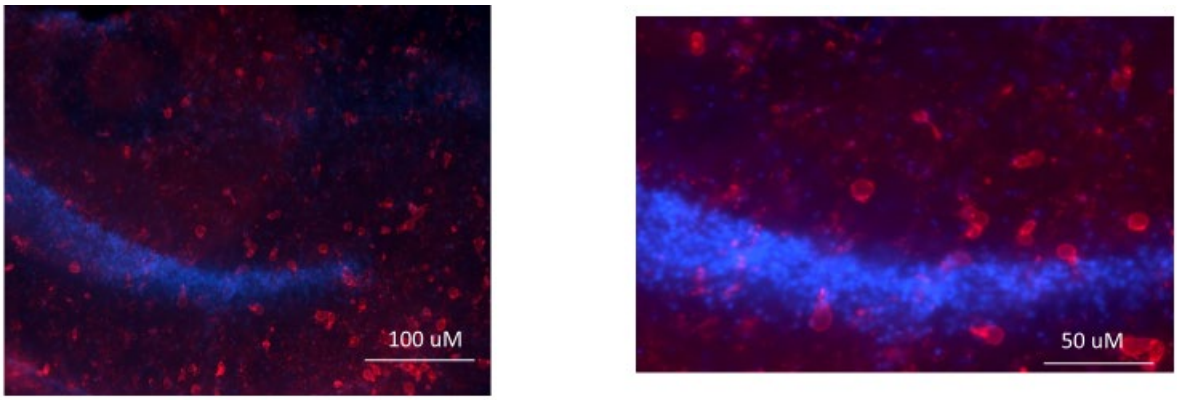

Figure 6: Hippocampal slice immersion studies

After immersion of slice into media (instead of resting on semiporous membrane) MG indiscriminately begin to take on ameboid shape consistent with M1, activated motif. In both treated and untreated slices resulted in same morphology pattern. This indicates that MG shape is sensitive to fluid turbidity and lack thereof attachment points.

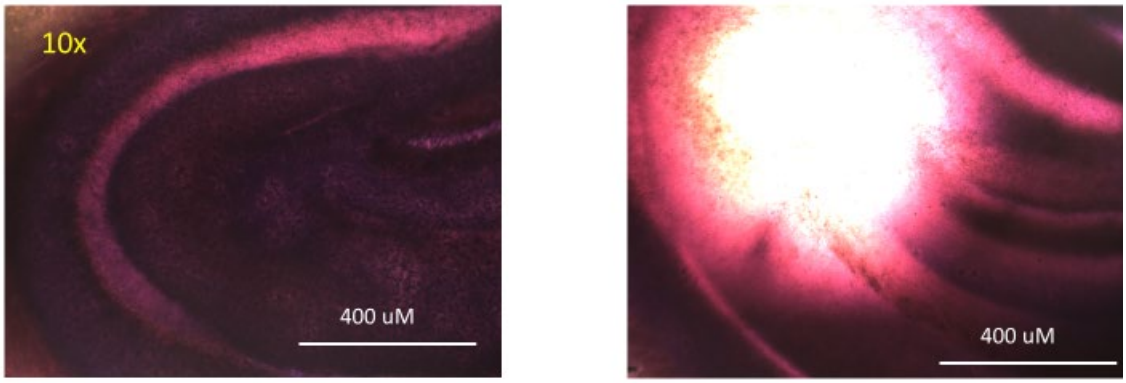

Figure 7: MTT viability testing after toxicant exposure

Control slice (left) contrasted with toxicant-treated slice after MTT exposure (1hr). Control slice converts MTT to formazan throughout the region of placebo (PBS) treatment versus pharmacotoxicant-treated region slice demonstrates a void of formazan formation (white spot) due to cell injury/death.

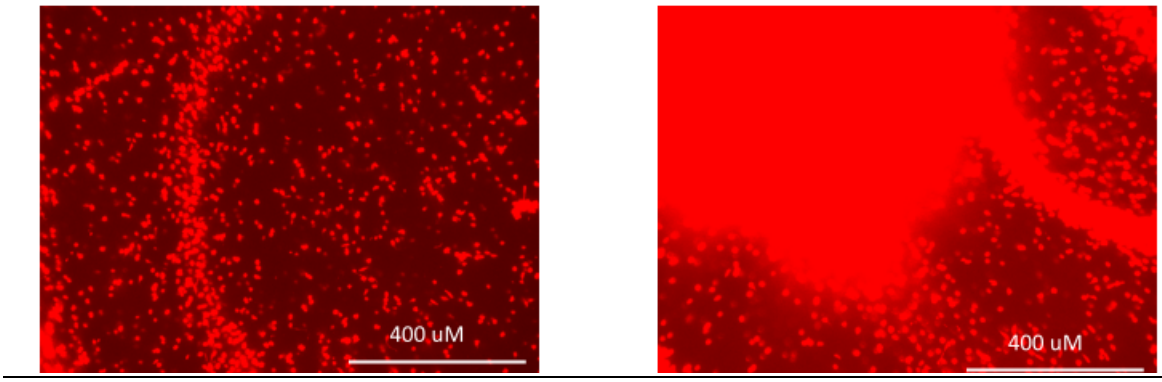

Figure 8: PI viability testing after toxicant exposure

Control slice (left) contrasted with toxicant-treated slice after PI exposure (30 mins). Control slice excludes much PI from cell nuclei throughout the region of placebo (PBS) treatment, versus, toxicant-treated region slice demonstrates a preponderance of red fluorescence (red spot) indicating that PI infiltrates in through damaged cell and nuclear membranes, also PI is reacting with spillage of nucleic contents from dead cells.

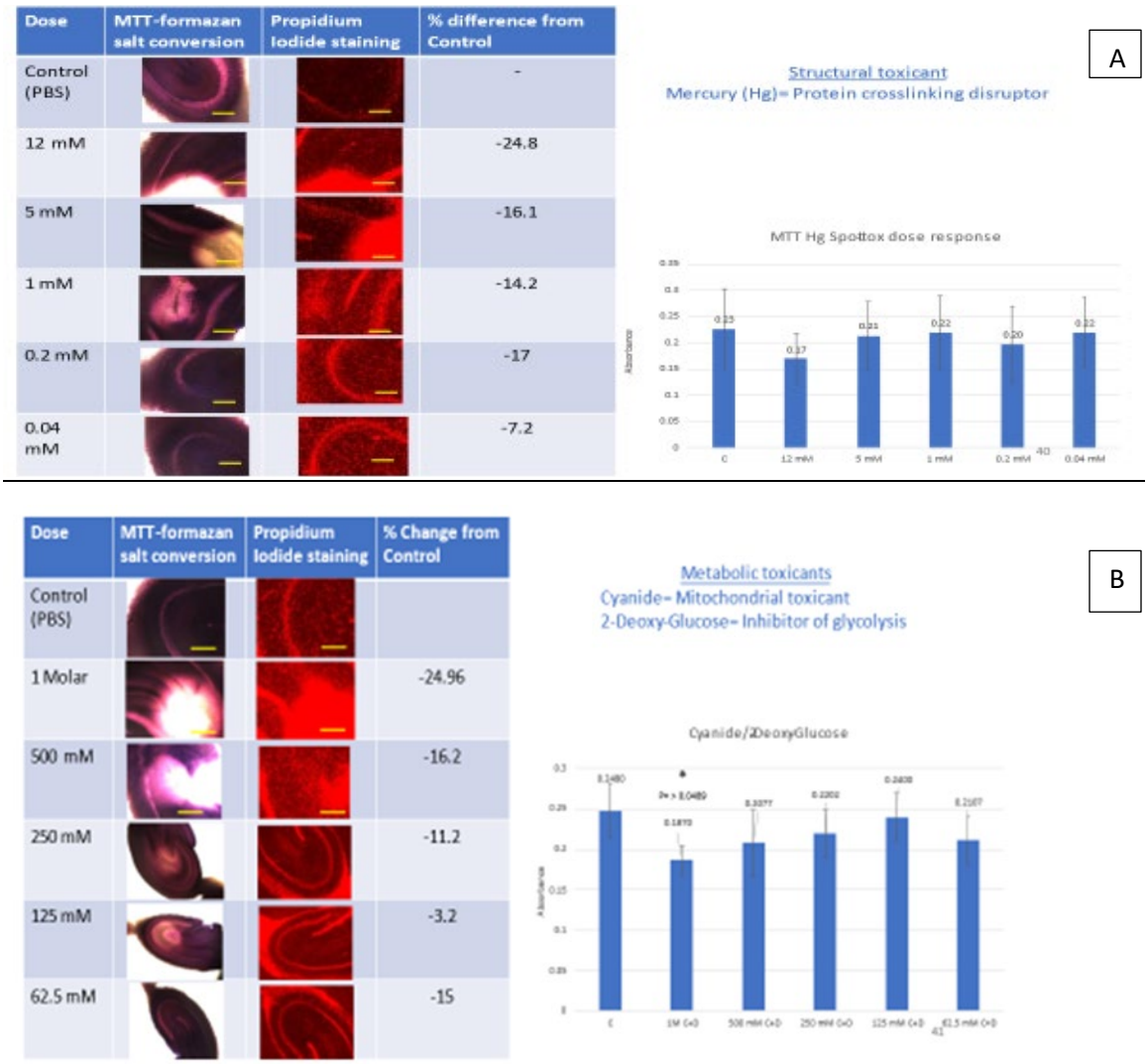

Figure 9: Simultaneous MTT and PI biochemical confirmation of cell death

Dose response to mercury (A). Dose response to Cyanide and 2-Deoxy-Glucose combination (B). After exposure to 2 toxic conditions mercury, or cyanide in combination with2-deoxy-glucose toxicity within a region of a slice was confirmed biochemically. Simultaneous probing with MTT and PI indicate confirm cellular toxicity within the hippocampal slice by scrutinizing the functionality of a mitochondrial reductase enzyme to reduce MTT (to a formazan salt) and the ability of the membrane to exclude a polar molecule (PI). Quantitative data indicate that the majority of the slice is viable, underscoring the regionality of the area of toxic insult and likely a region with increased activated MG. Other areas, such as the dentae gyrus region are viable and thus a good region to evaluate nonactivated MG still on their baseline morphology. Of note, the lower dose levels result in the appearance of white spots prior to red spots, suggesting that probing reductase function (MTT) is a more sensitive determinant of cell stress than an exclusion dye (PI). Yellow Bar: 400uM

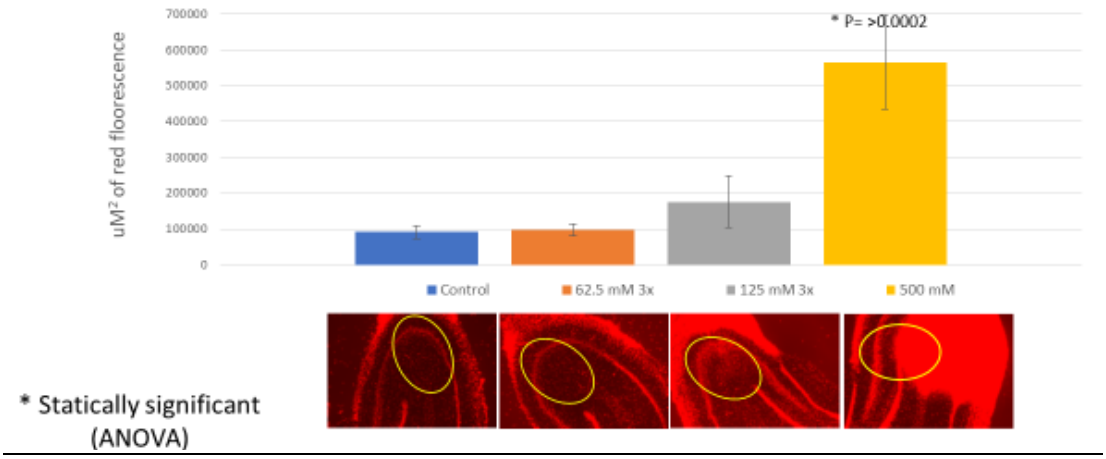

Figure 10: Image analysis of PI spot tox

*Image analysis of area of red fluorescence (PI staining indicates damaged membrane) indicate a threshold effect. This represents a quantitative analysis of PI staining in a dose-response assessment. Whereas in control slices indicate that there is some level of background PI staining, however, upon exposure to very high concentration of a polar toxicant (cyanide and 2-doxy-glucose) the staining area (and thereby PI interacting nucleoside induced fluorescence) is greatly increased. This not only represents damage membranes by PI reaching the nuclear compartment of dead cells, but also the spilled nucleoside contents of dead cells. * Statically significant (ANOVA)*

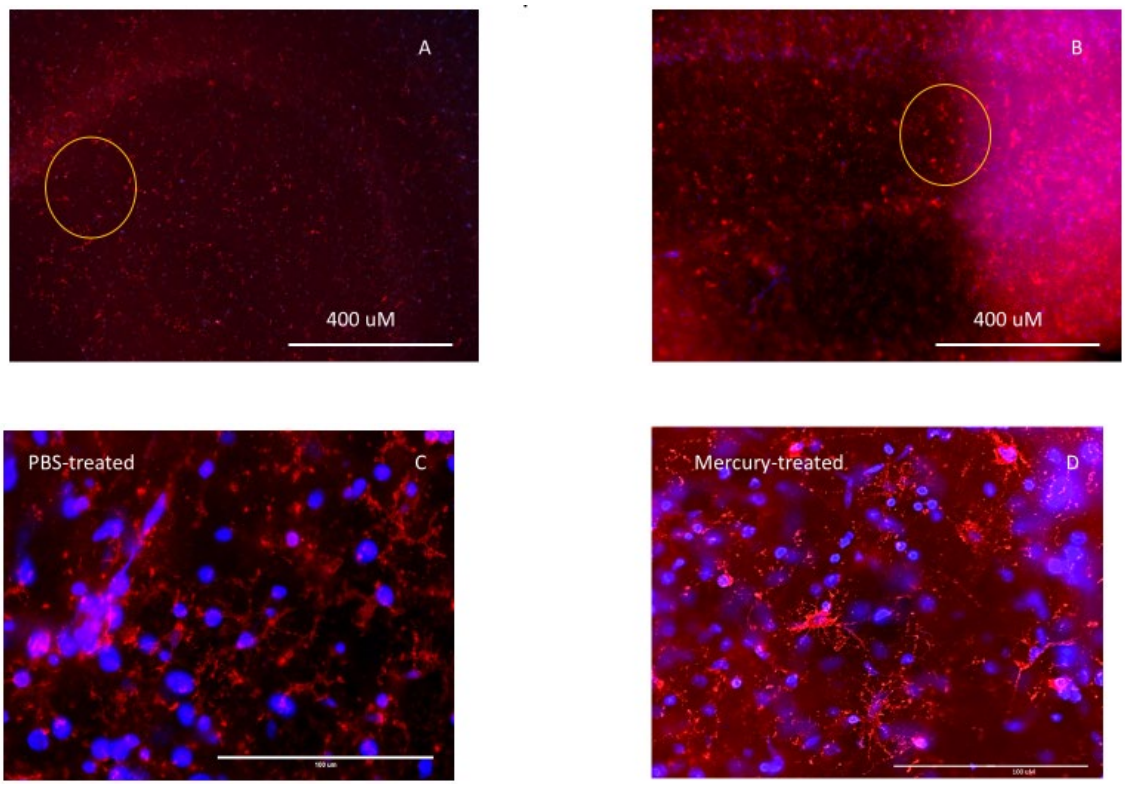

Figure 11: IHC of MG control vs treated

Images 11 A, B (10X) of immunohistochemistry of CD11+ microglia within untreated cultured hippocampal slice and slice treated spot tox. Low magnification of hippocampal slice indicates areas of toxicity by an increase in the appearance of ameboid MG proximal and distal to the area of toxicant exposure, especially at the edge of where background staining is greatest (yellow circle) and there likely is most cells that are stressed, but viable.

Images 11 C, D (40X) High magnification of MG field near at border of spot-tox area results in the appearance of MG mostly in their activated form (b). Compared to the PBS-treated slice (a) and the untreated portions of the slice, activated MG consisted of thickened cell soma and dendrites, in addition to the shortening of MG's dendritic processes.

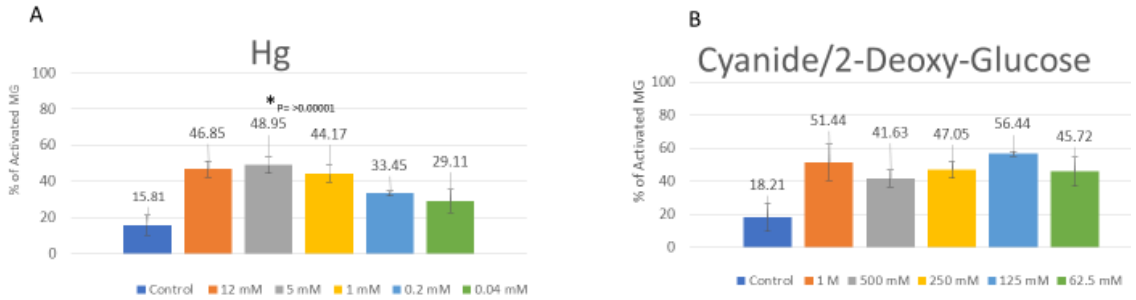

Figure 12: MG activation quantitative data

*Hg and CN-2DG –Quantification of activated MG within a 40x image field. Quantitative data from 40x fields indicate that there is up to a 30-33%+ increase in MG activation at the evaluated areas. The quantitative data for activated MG is similar for mercury and cyanide/2-deoxy-glucose. * Statically significant (ANOVA)*

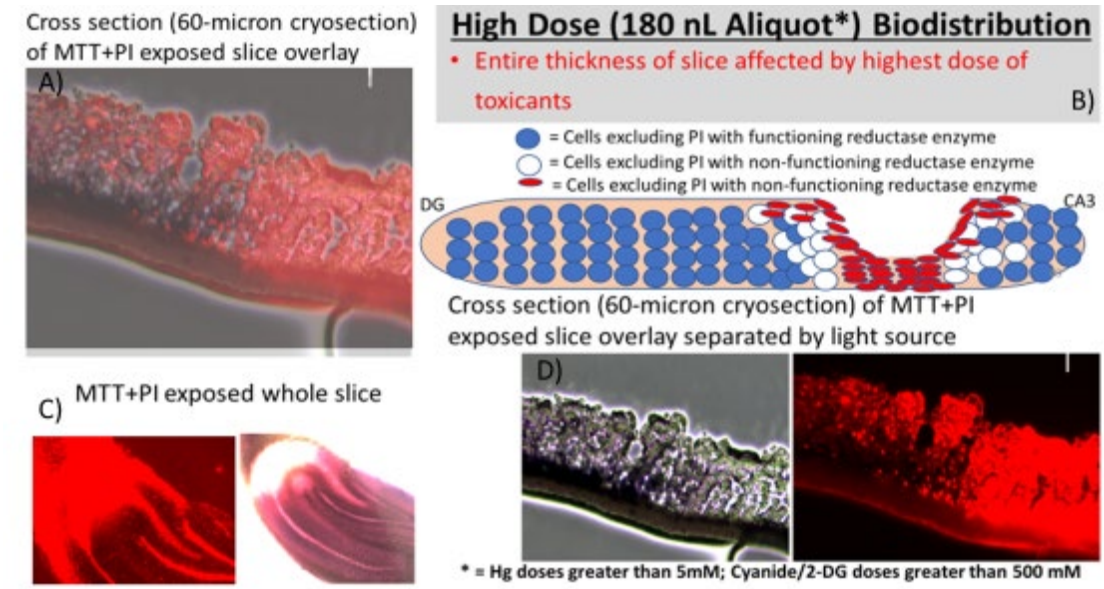

Figure 13: Cross section of slice treated with high toxicant doses

Cross section evaluation on bioavailability of high dose spot tox. The cross section overlay of figure 13c light and fluorescence 20x fields (A, D) of a hippocampus treated with a single high dose spot tox of toxicants slice indicate (B) that the absence of MTT conversion and PI staining permeates the entire thickness of the slice; whereas the untreated area in the far right of the image converts MTT to blue and excludes PI red out of viable cell nuclei.

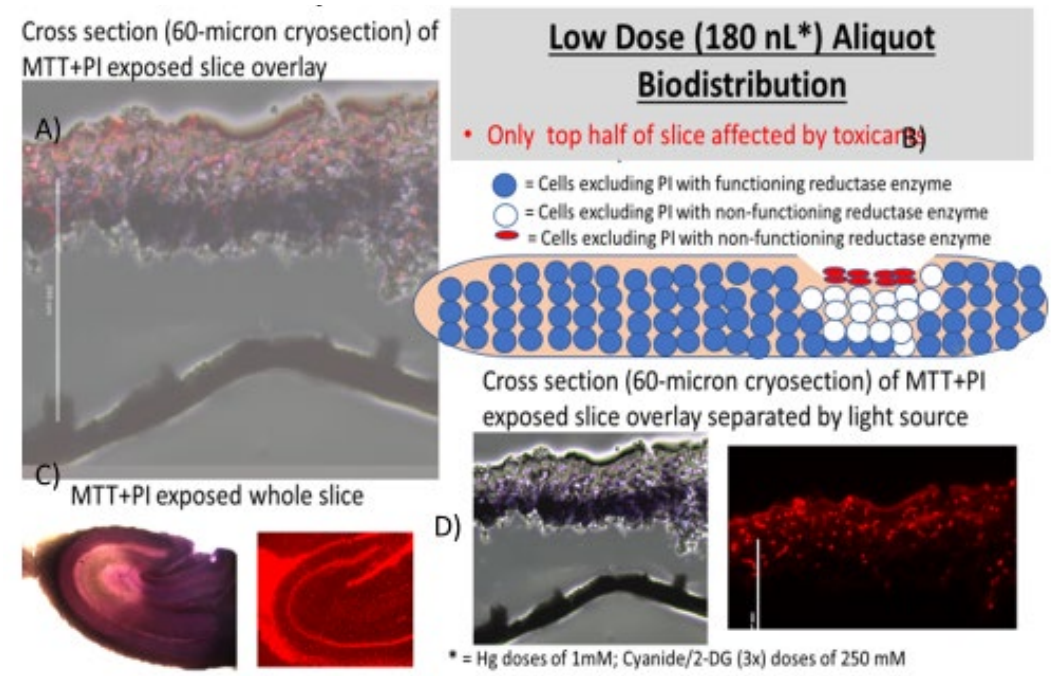

Figure 14: Cross section of slice treated with low toxicant doses

Cross section evaluation on bioavailability of low dose spot tox. The cross section overlay of figure 14c light and fluorescence 20x fields (A, D) of a hippocampus treated with a single low dose spot tox of toxicants slice indicate (B) that the absence of MTT conversion and PI staining does not permeate the entire thickness of the slice.

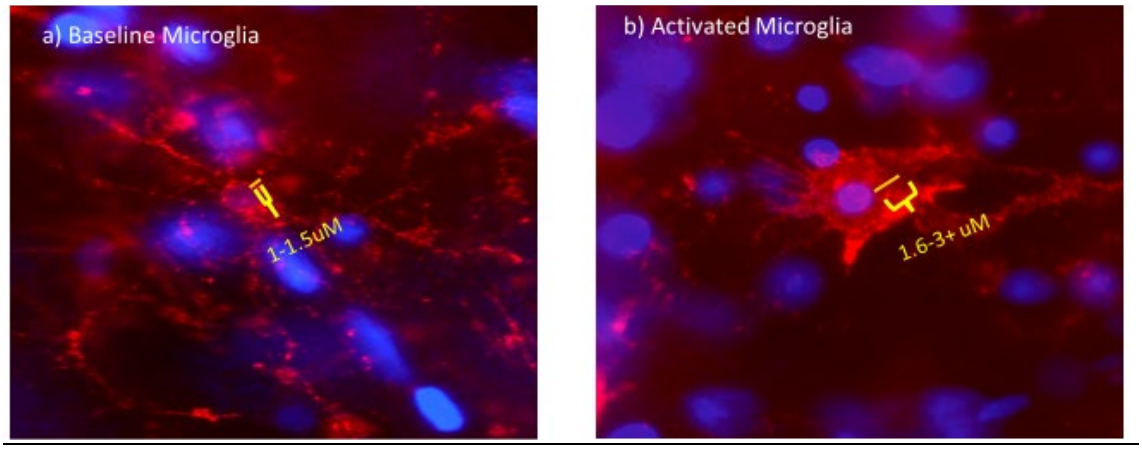

Figure 15: Quantifying MG's structural changes

MG distance of nucleus membrane from cell membrane. a) Baseline MG soma consists of nucleus enveloped by a thin cell membrane that ranges from 1-1.5 microns thick (distance from nucleus membrane and cell membrane). Also, several dendritic processes (up to 9) emanate out of the soma, usually 1 micron in thickness during baseline state and extend out 20-25 microns from soma's center.

b) Activated MG soma consists of nucleus enveloped by a thickened cell membrane that ranges from 2-6 microns thick (distance from nucleus membrane and cell membrane). Also, less dendritic processes emanate out of the soma, remaining dendrites are shorter and thickened to 3+ microns in thickness during MG's activated state and do not extend out very far from soma's center. Also, noteworthy that the most prominent dendrites are still present albeit as stumps, instead of branches.

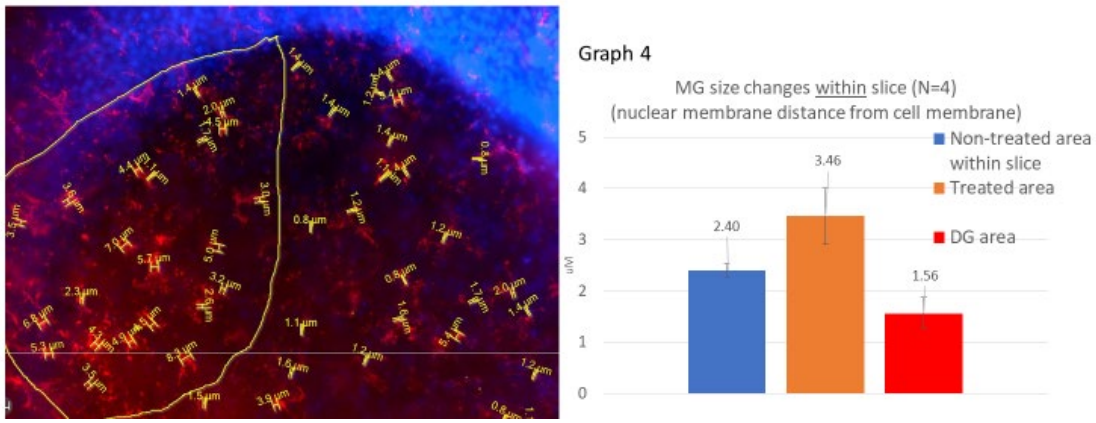

Figure 16: Quantifying MG's structural changes in different hippocampus regions

*MG's morphological variation adjacent (inside circle) and proximal to spot tox (outside circle). In this representative image the region of activated MG within the yellow circle is the area that toxicity was induced within the tissue. Across 4 experiments these cells had a nucleus membrane and cell membrane average distance of 3.46 microns. Outside the circle is considered near the area of toxicity, which consists of a mix of baseline dendritic MG and activated MG yielded a distance of 2.4 microns. Hippocampus slice region distal to toxic injury, the dentae gyrus, had membrane * Statically significant (ANOVA)*

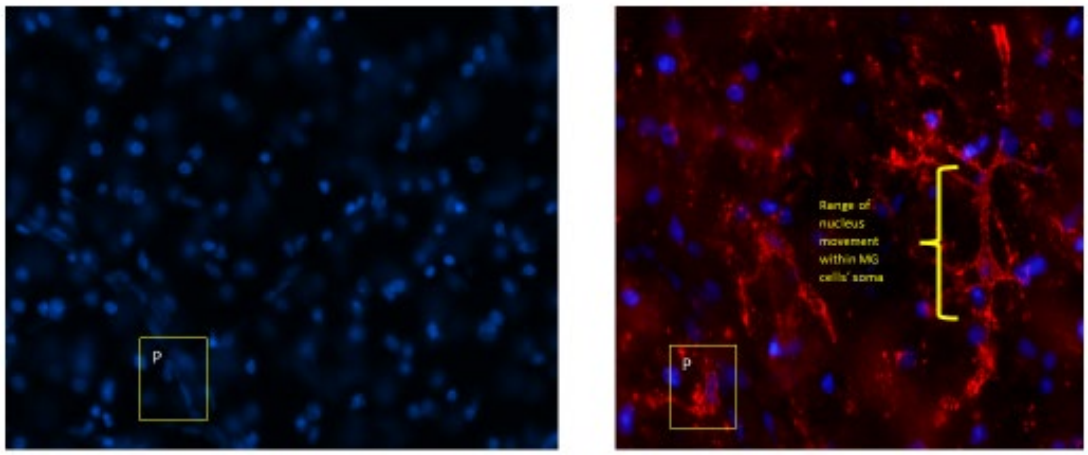

Figure 17: Location of the nucleus within the enlarged cell body; shape of the nucleus

MG's nucleus shape shifting and movement within the MG soma. Nucleus shape and/or placement within the MG can also be differentiated to describe the cell's activity. The microglia in captured within the yellow square (lower left corner) has a pinched nucleus which indicated that it is likely migrating through a narrow opening within the parenchyma. The microglia on the right have an elongated soma which postulates that the nucleus has ample room to move about that intracellular compartment.

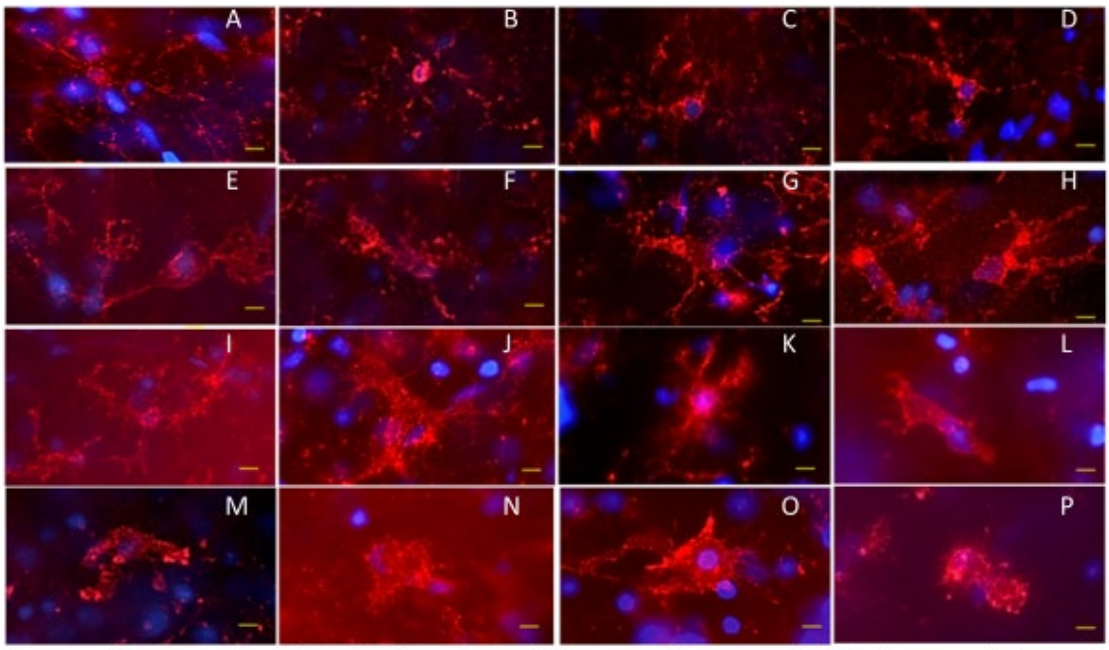

Figure 18: MG's distinct morphologies

In between baseline (M2) and activated (M1) morphologies MG exhibit many distinct structural characteristics and different forms. Microglia's shapes in between baseline dendritic morphology and activated globular morphology (A-P). MG's many forms indicate a progressive accretion of the cell membrane: Distance of cell membrane to nuclear wall increases. Also, there is a thickening and shortening of dendritic processes, which involute into the soma. Bar= 5 microns

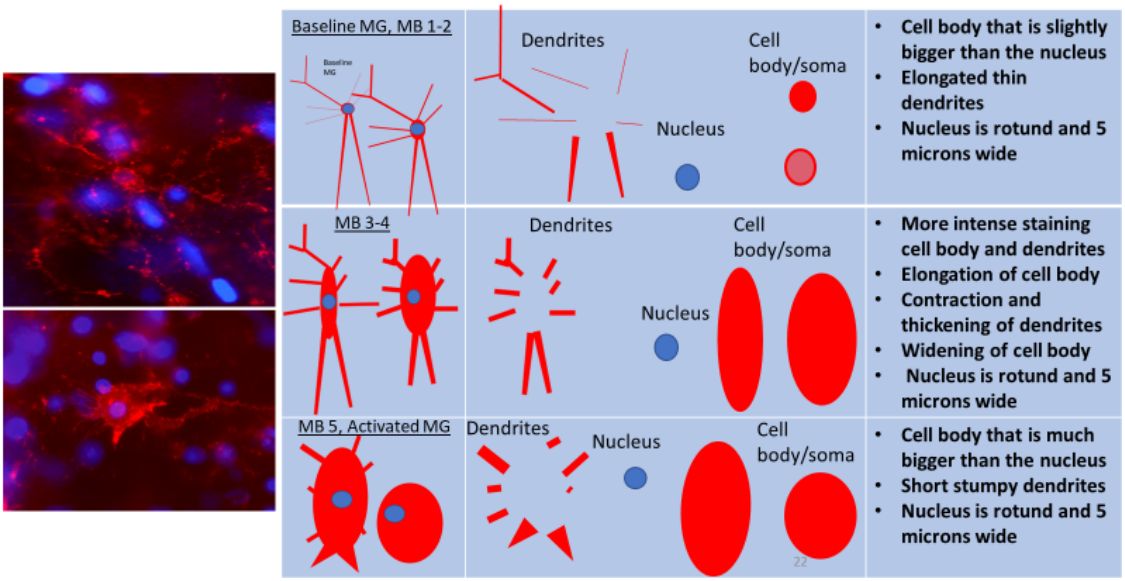

Figure 19: Breaking down MG structural components

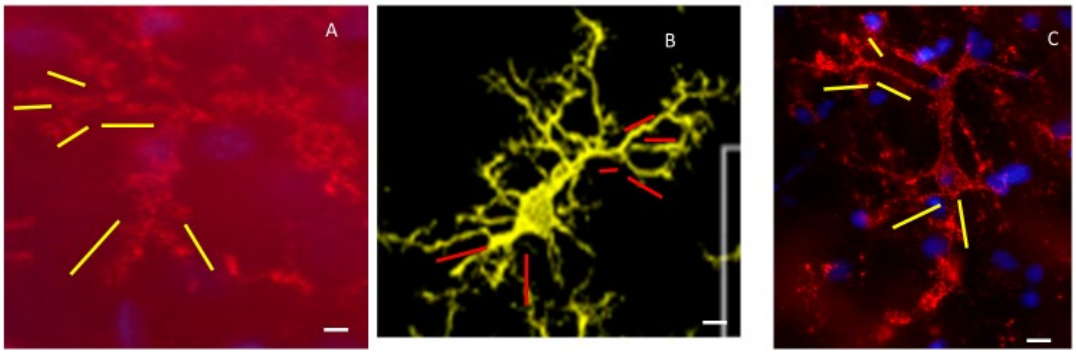

Figure 20: Qualitative assessment of dendrites'

A qualitative assessment of the size and thickness of the 6-10 dendrites that microglia present in dictates that major dendritic processes are part of the structural motif, an off-center lateral dendrite that culminates in a trifurcation, and 2 ends that split off the opposite end that bifurcate. Bar = 5 microns

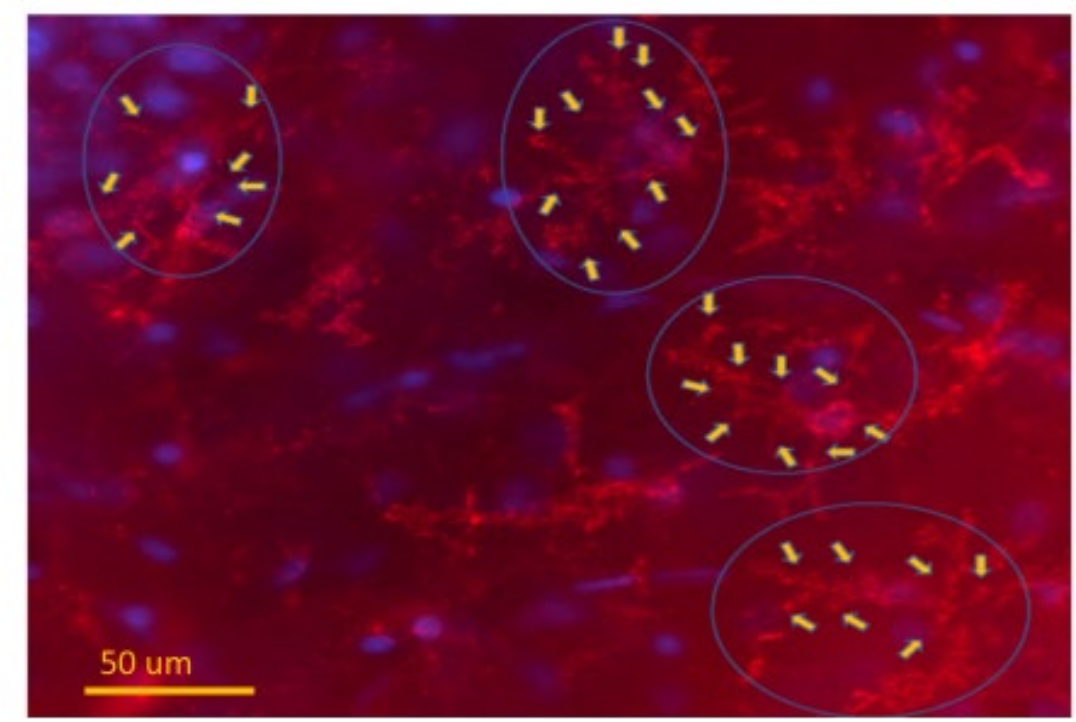

Figure 21: Number of dendrites

Microglia exhibit 6- 10 dendritic branches on a 2-dimensional plane within the cultured hippocampal slice. An analysis of branching out of the soma indicates that MG can exhibit 6-10 dendritic processes (arrows). These processes can bifurcate into other branches at varying lengths.

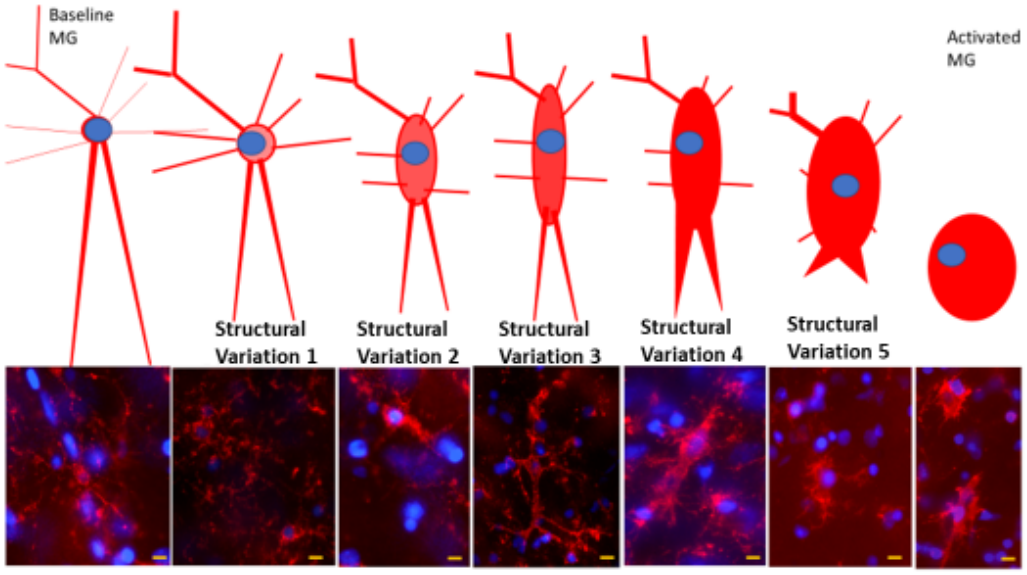

MG Structural Landmark	Baseline MG (BL)	Structural variation 1 (SV1)	Structural variation 2 (SV2)	Structural variation 3 (SV3)	Structural variation 4 (SV4)	Structural variation 5 (SV5)	Activated
Soma/Cell Body	Thin soma (~1 micron evenly wider than nucleus)	Thickening of soma (~1.5+ micron evenly wider than nucleus)	Elongation of (greater than 2 nucleus)	•Further elongation, polarization (greater than 3 nucleus) •Lateral **widening** 1.5+	•Elongated/ thickened (greater than 3 nucleus) •Further **lateral widening 2+**	Globular/ thickened (greater than 3 nucleus) **Wide lateral** 3+	Globular/ thickened
Dendrites	Barely visible (Dendrites ~1 micron wide)	More visible (Dendrites ~1 micron wide) and intense	Visible (Dendrites >1 micron wide) and intense	Visible and shortened	Visible, shortened intensely stained	Stumps	Not present
Length	30-40 microns from opposite dendrites tips	25-35 microns from opposite dendrites tips	20-30 microns from opposite dendrites tips	15-25 microns from opposite dendrites tips	15-25 microns from opposite dendrites tips	15-25 microns from opposite dendrite tips	10-15 microns from opposite reaches of soma

Figure 22: MG's five defined structural variations between baseline and activated state

Spectrum of 5 microglia's structural variations (behavior) in between baseline(M2) and Activated (M1) state. In between the 2 known states of microglia M2 (baseline) and M1 (activated), 5 intermediate morphological variation can be identified based on the shape of the soma, the contraction of the dendrites and the cells' overall size. Morphological variation greater than 3 indicate that microglia ceases being a stellate form and is becoming a dense cellular particle. Bar = 5 microns

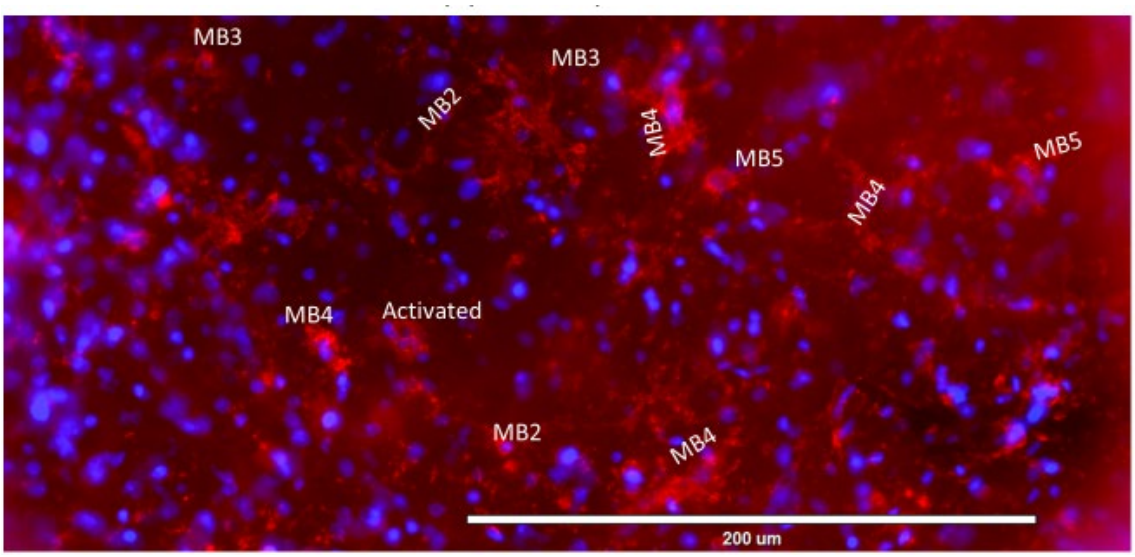

Figure 23: Microglia's structural variations within a 20x field of a toxicant treated cultured hippocampus slice

Contextualizing microglia's morphological variation within a region of toxicity within a cultured hippocampal slice indicate that as you get further from the region of toxic injury microglia appear less activated. Since there is very minimal microglia migration (and thus these changes do not represent newly arrived MG mid metamorphosis) within the slice after 2 hours these morphologies are stable indicators of cell stress. Ergo they could be associated with different levels of cell injury as it relates to the viability of a parenchymal cell or the MG cell itself.

CHAPTER 2: EXAMINATION OF EXTRACELLULAR SPACE WITHIN AN ORGANOTYPIC HIPPOCAMPAL SLICE AND SECTIONED WHOLE HIPPOCAMPUS

2.1. SUMMARY

Volumetric characterization of extracellular micro-spatial distribution within the CNS, is an underinformed component of biology. This condition enables 2 important factors of CNS biology, the flow of CSF fluid to maintain steady states and motile cells' movement. This postulate came about after a thorough evaluation of the surrounding micro-terrains of microglia (MG), a motile cell. Upon evaluation of fixed and unfixed thick undehydrated 60-micron cryosections the non-solid space within fresh and cultured CNS tissue was encountered and appraised to be highly porous. After ascertaining that these spatial observations were not artefactual, an image analysis of fixed cryosections from (fresh whole hippocampus tissue and cultured hippocampal slices) of solid vs empty space yielded that 40-25% of volumetric layout is devoted to empty space, which gives it the porosity appearance. The porosity was presented as narrow openings in-between tissue, and much larger voids adjacent to vasculature which ranged from 10-200 microns in diameter. In addition, qualitative assessments indicate that when tissue contains mostly dead cells with ruptured membranes it collapses thereby diminishing the volume of extracellular space. Fully activated MG (M1) are postulated to obstruct by containing spillages of potentially hazardous intracellular fluids. Using fluorescence, brightfield and phase contrast lighting on cryosectioned tissue cultures that has undergone regionalized toxic injury the loss of space is appraised. These finding are in line with what is understood about CSF flow and a peculiar similarity in the structure of CNS cells of post

blood-brain compartment. Taken together, the results of this study inform and reconcile spatial aspects of CNS tissue micro-volume layout.

2.2. INTRODUCTION

Distribution of extracellular space within the CNS warrants further characterization. The spacing between somatic cells within the CNS enables 2 important factors of CNS biology, CSF fluid flow and motile cells' movement. The assessment of spacing came about after a thorough evaluation of the surrounding micro-terrains of microglia (MG), a motile cell. Upon evaluation of fixed and unfixed thick undehydrated 60-micron cryosections the non-solid space within fresh and cultured CNS tissue was encountered and appraised as highly porous. After ascertaining that these spatial observations were not artefactual, an image analysis of fixed cryosections from (fresh whole hippocampus tissue and cultured hippocampal slices) of solid vs empty space yielded that 40-25% of volumetric layout within the border of a hippocampal section is devoted to spacing which presents as porosity within the tissue mass. The porosity was presented as openings (Figure 30, Figure 31) between tissue's solid components, indicative of empty space within the tissue. In addition, much larger voids adjacent to vasculature which ranged from 10-200 microns in diameter were found. In addition, qualitative assessments indicate that when tissue contains mostly dead cells with ruptured membranes it collapses, thereby diminishing the volume of extracellular space. Using fluorescence, brightfield and phase-contrast lighting on cryosectioned tissue cultures that has undergone regionalized toxic injury the loss of space is appraised. These finding are consistent with conditions that enable CSF flow and a similarity in the structure of CNS

cells of post BBB compartment. Taken together, the results of this study inform and reconcile spatial aspects of CNS tissue micro-volume layout.

Whilst considering and surveying the nature of CD11+ MG cell responses to injury, a factor in cell injury was unintentionally elucidated, microscopic cytospacing and the potential mechanism of its perturbation. Literature investigation of cell spacing, and interstitial space (defined as intercellular space) yielded very little historical and literature reference, indicating that this is an underappreciated component of the microenvironment [42]. Upon surveying the cell viability in this model, the empty space in between cells garnered some greater significance. Underscoring importance of not just static cells' placement, but the spacing necessitated to enable motile cells movement and extracellular fluid flow will be attempted through the data generated in this study. This finding was a byproduct of the initial investigation of CD11+ MG and through a series of raw observations from novel light microscopy and fluorescence image techniques reconciling the solid and non-solid volumetric nature of the CNS parenchyma, which necessitates the effective and efficient flow of fluid to properly maintain its homeostasis. There are many postulates as the significance of the movement of the interstitial fluid/CSF in and throughout the brain parenchyma (Hornkjøl etal., 2022) but visual descriptions as to what the conduits that enables fluid flow at the microscopic level have not been characterized in a reproducible manner.

Taken together, the results of this study attempts to inform the cytoarchitectural details of space, however, space not occupied by cells or scaffolding extracellular matrix. How wide is it? The greater the space the faster the movement of free-flowing fluid. This is a framework that enables the physiochemical properties of unidirectional cerebrospinal

fluid flow as it pertains to space allotted to move. Apparently upon seeking ways to identify a cell by its appearance, its motility function came into focus. CD11 staining empirically indicated that cells that move do not overlap. Likely because there is not space to get around the obstruction ahead within a limited volume of space to move about. This capacity to move about within complex biological systems enables a significant breadth of dendritic cells role, and overall, the spatial conditions needed for neurons to maintain ion concentration cycles, nutrient maintenance and the initial immune system's response activity.

Finally, the accrual of information from MG's structural variations and the structural details of cytospacing will be reconciled by combining these two distinct sets of data (chapter 3), which not only could explain some of the unanticipated results of this study, but also most importantly can inform important burgeoning fields of immune biology such as glymphatics [41]. An analogous description of the significance of this empty intercellular space would be cities; whereas the historically much detailed description has been given to the buildings and houses on a certain city block, and or the cars that move between them, the roads that enable the space between city blocks and the movement of cars has not been described in any referenceable manner. Therefore, the interrelationship of CNS cells, static and motile, and the spatial considerations can offer some resolution to the complex process of inflammation within the brain's post BBB parenchyma.

2.3. METHODS

2.3.1. Organotypic hippocampal slices

The best visualization of MG(CD11+ cells) is in the neonate rat 10-21 day old, due to the relative translucency of the tissue matrix. Older animals have more opaque tissue and therefore CD11+ cells cannot be visualized in fine detail beyond 10x magnification. Animals were sacrificed via decapitation and brain was immediately excised from cranium, the whole hippocampi were carefully dissected out and placed in ice cold calcium and magnesium free Hanks balanced salt solution. Hippocampi were then placed on top of a 1.5% agar block sliced at a thickness of 200 microns using a Syskiyou Tissue Slicer. Slices are then manually separated out individually. One rat (2 hippocampus) can yield 26-40 hippocampal slices.

2.3.2. Tissue incubation

Using a trimmed transfer pipette slices were removed from ice cold media into a 6-well plate with preincubated culture media as described in previous papers [18]; [15]); this media consists of 50% MEM, 25% Hanks Balanced Salt Solution (with calcium and magnesium) and 25% Horse serum. Excess calcium free and magnesium free media on the top of the membrane should be removed. Before any treatment with pharmacotoxicants, the tissue was equilibrated in a cell culture incubator for 1 hour.

2.3.3.Tissue treatment

Treatment with Mercury and cyanide/2-deoxy-glucose consisted of a “spot tox” within the CA3 region of the hippocampal slice; this was delivered as an aliquot of 180 nanoliters (using a micropipette calibrated to go down to 100 nanoliters); control slices were exposed to vehicle solvent used for both pharmacotoxicants (PBS). Pushing the 180

nL droplet out of the micropipette tip and placing on top of the CA3 region will allow the drop to dollop on top of that tissue region, eventually this dollop will be absorbed into the tissue. The Dentae Gyrus region was not treated in order to have a healthy tissue control within the slice. To enable an effective contrast of what MG/CD11+ cells look like within untreated and thus healthier regions versus what they look like in regions in and around the spot tox's unhealthy tissue. This enables not just contrast but also a gradation of changes in the space in between healthy and injured cells. MG cells and injury regions were evaluated 2 hrs after spot tox.

2.3.4. Biochemical Confirmation of Toxicity

To ascertain that toxicity was elicited within the spot tox MTT and PI were used as viability indicators. MTT was added immediately after the 2-hour incubation period was finished [23]. Propidium Iodide was added 30 minutes later [24]. After a 1 hour of incubation the entire slice turns dark blue; longer incubation time will lead to drying out and crystallization of the formazan salt. Within the slice some of the cells do take up PI however the slice is mostly dark and thereby excluding PI. To confirm, viability testing was also done with FDA, CCK-8 and rhodamine 125; however, the most clear and affirmative results based on color contrast was with MTT and PI. In addition, slices fully immersed in media with several concentrations of pharmacotoxicants was done to understand better elucidate the tissue slice's holistic toxic dose response.

2.3.5. Microglia Visualization

After isolation and/or treatments hippocampal slices were places in 4% paraformaldehyde for 15 minutes. Then slices were blocked with 10% FBS for 30 minutes. Primary Anti-CD11 Antibody (mouse anti-rat mAb Cat#: MA-9u29) was added to slice with 1.5% FBS

and 1.5% goat protein for 1 hr under slight shaking. Secondary Ab (goat anti-mouse Cat#:Fb106) was added to slices with 1.5% FBS and 1.5% goat serum for 30-60 minutes. Slices were visualized either right on the semiporous membrane or mounted into a glass slide and mounting media (Cat #-) and gently capped with cover slip. Slices were visualized with EVOS microscope (cat#) after mounting media dried. Images were surveyed for CD11 cells (in between the central portion of slice and the CA3 or DG row of cells) and their morphological categorization; baseline shaped (stellate with fine processes) or activated (enlarged cell body with thickened processes). Sequentially activated MGof 3+ are rarely observed in baseline untreated slices and therefore when this was observed they were indicative of site of pharmacotoxicant-related injury.

2.3.6. Hippocampal tissue sectioning

After isolation and/or treatments hippocampal slices were places in 4% paraformaldehyde for 15 minutes; full hippocampus fresh out of the animal was fixed for at least 5 hours. Afterwards slices or whole hippocampi were placed overnight in 30% sucrose until tissue sank to the bottom of vessel. After sucrose treatment tissue samples (slices or whole hippocampus) were equilibrated for 30 minutes in OCT media prior to freezing; samples were placed in freezer until frozen solid. After freezing, 60 uM sections were taken to ensure that whole intact MG were captured in imaging. No ethanol dehydration steps were applied in order to maintain tissue volumes and spaces intact. To evaluate tissue injury slices were sectioned vertically and horizontally to visualize the 200-micron thickness after MTT and PI assessment.

2.3.7. SEM

SEM processing of slice consisted of 3 hr treatment with glutaraldehyde , followed by dehydration steps using 30, 60, 90 and 100% acetone. Then samples were placed on a lyophilizer to eliminate the remaining acetone with vapor pressure. Slices were staged on SEM mount with adhesive.

2.3.8. Thick cryosectioning of CNS tissue

After isolation and/or treatments hippocampal slices were places in 4% paraformaldehyde for 15 minutes; full hippocampus fresh out of the animal was fixed for at least 5 hours. Afterwards slices or whole hippocampi were placed overnight in 30% sucrose until tissue sank to the bottom of vessel. After sucrose treatment tissue samples (slices or whole hippocampus) were equilibrated for 30 minutes in OCT media prior to freezing; samples were placed in freezer until frozen solid. After freezing, 60 uM sections were taken to ensure that whole intact MG were captured in imaging. No ethanol dehydration steps were applied in order to maintain tissue volumes and spaces intact. To evaluate tissue injury slices were sectioned vertically and horizontally to visualize the 200-micron thickness after MTT and PI assessment.

2.3.9. Fluorescence flooding/Light microscopy

This technique consisted of evaluating 60-micron thick cryosection from either fresh whole hippocampus (right after excision) or from a cultured hippocampal slice, on slide without a coverslip. Upon finding optimal resolution under, areas that reflected light source, areas that reflected light and dark areas in between were appraised.

2.4. RESULTS

2.4.1. Cross sectional evaluation of 200uM thick tissue slice injury

An evaluation of the cross sections of the slice demonstrated that cyanide/2-DG -induced toxicity shows that slice thickness can impact the visualization of a spot. At lower concentrations the depth of the biochemically verified toxicity did not reach the bottom portion of the slice. This is consistent with the results of earlier tox-spot studies with thicker slices (300 uM) where 1000 and 500 mM concentrations of cyanide/2-DG did not result in spots, however a thinner slice (200 uM) did result in the appearance of a spot at the same concentration. In places where toxicity was observed through the entire thickness of the slice there were regions that were absent MTT to formazan conversion (which yields a blue dye within tissue) but also maintained PI exclusion indicating that MTT is a more sensitive determinant of cell impairment than PI, similar to what was mentioned in the previous sections. Also, besides the pigment changes related to MTT and PI it was noted under light microscopy that the integrity of the tissue matrix was perturbed as the injured tissue appeared collapsed and more fragmented (Figure 13) than healthy tissue. A notable ancillary observation in these 60 uM tissue sections of hippocampal tissue under light microscopy was the remarkable porosity of the tissue (Figure 24). This porosity is initially manifested primarily by the prevalence of circular openings that vary in size from 20 microns to as small as 5 microns (Figure 30). Taken together, under the small volume administered, there was a dose response effect on the depth of injury and as such, toxicant volume and tissue thickness are important considerations to propagate cell death that traverses several cell layers within the

organotypic tissue sample that elicits the visualization of a spot of biochemically verified toxicity using cell viability probes MTT and PI.

2.4.2. Characterization Cytospacing observed during MTT cross-section imaging

The initial purpose of the cryosectioning was performed to yield tissue thickness thinner than 200 microns to better visualize changes in MG (with IHC staining) within hippocampal slices under higher magnification. Sections of 60 microns in thickness were selected to ensure that whole intact MG could be captured in the section (as MG can be 50-40 microns in size in its baseline state). Adequate baseline MG IHC visualization was not attained under these conditions as many of MG's fine structured processes are lost during the harsh section slicing procedure. Therefore, MG was not optimally visualized and after several attempts very few quality images of intact MG were obtained; evaluating non-sectioned fixed whole cultured hippocampus tissue yielded much better MG imagery.

Another objective of cryosectioning to 60-micron sections was done to ascertain the hypothesis of slice thickness affecting the appearance of a tox-spot insofar as higher concentrations of pharmacotoxicants will result in an injury of a greater area and of tissue and deeper areas of tissue (as demonstrated in-vivo with ATP by Jeong et al [33]) which manifests as a MTT-white (indicating the absence of MTT conversion to formazan and therefore mitochondrial disfunction), PI-red spot (indicating membrane damage by PI permeability). Indeed, lower concentrations of pharmacotoxicants did indicate that they do not reach the bottom of the slice but do affect the top of the slice (where 180 nL drop was placed). Cross sections of the slice demonstrated that the 180 nL dose of

pharmacotoxicants do not elicit a white spot-tox that reaches the bottom of the slice at lower doses; the red fluorescence spot-tox also does not reach these lower regions of the slice and both differences in pigment generally overlayed each other. Of note, that the white, which indicates absence of blue pigment and thereby cell injury/death, in several instances reached the bottom of the slice, but the red did not; corroborating a differential in cell toxicity sensitivity between both agents and indicated a region where the cells were metabolically stressed, not converting MTT to formazan but still impervious to PI. Albeit the original objective was to evaluate cultured tissue that had stained blue (MTT) or red (PI) or the absence of, eventually the observations expanded to the nature of the solid layout of the tissue, but more so, the space in between. The evaluation of these thick 60-micron sections (with and without blue formazan pigment) of hippocampus tissue underscored the dimensionality of this sample by the appearance of shadows that thereby indicated depth and therefore spacings within the tissue. These spacings were constant and appeared seemingly in balance with the solid components. Taken together, this took on the form of a very porous micro-landscape (Figure 26). This porosity was not only present throughout the entire hippocampus; the spacings that constituted it varied in size, from 5 microns to 200 microns. Albeit many appeared circular or oval, several of them were also elongated, as if they followed the form of a blood vessel. Irrespective of shape, these 60-micorn sections demonstrated a heterogeneity in solid and empty components within the borders of the tissue.

Porosity profile is the same in cultured tissue slices or sections cut from tissue that was immediately fixed after excision.

A comparison of cultured CNS tissue from cultured slice and tissue that is from freshly excised hippocampus tissue indicates that the porosity profile is maintained ex-vivo (Figure 26). This structural preservation lends credence to the electrophysiology investigations that demonstrated similar activity in-situ vs ex vivo. Therefore, based on this comparison the porosity profile in cultured hippocampal slices is contextual to the structure of in vivo settings.

2.4.3. Comparison of spacing of cultured and fresh tissue and fixed vs non-fixed tissue

Whether cultured or fresh tissue and/or fixed and unfixed hippocampus that has been flash frozen presents with same porosity profile as fixed tissue (Figure 27, Figure 28). Albeit most of the tissue did present as non-porous, black small linear spacing indicate that if tissue is not fixed the spacings within will collapse. This indicates that the spacings that demarcate porosity are not artefactually related to fixation artefacts.

2.5. Quantifying space within the 60-micron sections

Upon examination of brightfield (At 10x and greater magnifications), of sectioned CNS tissue resembles a layout with abundant quantifiable porosity (Figure 26, Figure 29). Quantifying the overall space, it yields that 75% of space is taken up by cells/matrix and remaining 25% is constitutes up by empty spacing. Also worth considering, that the spacing is arranged in a manner that is indicative of fluid flow; underscored by deep circular openings that resemble tunnels. Image analysis was conducted with a Halo setting that captured the colors consistent with empty space, black. Furthermore, during microscopic evaluations, focus could not be maintained under the same stage distance,

thus upon movement of stage different areas came into focus thereby indicating that these surfaces were not in the same plane of vision and indicated surface voluptuousness.

Closer examination of porosities under the condition of fixation and processing (4% paraformaldehyde, embedded in OCT and 60microns section) spacings that range from 10-200 microns wide (Figure 30). The spacings that constituted the porosity profile were often close to circular, regardless of size, as such measurement consisted of measuring the diameter of these spacings as they appeared in the image of the 60-micron thick cryosection. Other openings where non-circular and as such the widest point of separation was measured. Irrespective of size opening always had rounded edges and seldom where they associated with rectilinear outlining when the spacing appeared to be parallel to a blood vessel.

Tissue porosity was evaluated under dapi staining in Figure 31; in a region of a sectioned portion of CNS tissue demonstrated that nuclei and spacing are evenly distributed. Reconciliation between nuclei placement and openings indicate that multiple nuclei surround opening thereby suggesting that there is a multicellular cooperation that encompasses these openings (Figure 31)

Evaluations of 60-micron images with fluorescent flooding and brightfield demarcates that a cross section of tissue consists of solid components (cells, extracellular matrix, etc) and empty space. The solid components of tissue were consistently observed as the presence of red (under red fluorescence), or beige (under brightfield) as light is being reflected from the light source. Conversely, the tissue does not all light up homogenously as there are portions of black indicating that there is spacing in between the solid components of the tissue matrix. In particular, during fluorescence imaging that flooded

all the solid components of tissue demonstrated the spacing, which simply appears as black, with greater resolution (Figure 32). Phase contrast imaging overlayed with fluorescence imaging corroborated the spacing; furthermore, this contrast indicated that only the topmost portion of the section only reflected the red fluorescence, whereas the fluorescent lighting did not visualize deeper solid components that were visualized by phase contrast lighting (Figure 33 with both light sources overlayed). This indicates fluorescence is more sensitive to the loss of space as it cannot reflect off deeper solid components of the section. Evaluating the hippocampus spot-tox injury model under fluorescence indicated that there is a perceptible loss of space when this tissue is injured. As demonstrated in Figure 11, an injured portion of the slice results in crater of red fluorescence that is indicative of non-specific staining; however, the surrounding area where MG are clearly visualized have abundant areas of black (spacing) in between. The preponderance of non-specific staining within the injured area indicated that the solid components of that region of the slice were in close proximity to each other and thus there was less spacing in between. If a treated hippocampal slice is surveyed and an image analysis is done for the amount of black areas with a treated and a non-treated area there is difference noted in the total amount of spacing. Also, since in these images the black is clustered each individual black area can be compared between treated and non-treated areas of the same size, thus the treated area had smaller black regions that the non-treated region. Thereby indicating, cell collapse and thus tissue volume redistribution and perturbation of normal layout.

2.5.1. MG within spacings

Taking into account that the cells that are most likely to be found within the walls (or borders) of extracellular passages are motile cells such as MG, a survey of cells shaped like the circles akin to the openings was performed. MG could not be visualized in the 60-micron sectioned samples, which best displayed the openings. Reconciling the intricate shapes of MG and the openings in 60-micorn sections was fraught with visualization challenges, as the harsh cryosection procedure yields poor image quality of MG in under a microscope. The most optimal evaluation of MG came from observing it from whole 200-micron slice of cultured tissue that has been fixed right after culture. However, the 200-micron thickness of cultured slice was too thick to observe the openings/spacings as the openings are likely getting occluded by the tissue collapsing onto itself and thereby blocking the openings, but MG visualization was optimal. The porosity/spacings were best visualized when the slice was cryosectioned to 60 microns; however, MG was damaged and not captured in the same quality as it is observed when it is within a 200-micron slice of non-cryosectioned tissue. Nevertheless, there were some hints of MG placement withing the images acquired from unsectioned tissue based on the capture of MG's shapes and the non-specific background staining or lack thereof staining (Figure 35).

An attempt was made to get MG IHC staining and placement within voids under phase-contrast. Albeit some MG were captured, and a plethora of openings (areas of black) were within image the resolution was very poor and thus difficult to draw conclusions from. Thus, when doing a survey in whole intact cultured slices that were stained for IHC CD11+ cells the shapes of these cells were evaluated. In this image (Figure 35)

there are what appears 4 MG in a circular shape, albeit there seems to be cells in the inside of the circle the lack of staining indicates that they are out of plane and therefore deep within.

In an experiment where a 60-micron section was stained with PE conjugate Ab and dapi a rather remarkable staining profile was captured (Figure 32). In this attempt, slices were slightly airdried (5-10 minutes) without a coverslip, what ensued was the visualization of a red and blue wash of nonspecific florescent staining. This nonspecific staining was indicative of a fluorescent flooding that seemed to capture all solid components of the slice. Upon nonspecific flood staining the porosity (spacing between solid components) was observed in greater resolution. The space in between within this fluorescence was vast and open; furthermore, the central portion of the image has the biggest openings and the openings got smaller as they got further from the larger ones. Brightfield microscopy corroborated the findings during fluorescent flooding, albeit there were more detailed images of a deeper portion of the section, which was not present during fluorescent capture. Dapi staining indicated that these openings consisted of several cells and thus is a multicellular construct that enables these openings to hold shape (Figure 31). Nonetheless, within the confines of microscopic layouts, this is indication of an appreciable volumetric distribution of space and the solid components placement therein.

2.5.2. Observation of macro spacings (greater than 50-microns wide) within 60-micron thick hippocampus tissue section

Whereas until now the observational focus has been on the tunnels or small openings ion between cells 5 to 25 microns wide, there are also other types of spacings that were observed (Figure 36, Figure 38), these were much greater in size and less common than

the smaller openings. In several instances during surveying of thick cryosections there was larger spacings observed, these spaces were up to 200-300 microns wide, however they were thinner when measured perpendicularly, around 120 microns. In several of the observations these larger spacings straddled what appear to be micro vasculatures (red arrow in Figure 36). In addition, in several instances when the 200-300 micros size openings were evaluated in there was a large opening that culminated at the end (Figure 38), which indicates that it is an outlet opening from this chamber.

2.5.3. Scanning electron microscope images revealed in greater detail the extent of this microspacing and porosity

At 2,500x magnification we can see a cellular landscape that entails several aligned cells and the presence of a red blood cell (Figure 37). The flawless shape of the RBC suggests that the structural aspects of this space are also well maintained and reflects the structures accurately. Furthermore, the porosity is predicated upon the specific placements of circular channels or tunnels of varying diameters that are regularly spaced.

2.6. DISCUSSION

2.6.1. Characterization of terrain

During the investigation into the morphological variation of microglia (MG) cells the spacing needed for them to comply with motility was encountered. Namely, whereas the investigation anticipated that MG motility would be perceptible in the hippocampal model, it turns out it isn't quantifiable by cell counting, as injured regions exhibited the same number of cells as non-injured regions and regions treated with placebo controls (data not shown, but on average there were 15-25 MG in a given 40x image field). As mentioned previously, there is likely a contribution to fluid pressure that assists not just

in the motility of MG, but also the speed of the extracellular fluid flow. This finding is consistent with studies that evaluated the dynamics of in-vivo MG motility vs ex-situ assessments on brain slices [19]. Based on extensive characterizations of the properties cerebrospinal fluid it can be postulated that this fluid is an important component of the extracellular constituents of the brain interstitium ([43]; [44] [37]). Therefore, it is noteworthy to point out that one of the limitations of the hippocampal slice if the absence of this fluid pressure gradient on MG motility. In any respect, albeit MG was not perceived to undergo much motility, the spacing for such motility to occur was characterized in the form of a high porosity within thick 60-micron cryosections of cultured and non-cultured hippocampus tissue (non-cultured tissue removed right after animal sacrifice); there is also evidence of this in non-frozen tissue. According to the first images in which this porosity was observed (Figure 26,Figure 30), typically, the rim of these openings that demarcate the porosity is an opaque structure that is likely a rigid structural component of indwelling CNS cells. Due to the depth of the tissue (60 microns) and the angle of the microscope's light source the inside of many these circular openings appear darker, insofar suggesting a shadow effect and thus that the opening is continuous beyond superficial opening; in several other instances the opening is white and thus indicative of opening, and thus undisturbed passage of light, all the way through the other side of the 60 micron section and thus a "tunnelation" effect within the microspacing.

2.6.2. Weight of evidence of veracity of terrain and porosity profile in the observed CNS tissue sample

Microglia and extracellular fluid do share an important characteristic in common, they both need space to act on its roles in the CNS. While investigating the staining patterns on MTT conversion (in light microscopy images) based on cell injury, it seems like this space was characterized in some rudimentary manner. This weight of evidence that these spaces are microanatomical -and not artefactual- is accrued through 9 empirical observations from this research, an observation about the nature of parenchymal brain cells, and the logistics of cerebrospinal fluid flow:

1-Shadows/depths focus. Sections of hippocampal slice were evaluated under light microscopy without a cover slip to appraise cross-sectional MTT staining in the injury model as there seems to be a dose response effect on injury depth. As described above in Figure 26 there are several instances of circular shadows consistent with microlumens and empty spacings, conversely there were also instances of white circular shapes insofar as to suggest an opening that reached the other side of the 60-micron section. These shadows and areas of non-obstruction (white) represent a space withing the solid components of the slice. During microscopy reviews of these slices' focus could not be achieved homogenously across the slice; furthermore, when the focus was adjusted the portions that had not focus eventually focused, indicating a difference in depth of solid components. Once it was ascertained that these were not fixation nor freezing artifacts, or an artifact of mechanical tissue damage (as light microscopy sections from whole hippocampus had the same spacing profile as the sections from a 200-micron slice) its contents were evaluated for MG.

2-The motility of fluid within the hippocampal slice. A 200-micron slice resting on a semiporous membrane that is on top of a well with 1 mL of media will uptake media fluid and its content in and within the spaces of the tissue matrix. This is evidenced by the uptake of MTT and PI (decanted onto the media pool) that yields staining of the uppermost cells of the slice, furthest away from the media pool (Figure 25.). These cells turned blue and/or took up PI and turned their nuclei red. Thus, in order for the contents of the media pool to reach the topmost portions of the slice it stands to reason that there were openings, or spacings, within the tissue that enable this transit of MTT and or PI the thickness of the 200-micron slice. Had this space or openings between cells not been available the topmost cells would have not consumed the MTT and PI from the media pool and not changed colors corresponding with these two reagents.

3-Pictorial evidence of MG filling the void. Immunohistochemistry of CD11-staining of MG within 60-micro sections was initially conducted to better appraise MG shape at higher magnifications, however when contrasted with properly visualized phase contrast images MG appeared to be indwelling within these openings (Figure 35). This is consistent with the motile properties of these cells as they necessitate space to move within the brain parenchyma to fulfill their roles as responders of cellular damage and or cellular maintenance. Furthermore, one of the most remarkable initial observations of MG is that they seldomly, if ever, overlap; this is perhaps because the attachment points to the extracellular matrix of the CNS permit only one MG to adhere at any given extracellular region. Therefore, MG adhesion is dependent on acquiescing to an available set trail of CD11-receptors (ICAM-1, ICAM-2) that interact with MG's CD11 protein. ICAMs are an omnipresent receptor in the CNS [20]. Therefore, MG trails within the

extracellular matrix are also evidenced by the presence of these adhesion proteins laid out throughout regions of space for CD11-bearing cells to move about. And finally, during IHC evaluations, it was noted in several instances that MG arrange themselves in a circular manner. This arrangement is consistent with the shape of the openings and porosities being described. This indicates that MG take on the shape of the openings to permit max lumen opening. In published studies ([18] and [17] that introduced cultured MG to a cultured hippocampal slice mentioned that MG would infiltrate the tissue and distribute within. Such is that this indicates that there is a spatial aspect to MG movement in similar experimental paradigms that lend credence to the ability of motile cells such as MG to move about freely into and within CNS tissue.

4-Fluorescence-superfluousness/phase contrast. To appraise the solid and empty aspects of the CNS matrix at it appeared in 60-micron sections of whole hippocampus, and 60-micron sections from 200-micron slices (without a coverslip) a technique of fluorescence flooding was applied, this saturated and reflected all components were solid, but what was empty is does not reflect and is simply black amidst all the fluorescence intensity (Figure 32, Figure 33). Interestingly, this technique captures the topmost portion of the sections, however it could not capture deeper solid components, as when phase contrast was applied it demonstrated that there were other solid components present deeper in the tissue that were appearing as black in fluorescence lighting (Figure 33). This indicates that fluorescence lighting is more sensitive to volumetric changes of solid components as it pertains to tissue thickness, ergo if the tissue collapses the black could be filled in with lower ECM if spacing is lost.

5-Blackness/black areas. During IHC of MG in 200-micron slices to determine their morphological variation in response to toxic injury, there was always slight background fluorescence from the EMC, however there was also pitch-black areas that exhibited no fluorescence (Figure 11, Figure 34) The resolution of the fluorescence in the 200-micorn slice was not as pronounced as the 60-micron slice, likely due to sample thickness, however the black was consistently present as mostly circular spacings that were similar to what was observed in phase contrast and light microscopy. It is worth noting that albeit the resolution of the spacing was not optimal, the presence of the spaces (by the preponderance of pitch-black regions) indicates that the spacing is not a freezing artifact as when slices were processed for IHC they were never frozen (Figure 28).

6-Cell collapse. Evidence of cell/tissue collapse in way of decrease spacing was seen in light microscopy and fluorescence microscopy images (Figure 11,Figure 13, Figure 14, Figure 34). In several instances during the evaluation of MTT-treated tissue the appearance of tissue collapse (loss of space) was observed, this was manifested as an increased incidence of the fragmentation of the solid components of the injured regions of tissue compared to other portions of the slice that were adjacent but, based on formazan content (from MTT), were healthy; in addition, this portion of the tissue was depressed compared to the rest of the slice. During IHC evaluation one of the hallmarks of a spot tox was the appearance of a large circular region of red fluorescence staining in the middle of the non-fluorescence (black) regions that surround it. In fact, image analyses of black regions (regions of space, not illuminated by fluorescence) comparisons to equal areas of healthy tissue indicated that there's an appreciable quantifiable loss of space that occurs because of cell injury and or death within the tissue. This is consistent

with the notion that CNS cells survival also serves to maintain extracellular matrix structure needed for fluid passage (more on this below).

7-Tissue bioavailability limited by cell collapse. Volumetric/concentration limitations- As mentioned in the previous sections, fluorescence lighting is more sensitive to capture of the topmost solid components as it will only reflects off the top layer of solid within the slice. This collapse is thought to contribute to the impermeability of pharmacotoxicants (in particular, polar ones such as cyanide) at lower concentrations added to the top of the slice, as when the top tissue/cells collapse it results in lipophilic barriers that prevent the rest of the toxic fluid from reaching the lower portions of the slice and therefore a slice-wide spot-tox is not visible. In addition, during the model workup of the hippocampal slice it was noted that thicker slices would not yield a spot tox because the 180 nL volume of toxicants was not enough to reach the bottom of a 400-micron, nor a 300-micron thick slice; however, at 200 microns a spot appeared. This is likely a manifestation of tissue collapse preventing the toxic fluid from reaching the lower portion of the slice in thicker slices, whereas a 200-micorn slice represented a thickness of full permeability at the toxicant concentrations used. This was also corroborated during slice-immersion toxicity studies, the abundance of fluid surrounding the tissue matrix was able to permeate entirely at high toxic concentrations, however, at lower concentrations the core of the slice was viable whilst the edge of the slices was categorized dead as PI had infiltrated those cells, but not the cells within the inner core. Another remarkable observation is that when the slice is immersed MG expand into large globular forms. As mentioned previously MG seem to need something to attach to maintain its fine stellate shape, in the presence of fluid turbidity the soma becomes

enlarged and globular. This expansion (in combination with tissue collapse) seems to limit the amount of toxic fluid that reaches the core of the slice (via space openings) and thus in some manner protects the cells within the deeper tissue core compartments. One inexplicable aspect to this observation, is why is it that at lower toxicant doses the sides of the slice only turn red (insofar as suggesting a preponderance of PI uptake) and the topmost region (as it appears on the microscopy image) are still black and thus, maintaining PI exclusion.

8-Strategic vasculature around large chambers of empty space. During light microscopy large spacings of 100-200 microns were noted (Figure 36, Figure 38). These larger chambers of space seem to be arranged around a small plexus, or vasculature. And albeit they measured at 200-microns wide they were rather narrow as when the tissue was sampled perpendicularly these openings were 120-microns wide. These openings/vessel arrangements may be consistent with the postulates of [45] which suggested that there is CSF regulation within the brain parenchyma, and not just within the choroid plexi of the ventricles. This spacing may reflect an interface between the fluid of the vasculature and the fluid of the brain interstitium. Further this structure bears resemblance to the arachnoid villi [44]. Considering that from the presupposition that any CNS fluid can is sourced/replenished and or eliminated through the vasculature this morphological arrangement is perhaps a representation of this aspect of fluid input or output within the brain's interstitial compartment.

The evidence of porosity being anatomical is not just the data/images generated but also a historical acknowledgement regarding the nature of CSF and CNS cells. The most obvious one, which has been mentioned, is the nature of CSF and its passage through the

brain parenchyma, the kinetics has been described as relatively fast moving and unidirectional ([37]; [45]; [36]). This is consistent with what is known about action potentials (Hodgkins et al. 1939 [46]; [38], [47]), that is, as soon as sodium and potassium ions are taken up by a neuron's sodium-potassium ATPase the void of ion unavailability should be replenished by the speed of fluid expediently bringing in the next ions to facilitate availability for the next ion channels. Therefore, space to maintain this ionic balance within the microanatomical volume is allotted (as it relates to speed of CNS interstitial fluid flow). The other historical information that fits within the context of some of these pictorial findings, is the shape of parenchymal CNS cells. The parenchymal cells of the CNS (specially neurons, astrocytes, microglia, oligodendrocytes) share a peculiar specific and common structural motif, that is, immediately after the soma of these cells all processes emanate out with ample space in between them; the best way to describe it is as a C-curvature between the cell body and the axon or dendritic extension (Figure 39). The spacings within these cells suggests that this allows the unperturbed flow of fluid near the soma. It is important to bear in mind that a significant amount of ion channels are present on or at near the soma [48] and thereby within the C-curvature lending strategic placement of these ion-channels. The filaments described earlier all fit within the profile that almost all CNS cells have a process emanating out of it, and further, the ample spacings that surround these filaments. Upon closer examination of these cell's shapes these peri-cell body C-curvatures indicate a common structural motif within the cells of the CNS that enables the shape and form of these circular channels/openings observed in the raw observations of the 60-micron hippocampus sections. As such, these channels arise from an accumulation of cells

sequentially arranged, so much so they start to resemble a tunnel. In all essence of prime form follows function and this structural motif seems to serve as stationary rudders of fluid flow. The mere sequential and adjacent placement results in a controlled passage of fluid and its directionality; and perhaps even speed (due to lack of solid stationary impediments within). Thus, these 2 know and verified aspects of the nature of CNS, the importance of interstitial fluid flow and the shapes of CNS cells, lend credence to the microspacings being important micro-anatomical components described in this investigation's report.

2.6.3. Why have these spacings not been seen before?

Microspacing as described in this investigation's definition is the space in between cells that enable the efficient flow of interstitial fluid or cell movement withing the parenchyma of the brain (or any other organ) without disrupting anatomically important tight junctions. Classically, empty spacing observed within a microscopic evaluation were described as "vacuoles" which are non-contextual to the conditions described in this study as those are usually "intra"cellular rather than "inter"cellular. Recent articles have alluded to this spacing [42] and the importance of appraising it. The definition of micro spacing is not described in any appreciable level in the literature and thus, if this is indeed a void of biological information, this investigation will attempt to account for some of the details of it within the CNS tissue. Typically, during most of all scientific explorations of the microscopic environment the majority of the focus is on the solid components of biology, the cellular and biological matrix structures. In the typical Hematoxylin and Eosin procedures for histology a dehydration step is required to better visualize these important solid components, however it appears as this dehydration also leads to a

collapse of the microspacing needed for interstitial fluid flow. And therefore, most of the microspacing's representation might have been unaccounted for when histological characterizations and investigations were done. Furthermore, the typical H&E tissue sections usually evaluated where very thin, 5-10 microns; this relegates observations to be mostly 2-dimentional. During this investigation 60-microns were selected to ensure a MG (which are usually 40-50 microns wide) was captured in an IHC section. The thicker the section the greater the depth dimension is appraised and thus visualized through shadows. Such is that these shadows were observed first during light microscopy of MTT stained tissue and then the evaluation progressed to evaluations of unstained tissue under light microscopy and fluorescence reflections contrasted with phase contrast visualizations as described within this investigation's results. The possibility that these spacings being artefactual cannot be absolutely refuted, however, based on the weight of evidence presented, it appears that microspacing indeed is a natural separation of the microenvironment's solid and static components (non-mobile cells, extracellular non-soluble matrix proteins) and motile components (interstitial fluid, motile cells). Even if these findings are proven to be an artefactual element, and thus unnatural spacing, the question of how fluid flows and motile cells migrate through the microenvironment still stands and thus something that ought to be more deeply comprehended. Biology is predicated on steady states and thus a flux of replenishment, consumption and elimination or the contents of the interstitium and thus the fluid flux needed to achieve these steady states is an important consideration, and therefore also the space for the dynamics of interstitial fluid to permeate and decant from parenchymal microcompartments is also important and underappreciated component of tissue

histology. As described above, motile cells like the MG and interstitial fluids benefit from having relatively ample micro space to conduct their biological roles in an efficient manner as it relates to spacing necessitated to enable biochemical reactions, ionic concentration cycles, etc. These visual mathematics of openings and porosity within CNS hippocampus tissue suggest that mobile phases of biology are being accommodated, in the form of fluid transits or space for MG (or other motile cells) to move about (Figure 24, Figure 26, Figure 36, Figure 38, Figure 39).

Albeit an inadvertent observation, but upon consideration, highly relevant, it accounts for the volumetric considerations of the solid components of cells and the fluidic components outside the cell. From a purely empirical standpoint, it appears as if solid and non-solid arrangements are an important factor in micro biological layouts. Taking into account that the capturing of only solid components indicates a topography of cells and extracellular matrix that is very voluptuous indicates that spatial distribution is balanced between solid components and empty space; based on the image analysis of this study empty space between CNS cells in the hippocampus constitutes anywhere from 25-50% of the spatial layout (Figure 29), ergo information about microcytostructure that is permissive for normal fluid flow. If corroborated outside of this lab intercellular space can add further resolution to controversial topics (amidst others) of the hippocampus such as lamellar hypothesis ([49]), as the spacing itself could be part of the excitatory pathways investigated in electrophysiology paradigms. There is a balance of the overall volume devoted to space and volume devoted to solids that seems to be in exhibit in this controlled CNS sampling of tissue and hence in some extent considering these cells that are still viable within the cultured sample and likely simulating what they were just doing

inside the whole brain. The area devoted to empty space is also functional volume, for this permits the non-static components of the CNS (CSF fluid, motile cells) to conduct important functions in biology, the maintenance of a steady state.

2.7. CONCLUSION

If indeed it is proven that the spaces observed under the proposed treatment of tissue are not artefactual effects, by manner of 25-50% is devoted to the empty space volume –as reported in the results of the sample and sample treatment. And therefore, the alteration of this volumetric distribution should be a factor in microtopography-related pathogenesis, as it allows for the effective and efficient flow of interstitium fluid that enable optimal neurophysiology. Such is that when the interstitial conditions that enable optimal neurophysiology is no longer "optimal" potentially neither is neurophysiology, and hence neuropathophysiologies are likely to ensue; the same deductions are made by Bich et al (2019 [42]). Such could be regarded in the crater that appears in the region of the spot-tox thereby indicating that cells when they die (by having a ruptured cell membrane) also deflate, and therefore alter volume of free fluid flow (taking for granted the notion that "nature hates a vacuum") under and above the crater. Structurally reverse to the previous postulate, the volume of fluid flow can also be altered with cells that overly-inflate; that is if, despite their fluidic content, cells in it of themselves are considered solid particles and therefore alter the free extracellular fluid flow. Activated globular CD11+MG can narrow openings for fluid, motile cell piling on top of each other, or remnants of piled fibrotic-like deposits (or other non-live extracellular composites, such as APP-rich amyloid deposits (as described in vivo by [50] and thus in its alteration of volume devoted to solid and volume devoted to space and in turn can

impact the effective flow of interstitial fluid. The appreciation of spacing can be a worthy contributing factor to the recent burgeoning discipline of glymphatics [51], postulating that most cells associated with lymph nodes are motile and thereby need microspacings to move about without interrupting important parenchymal cell junctions.

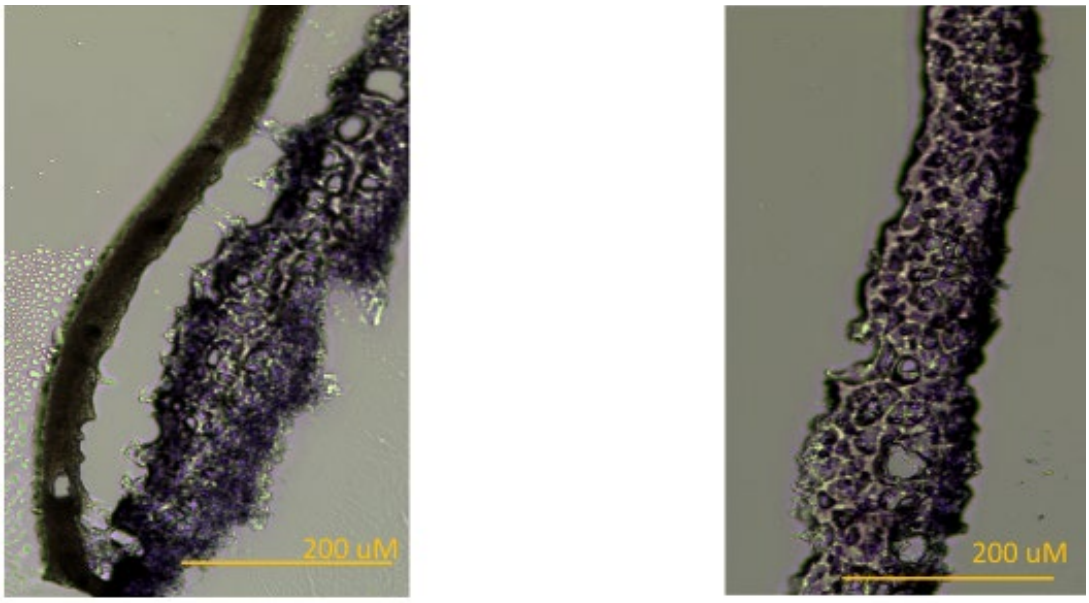

Figure 24: Hippocampal slice cross-section and porosity profile

Porosity profile of cultured hippocampus tissue cross section (post MTT exposure, formazan stained) of a 60-micron cryosection. This cross-section of the tissue slice demonstrated the uptake of MTT throughout the entire thickness of the slice.

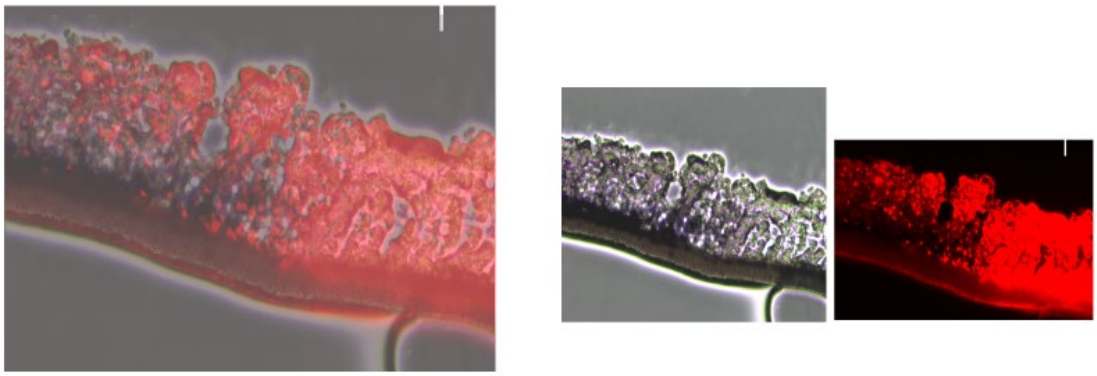

Figure 25: Cryosection cross section of spot tox injury within a cultured hippocampus slice

This 60-micron thick cryosection of the tissue slice demonstrated the uptake of MTT and PI throughout the entire thickness of the slice. The areas that are white and red represent injured or dead cells within the tissue. The other areas are blue and have minimal red indicating that those cells are viable and by large most have intact membranes excluding PI.

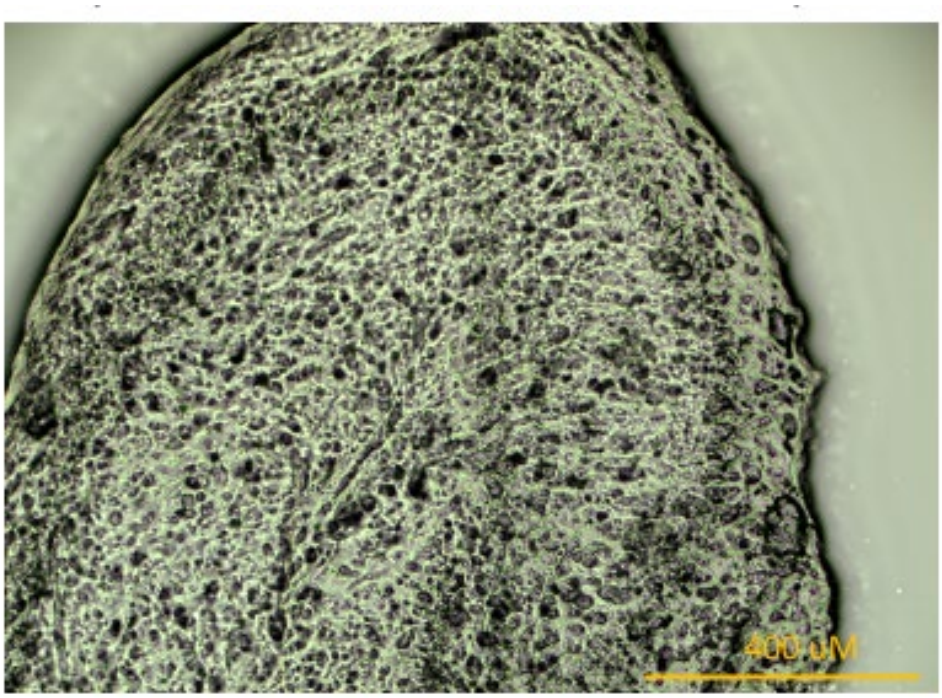

Figure 26: Porosity profile of cultured hippocampus 60-micron tissue cryosection (no stain)

This unstained light microscopy 10x image of a 60-micron thick section of a whole hippocampus demonstrates the impressive porosity of the tissue's microterrain. The black areas within the yellow-beige portions of this tissue section represent shadowed areas for which the light does not reach and thus indicates a depression in the tissue's plane and thus an empty space within the tissue section.

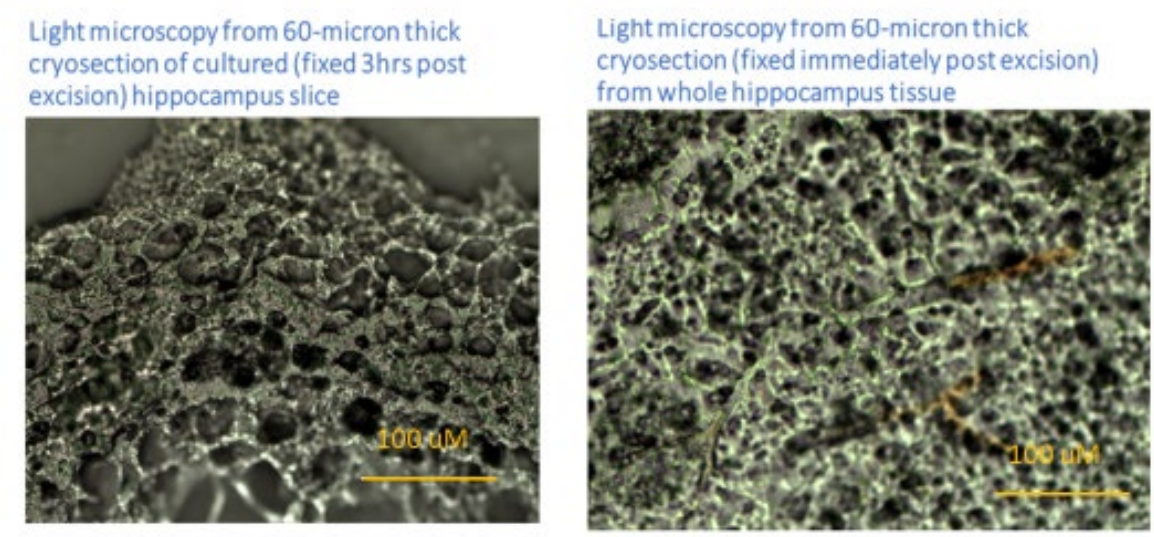

Figure 27: Cryosections from cultured slices vs cryosection from fresh hippocampus tissue

No difference in porosity profile of cryosectioned cultured hippocampal slice and cryosectioned whole hippocampus tissue. These two light microscopy images of a 60-micron section of hippocampus tissue demonstrate the similarity in the porosity profile between a 60-micron section from a cultured hippocampus tissue (fixed after 3 hours of culture) and a 60-micron cross section from whole hippocampus (fixed immediately after dissection of hippocampus from whole brain).

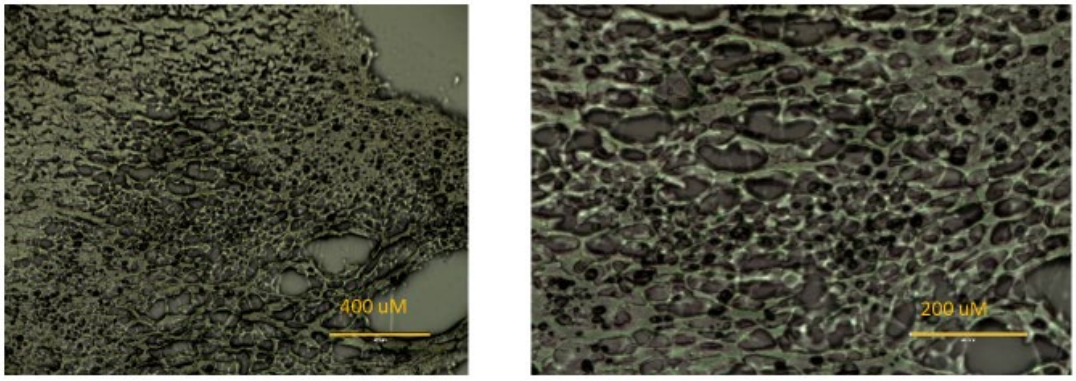

Figure 28: Cryosections from unfixed hippocampus tissues

No difference in porosity profile of unfixed flash frozen cryosectioned cultured hippocampal slice. This light microscopy image of 60-micron thick unfixed tissue demonstrates that despite not being fixed the porosity profile is still maintained.

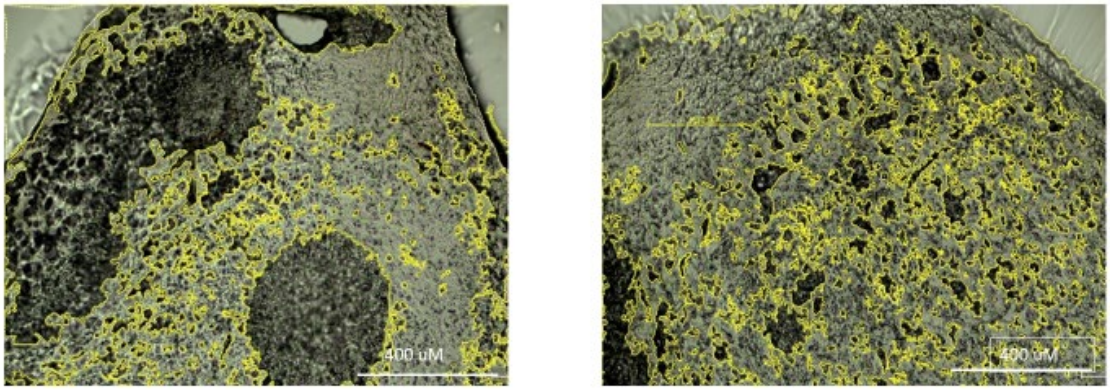

Figure 29: Image analysis of porosity

Image analysis of empty spaces within 60-micron section of hippocampus. This image analysis (demarcated by yellow lines) of a 60-micron cryosection of a whole hippocampus indicates that when empty space vs solid space is appraised, the volumetric distribution of empty to solid space is 25% to 75% respectively. In other cryosections of the hippocampus there is greater empty space; estimated to be 50% empty space vs 50% solid space.

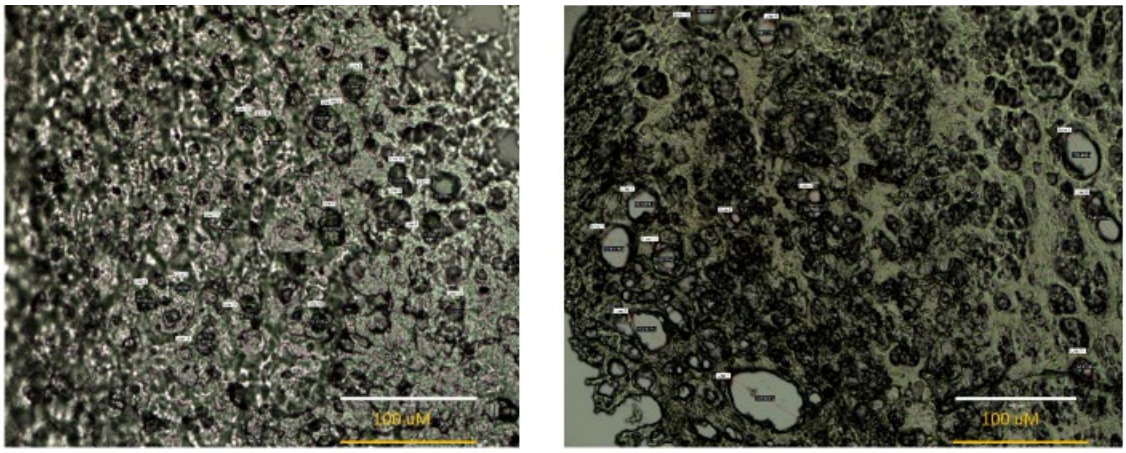

Figure 30: Characterization of openings

Characterizing openings within cryosectioned whole hippocampus. Light microscopy image of a 60-micron cross section demonstrates that the empty spaces can be either black and or white, the former being representative of an opening that ends in a shadowing effect and the latter represents simply a hole that is open all the way towards the other side of the 60-micron this cryosection of tissue. In addition, this image measures the different size and shapes of the openings that represent porosity of tissues, indicating a heterogeneity in its size (diameter) characteristics. Some openings were as small as 20 micron whereas others where as large as a 100 microns.

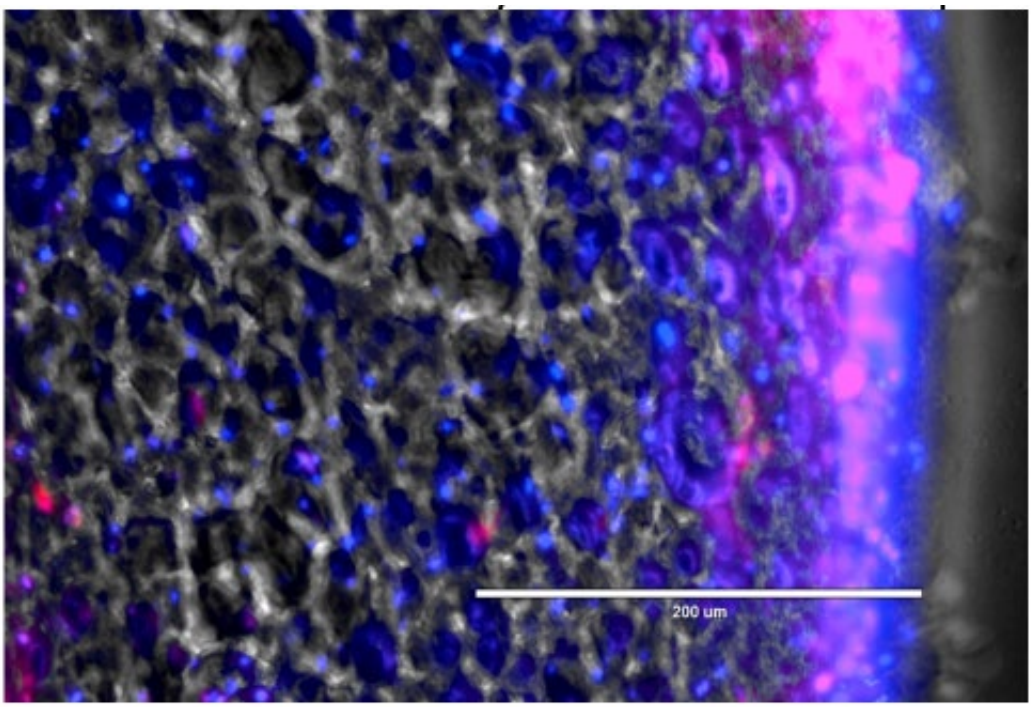

Figure 31: Cell nuclei layout relative to porosity openings

This fluorescence image overlayed with a phase contrast of a 60-micron cryosection represents tissue stained with dapi and PI demonstrating that many cells are viable and how the nuclei of cells that constitute the tissue are presented within the porous tissue matrix.

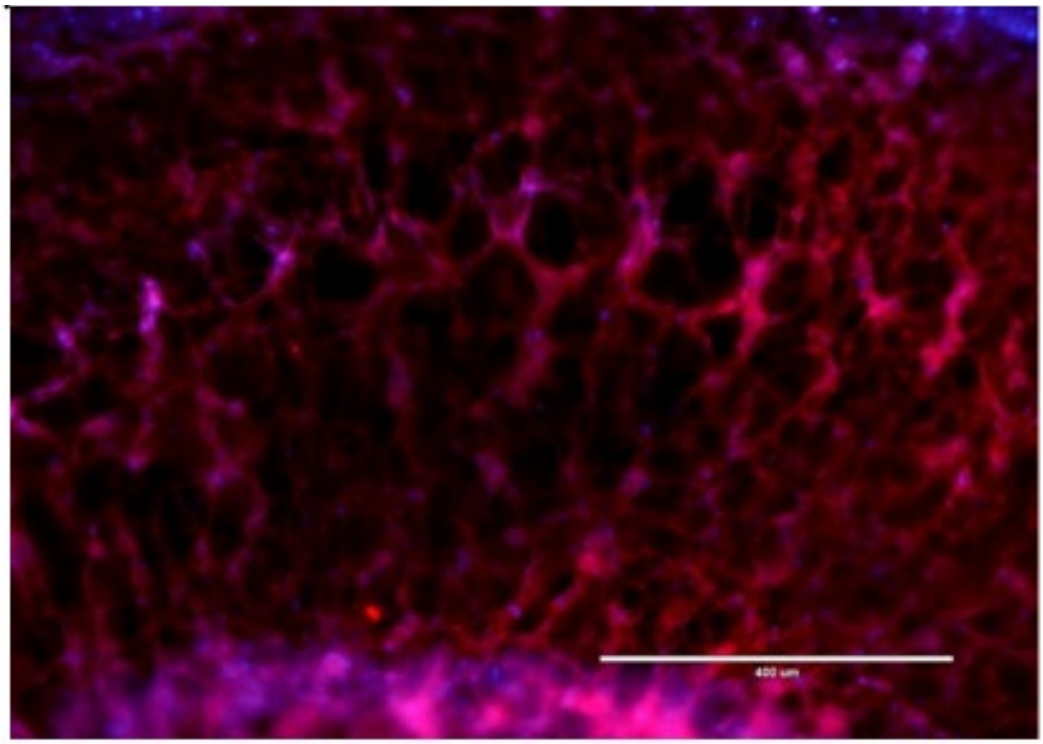

Figure 32: Fluorescence flooding of cryosectioned whole hippocampus tissue

This 10x fluorescence image of the CA3 portion of a hippocampus 60-micron cryosection demonstrated that under this light source porosity is more pronounced than what was observed under light microscopy. Bar = 400 um

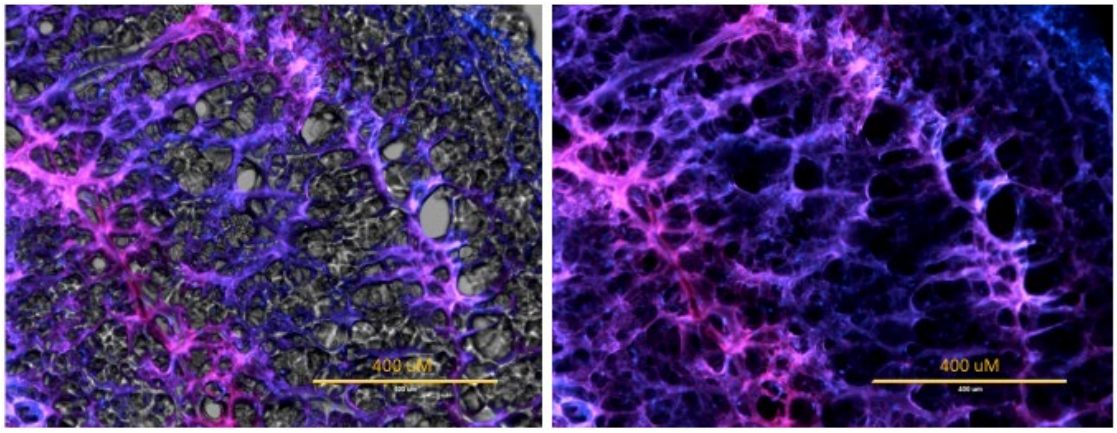

Figure 33: Fluorescence flooding of cryosectioned whole hippocampus tissue contrasted with phase contrast

These are 10x images of 60-micron thick cryosection comparing the impact of different light sources. The image on the left is an overlay of a fluorescence image with that of a phase contrast image, whereas the fluorescence light only reflects the topmost portion of the slice, the phase contrast captures more deeper components than the fluorescence lighting does. This indicates that the porosity can be more detailed under a fluorescence light source.

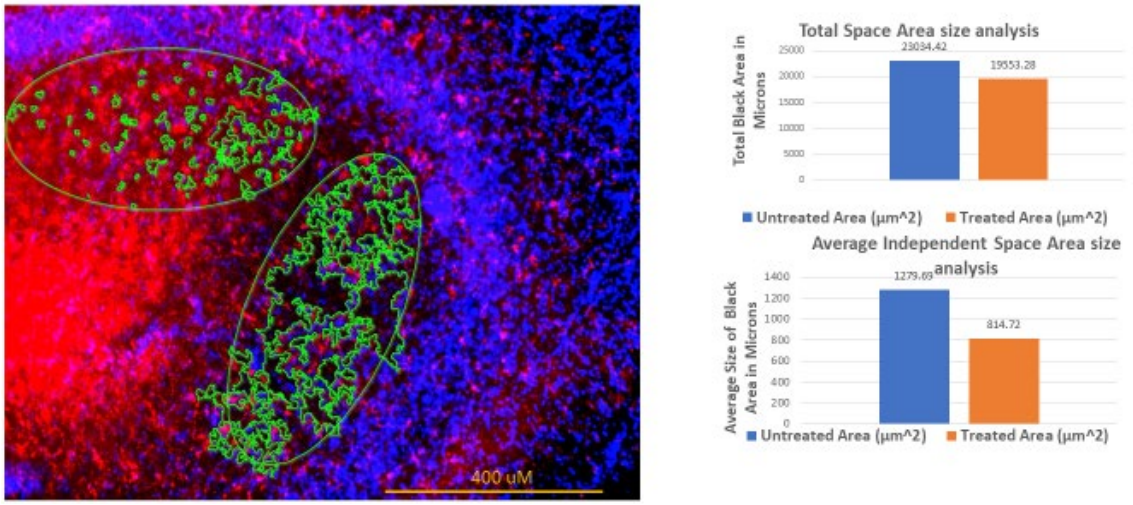

Figure 34: Quantitative Analysis of space loss in a sample of IHC of cultured hippocampal slice exposed to toxicant

This is a representative analysis of the impacts of toxic injury on intercellular spacing in single cultured tissue. An image analysis (using HALO software) of black area size in toxicant treated areas size vs untreated area size indicates that a decrease in area could be appraised numerically based on black area size in areas of the same size (oval). Upon cell injury tissue structure collapses and decreases the amount of black area as red fluorescence reflects (total area:19,553 um) off tissue surface; in non-injured tissue the spacing is maintained to prevent fluorescence reflection (total area: 23,034 um). In addition to greater total area, the individual areas are smaller in the treated (814 um/area capture) areas vs non-treated areas (1,279 um/area capture).

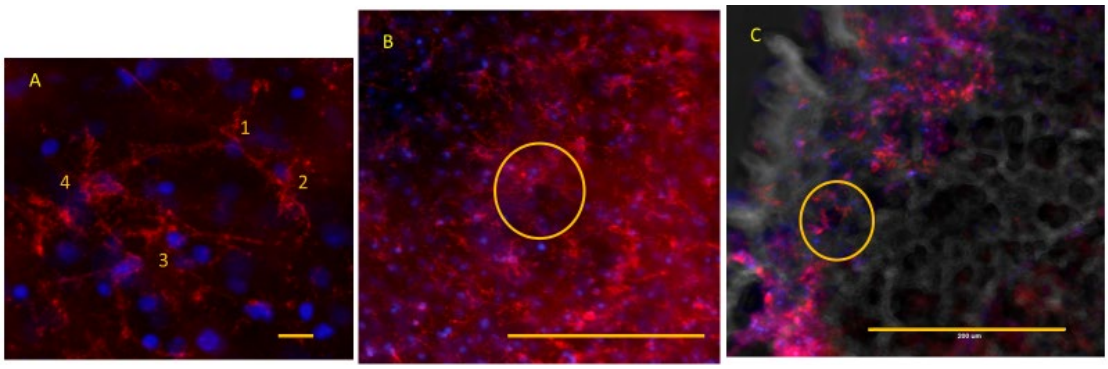

Figure 35: MG and openings

Visualization of MG in whole hippocampus IHC (A) vs cryosection of hippocampus with phase contrast (B). A) In this representative 40x image, 4 MG (numbers 1-4 adjacent to the outer portion of cells' nuclei) surround circular empty spacing, these MG are likely attached to the walls surrounding the opening. Lack of fluorescence within the inner border of the MG indicate that there is empty space. This indicates that baseline MG can be a non-obtrusive element of extracellular spacing. Bar= 20 um B) Representative 20x image of fluorescence image of CD11 tagged microglia (counterstained with dapi) surrounding an empty space (yellow circle). Bar = 200 um C) Representative 20x image of fluorescence image overlayed with phase contrast image; phase contrast image demonstrates that the black between MG (yellow circle) is empty space. Bar = 200 um

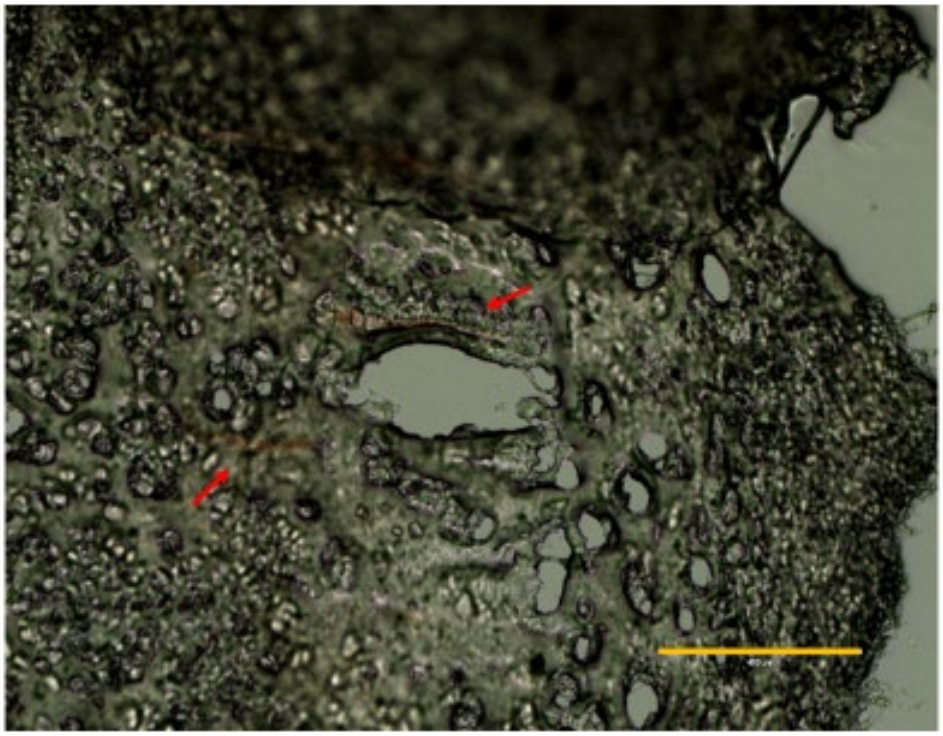

Figure 36: Macrospacing within cryosections

Macro spacing observed within cryosections relative to vasculature. This representative 10x image exhibits blood vessel (arrows pointing to red lines, which are likely capillaries containing red blood cells) parallel placement relative to a large chamber of empty space. The presence of these blood vessel indicate that these large empty spaces are anatomical layouts. Bar = 400 uM

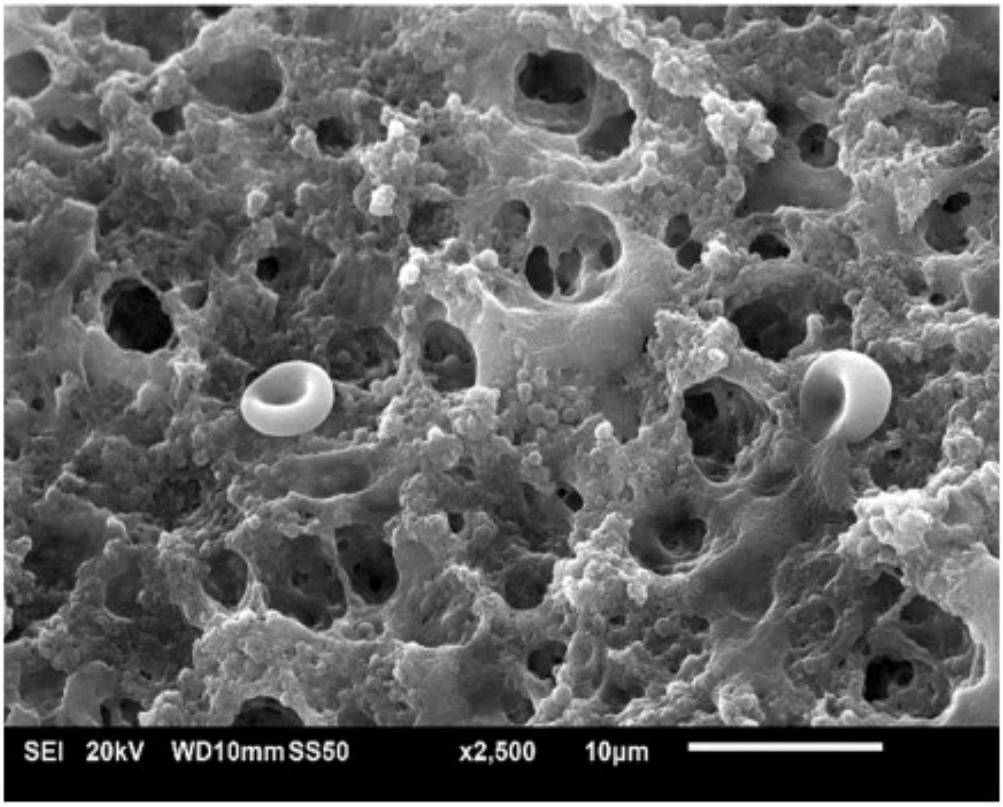

Figure 37: Scanning electron microscopy of porosity

This 2500x scanning electron image appraises the porosity at greater magnifications. The presence of an intact red blood cell indicates that the processing of tissue did not affect cellular structures.

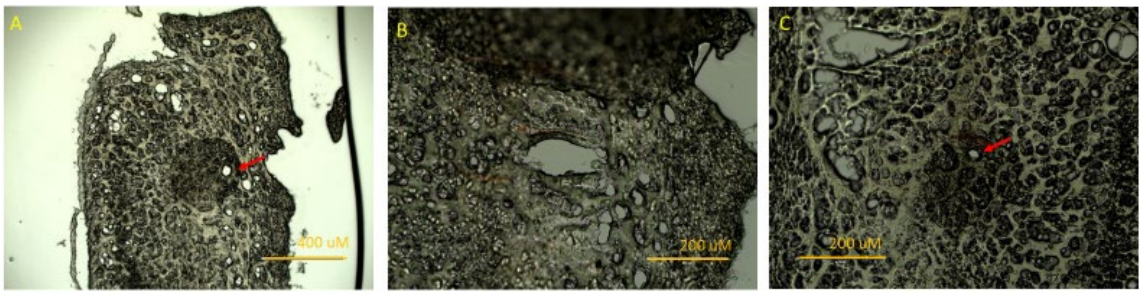

Figure 38: Macro spacings within cryosection of whole hippocampus

These representative images A, B, C (10x, 20x, 20x respectively) appraise the appearance of macro-sized empty spaces. One similar characteristic is that they are 200-300 microns wide and often present with a single opening on one end (red arrow). This indicates that empty space can consist of greater sizes to accommodate unbeknownst fluid dynamic of the brain's interstitial fluid/CSF flow.

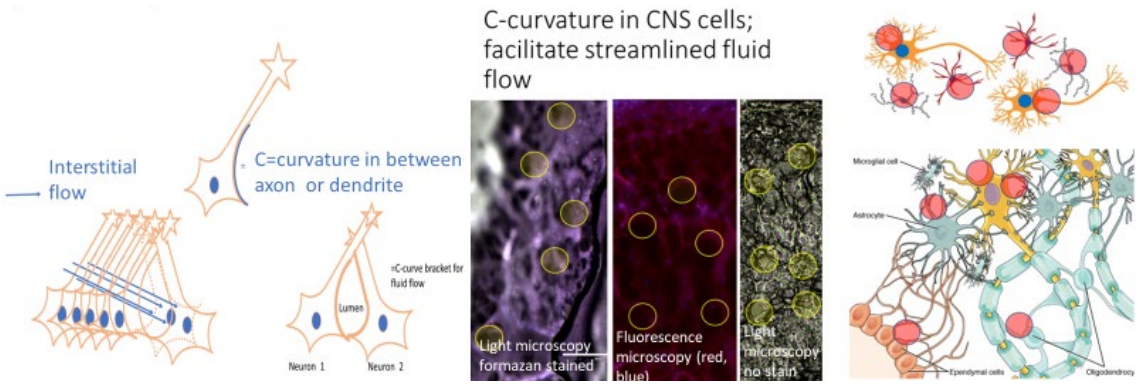

Figure 39: Conjecture of CNS's cells shapes as it relates to porosity of CNS tissue that enables interstitial fluid flow

One of the distinguishing characteristics of neuron, astrocytes and microglia as parenchymal cells within the CNS is the preponderance of processes, dendrites and/or axons emanating out of the main cell body. One of the consequences of this structural motif is the presence of a curve in between each dendrite, process and axon. In particular, axons being the largest structural process emanating out of the cell body, create a larger curve, described as a c-curve. Per the investigations of French et al [48], many ion channel are present within this region of the neuron; these channels are responsible for action potentials. If neurons are placed sequentially then they can create a tunnelation effect that will direct fluid towards a certain direction, which could correspond with the creation of a channel that is guided by action potentials.

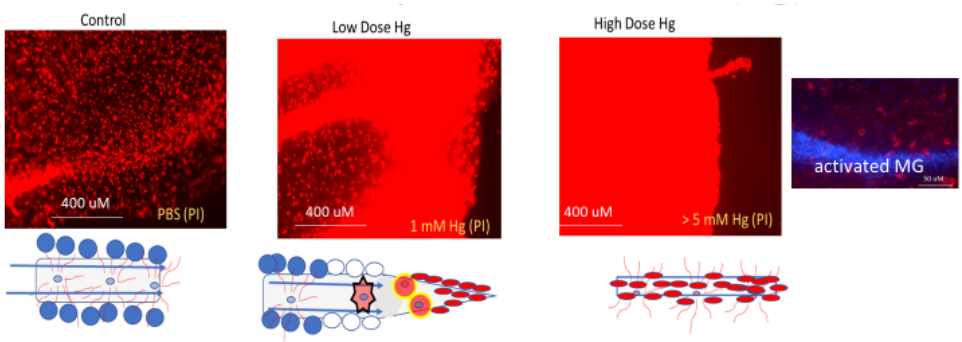

Figure 40: Loss of fluid permeability during whole slice immersion into media with toxicant (Hg)

Control slices have sporadic dead cells that, however by in large most cells are excluding PI dye. High doses of toxicant (mercury) the entire slice turns red not just due to PI infiltration into the cell but also due to leakage of nucleic contents into the extracellular space that also interact with PI. During low doses only the outer portion of the slice turn red indicating toxicity in only that portion of the slice; this indicated that the inner portion of the slice is protected by some factor that impedes access of toxic fluid into that compartment of the slice, likely activated MG.

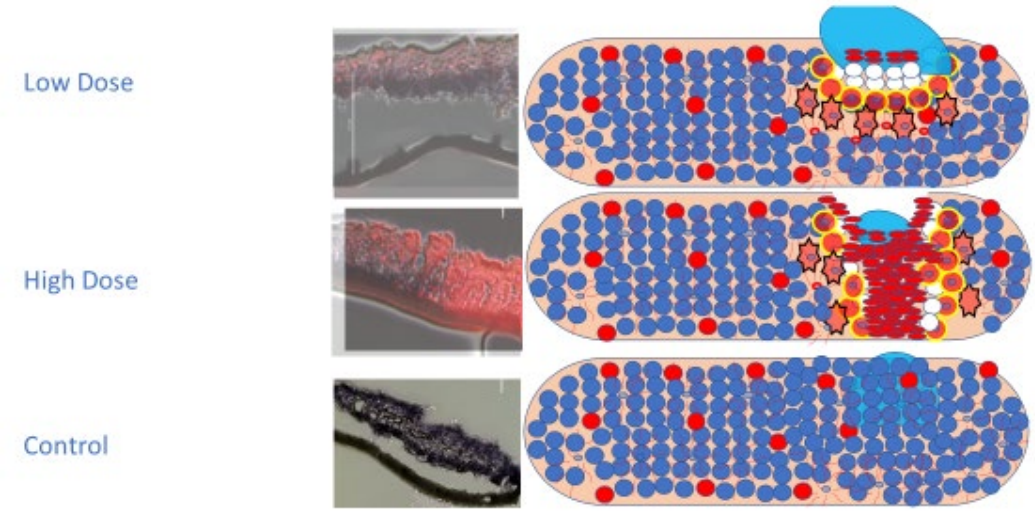

Figure 41: Proposed mechanism of biodistribution of 180 nL aliquot of toxicant at high and low doses compared to control

Lower doses of toxicants cannot reach the bottom of the slice likely dues to activated MG obstructing passage of toxic fluid to the bottom portion of the slice and thus are protected from toxic insult. At high doses, likely due to osmotic pressure gradients and induced toxicity the MG barrier is lost, and the bottom portion of the slice is exposed to toxic insult.

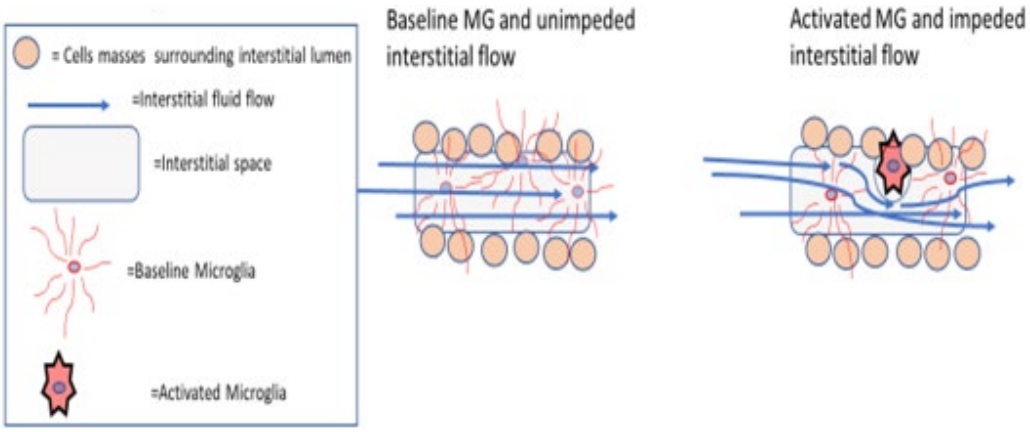

Figure 42: Proposed mechanism of impact of activated microglia (M1) on interstitial openings within the CNS parenchyma

This abstract image of the significance of interstitial space demarcates 5 important components: parenchymal cells that surround the lumen (and that are also immobile), empty interstitial space microcompartment, baseline microglia cells and activated microglia cells and the unidirectional fluid flow. In left figure during baseline state MG are thin and spread out and thus do not present much obstruction to the unidirectional flow of interstitial CSF fluid, which is represented by straight lines. In right figure during activated state MG occupy more volume and disrupt the flow of fluid. As a result of this obstruction fluid is no longer linear and thus to circumvent the enlarged MG interstitial fluid's speed and direction is slowed and interrupted. This postulate indicates that post activated MG microenvironment is not optimally replenished with fresh interstitial fluid.

CHAPTER 3: DISCUSSION OF MICROGLIA AND INTER-CELLULAR SPACE

3.1. DISCUSSION

With these aspects in consideration, that is, the details of MG morphology, and biochemically confirmed cell death (part 1) described in this investigation relates to the details of the observed spacing (part 2) allotted for cellular motility and fluid flow. This was mostly evident in two instances from the above data on hippocampal slices; during slice immersion toxicity study and the lack of permeability observed during lower toxic doses of the spot tox. When slices were immersed and compared from control to low and higher doses of pharmacotoxicants the penetration of the toxicant was predicated on the concentration of pharmacotoxicants, whereas higher doses lead to complete PI penetration and the entire slice turning red, lower doses only lead to PI in the rim of the slice, but the center was still excluding PI and thereby indicating cells with intact membranes were still present and hence viable. When MG were evaluated under these immersion conditions there was a preponderance of ameboid MG present, which indicates that in extreme activation (or extreme morphological change) the ameboid shape creates a barrier within the spacings and thus toxic fluid is excluded from the slice core and protecting cells in the inner core of the slice from Hg toxicity (Figure 40, Figure 41, Figure 42). It seems like this threshold is lost at higher concentrations of toxicants are enough to elicit more widespread diffusion of fluid and more widespread toxicity. It is uncertain if this is occurring because of MG lethality or, more thorough permeation through collapsed tissue barriers, or a combination of both at these concentration gradients. The other instance where similar observation and inferences are made is when a 180nL aliquot is placed on the top of the slice, the propagation of cell death was confirmed with MTT in combination with PI; and thus when the area did not convert

MTT to the formazan salt (and hence turned blue) a white spot was left in that region of the aliquot, whereas the rest of the slice turned blue; conversely with PI, the a red spot indicated that this molecule was reacting with intracellular RNA and DNA as well as RNA and DNA spilt from cells with damaged membranes.

Similar to the observations during the immersion of slices, a white or red spot only appears in the highest pharmacotoxicant doses indicating that 180 volume is sufficient, but the concentration predicates how much tissue area is affected. Since cells when they die deflate and then collapse in essence create a lipophilic barrier a closure in the fluid passage is created (Figure 41); furthermore, in the first regions of the area where the most activated MG are found and thus their expansion within the microspacing allotted can potentially create another barrier on top of the deflated, lipophilic dead cell remnants. It is therefore postulated, according to the above evidence, that MG in the M1 state (ameboid) can impact fluid flow (Figure 41, Figure 42), and in fact its preceding morphologies where it is extensively retracting and rearranging its membrane placement and accruing it in its soma, therefore leading to its expansion can, based on their placement and the size of the opening they are navigating through in the brain parenchyma, alter the flow of fluid and thus create interstitial fluid access disruption in the spaces post blockage, bearing in mind that interstitial fluid flow is postulated to be unidirectional based on previous experimental evidence [36].

The data yielded in this investigation is a step to adding further resolution to the volume occupancy of biology. Traditionally this has not been accounted for histopathologically as many of the processing steps taken in the visualization of microanatomy requires dehydration steps that collapse most intercellular spacings. In this experimental

paradigm dehydration steps were generally avoided during IHC evaluations and light microscopy of formazan-stained and PI-stained brain tissue; that in conjunction with the utilization of appropriate OCT processing and slow freezing enabled the preservation of the intercellular spacings described above. Then qualify the spacings by evaluating its alteration; that is, take a piece of CNS tissue and evaluate if the spacing is impaired by cellular injury. Taking the gradient of utilizing a marker for mitochondrial health such as MTT and a marker for membrane integrity, PI, stressed cells can be characterized by the non-conversion of MTT to formazan but maintaining PI exclusion. This marker of stress can be the beginnings of cellular impairment as once the mitochondria is damaged, ATP is decreased and thus priority is given to maintaining an intact membrane. However, is this decreased concentration of ATP sufficient to maintain the actin-tubular structures that shape neurons macrostructure to hold up a certain overall cellular shape, which in turn enable optimal extracellular fluid flow? If the same could be done for other organs' tissues (besides CNS) the impacts can be related to the importance of *in-situ* space of a biological system; provided that these excised tissues can effectively maintain suffusion and thus survive ex vivo for at least 4-5 hrs, the way the slices in this model did. The brain facilitates ex-situ preservation as it is accustomed to maintaining itself suffuse without as much blood-derived hydrostatic pressure as that of other organs (but it isa an important consideration with regard to the pressure of fluid flow (as demonstrated by Császár et al. 2022 [52]and [19]). This was directly observed in the slice model membrane areas immediately surrounding the slice exhibited wet regions where media fluid was present; when the slice went days without media changes and started to lose viability this wet region got smaller, indicating that the slice was drying out and it no

longer was maintaining its ability to be covered in fluid. This indicates that cells must be alive to maintain this suffusion mechanism, which in turn, fluid flow necessitates an appreciable amount of space for the fluid to permeate through. The next step would be the evaluation of such space using bioimaging techniques which is already a fully burgeoning field that is ever improving resolution as it pertains to magnification of biological structures in an *in-vivo* setting.

If this is indeed an accurate inference of the dynamics of fluid flow amidst halls of stationary cells with motile cells flowing within (AKA intercellular lumen) it can fill in some of the voids in pathological processes as it relates to the initial inflammatory response (Figure 42). In fact, upon closer consideration, it could be defined that MG shapes after structural variation 3 (when the lateral membrane gains further separation from the nucleus membrane) begin to bear some impact on fluid flow as it is now becoming a denser cellular particle that is likely to redirect fluid. These observations/deductions from the biochemical data, visual imagery of thick CNS sections and evaluation of a dendritic cells structural variations and as such could transcend the CNS compartment into extra CNS compartments, for example, the advent of edema is the rearrangement of space due to high fluid occupancy. Thus, putting this into therapeutic context, agents that will deescalate MG from the M1 state and thereby return the intercellular lumen back to its optimal diameter. Hence, the M1's structural variation impetus is that of containment of bad intracellular fluids (from dying/dead cell spillage) and therefore limits collateral damage to the surrounding tissue that is healthier and thus more viable for proper inherent cellular functions.

3.2. OVERALL THESIS CONCLUSION

The visual ma*t*hematics of stress dependent cell s*h*apes within tissu*e* and empty spaces, and loss the*r*eof within tissu*e* descr*i*bed i*n* th*i*s re*s*earch lend credence to *t*he dynamic states of biology. As suc*h*, much information has and can b*e* furtherly gathered with re*s*pect to the activities occurring within a holistically re*p*resented t*i*ssue-space volume. The ve*r*satility of MGs ab*i*lity to shape shif*t* is a meaningful characteristic of its identification; that is a cell that is spread out within the extracellular matrix via dendrites and can readily move about through several interstitial locations. Further, this cell is not only considered an initiation point of the immune response within an immune-privileged compartment of the post BBB interstitium, but also an active participant in the plasticity of synaptic pruning, underscoring just how versatile this dendritic motile cell is and thus could be ascribed a structural variation. Such is that in this investigation of MG presented the 2 opposing ends of MG morphological variation and characterized a spectrum of five intermediate behavioral morphologies after inducing toxicity to a region of CNS tissue. Based on MGs placement within biochemically confirmed cell stress (impaired mitochondria within an intact cell membrane) and death (porous cell membrane) morphologies can serve as a potential basis for determining and potentially reading stressed cells within tissue which is antecedent to irreversible cell death. Such is that the 5 newly identified MG morphologies within the tissue matrix can be further investigated towards better defining cell stress during CNS inflammation.

The space and terrain from which MG likely lays its trails was also described and characterized in some manner during this study. The theme of intercellular spacing has historically not benefited from as deep examination as the cells themselves being solid

components, such is reflected in the dearth of published literature. The space needed to main*t*ain porosity -and ergo optimal fluid flow- observed underscores the importance of the CNS' parenc*h*yma's n*e*ed fo*r* pristin*e* un*i*directional i*n*terstitial flu*i*d's efficiency needed to generate ion-concentration dependent action potential*s*. Fur*t*hermore, t*h*e uniqu*e s*hape of CNS cells, namely the C-curvature that they all exhibit next to their soma lends credence to this *p*orosity prof*i*le. Such is that the placements of neu*r*ons, *i*f indeed *t*he interstitial fluid flow is a significantly important component of the neurobiological composition, is not just predicated on cells' sequential placement, but the spacing in between them is a relevant volumetric consideration of its normal relative distribution. Thereby indicating that these solid placements are also dictating the direction of fluid as a conduit of spatial allocation this adds some dimensionality to the conditions of biology, as elucidated and demonstrated by examining dendritic cells' responses to precise toxic injury, albeit inadvertently. Ultimately a study that sought out to understand MG morphological variation in the context of the brain parenchyma yielded a greater impression; that is of the spatial-volumetric consequences of those variation that entail the micro-CNS volume. With this greater understanding of MG so is such the understanding of its immediate microenvironment as it pertains to spatial considerations under a contained volume of functional biology.

REFERENCES

1. Li, Q. and B.A. Barres, *Microglia and macrophages in brain homeostasis and disease.* Nat Rev Immunol, 2018. **18**(4): p. 225-242.
2. Ginhoux, F., et al., *Origin and differentiation of microglia.* Front Cell Neurosci, 2013. **7**: p. 45.
3. Herculano-Houzel, S. and S.E. Dos Santos, *You Do Not Mess with the Glia.* Neuroglia, 2018. **1**(1): p. 193-219.
4. Wirenfeldt, M., et al., *Population control of resident and immigrant microglia by mitosis and apoptosis.* Am J Pathol, 2007. **171**(2): p. 617-31.
5. DiSabato, D.J., N. Quan, and J.P. Godbout, *Neuroinflammation: the devil is in the details.* J Neurochem, 2016. **139 Suppl 2**(Suppl 2): p. 136-153.
6. Schneider, U.C., et al., *Microglia inflict delayed brain injury after subarachnoid hemorrhage.* Acta Neuropathol, 2015. **130**(2): p. 215-31.
7. Tang, Y. and W. Le, *Differential Roles of M1 and M2 Microglia in Neurodegenerative Diseases.* Mol Neurobiol, 2016. **53**(2): p. 1181-1194.
8. Paolicelli, R.C., et al., *Synaptic pruning by microglia is necessary for normal brain development.* Science, 2011. **333**(6048): p. 1456-8.
9. Fernandez-Arjona, M.D.M., et al., *Microglia Morphological Categorization in a Rat Model of Neuroinflammation by Hierarchical Cluster and Principal Components Analysis.* Front Cell Neurosci, 2017. **11**: p. 235.
10. Kamphuis, W., et al., *Transcriptional profiling of CD11c-positive microglia accumulating around amyloid plaques in a mouse model for Alzheimer's disease.* Biochim Biophys Acta, 2016. **1862**(10): p. 1847-60.

11. Minami, S.S., et al., *Selective targeting of microglia by quantum dots.* J Neuroinflammation, 2012. **9**: p. 22.

12. Keren-Shaul, H., et al., *A Unique Microglia Type Associated with Restricting Development of Alzheimer's Disease.* Cell, 2017. **169**(7): p. 1276-1290 e17.

13. Prinz, M., S. Jung, and J. Priller, *Microglia Biology: One Century of Evolving Concepts.* Cell, 2019. **179**(2): p. 292-311.

14. Xiang, Z., et al., *Microglial morphology and its transformation after challenge by extracellular ATP in vitro.* J Neurosci Res, 2006. **83**(1): p. 91-101.

15. Stoppini, L., P.A. Buchs, and D. Muller, *A simple method for organotypic cultures of nervous tissue.* J Neurosci Methods, 1991. **37**(2): p. 173-82.

16. Stanton, P.K. and J.M. Sarvey, *Blockade of long-term potentiation in rat hippocampal CA1 region by inhibitors of protein synthesis.* J Neurosci, 1984. **4**(12): p. 3080-8.

17. Coleman, L.G., Jr., J. Zou, and F.T. Crews, *Microglial depletion and repopulation in brain slice culture normalizes sensitized proinflammatory signaling.* J Neuroinflammation, 2020. **17**(1): p. 27.

18. Masuch, A., et al., *Microglia replenished OHSC: A culture system to study in vivo like adult microglia.* Glia, 2016. **64**(8): p. 1285-97.

19. Krabbe, G., et al., *Functional impairment of microglia coincides with Beta-amyloid deposition in mice with Alzheimer-like pathology.* PLoS One, 2013. **8**(4): p. e60921.

20. Meerschaert, J. and M.B. Furie, *The adhesion molecules used by monocytes for migration across endothelium include CD11a/CD18, CD11b/CD18, and VLA-4*

on monocytes and ICAM-1, VCAM-1, and other ligands on endothelium. J Immunol, 1995. **154**(8): p. 4099-112.

21. Jurga, A.M., M. Paleczna, and K.Z. Kuter, *Overview of General and Discriminating Markers of Differential Microglia Phenotypes.* Front Cell Neurosci, 2020. **14**: p. 198.

22. Gallizioli, M., et al., *Dendritic Cells and Microglia Have Non-redundant Functions in the Inflamed Brain with Protective Effects of Type 1 cDCs.* Cell Rep, 2020. **33**(3): p. 108291.

23. Mewes, A., H. Franke, and D. Singer, *Organotypic brain slice cultures of adult transgenic P301S mice--a model for tauopathy studies.* PLoS One, 2012. **7**(9): p. e45017.

24. Vinukonda, G., et al., *Novel organotypic in vitro slice culture model for intraventricular hemorrhage of premature infants.* J Neurosci Res, 2012. **90**(11): p. 2173-82.

25. Lana, D., et al., *Microglial distribution, branching, and clearance activity in aged rat hippocampus are affected by astrocyte meshwork integrity: evidence of a novel cell-cell interglial interaction.* FASEB J, 2019. **33**(3): p. 4007-4020.

26. Chauhan, P., et al., *The Anatomy of the Hippocampus*, in *Cerebral Ischemia*, R. Pluta, Editor. 2021: Brisbane (AU).

27. Tian, L., et al., *Binding of T lymphocytes to hippocampal neurons through ICAM-5 (telencephalin) and characterization of its interaction with the leukocyte integrin CD11a/CD18.* Eur J Immunol, 2000. **30**(3): p. 810-8.

28. Tian, L., et al., *The neuronal glycoprotein telencephalin is a cellular ligand for the CD11a/CD18 leukocyte integrin.* J Immunol, 1997. **158**(2): p. 928-36.

29. Bernhoft, R.A., *Mercury toxicity and treatment: a review of the literature.* J Environ Public Health, 2012. **2012**: p. 460508.

30. Egekeze, J.O. and F.W. Oehme, *Cyanides and their toxicity: A literature review.* Vet Q, 1980. **2**(2): p. 104-14.

31. Laussel, C. and S. Leon, *Cellular toxicity of the metabolic inhibitor 2-deoxyglucose and associated resistance mechanisms.* Biochem Pharmacol, 2020. **182**: p. 114213.

32. Malenka, R.C. and M.F. Bear, *LTP and LTD: an embarrassment of riches.* Neuron, 2004. **44**(1): p. 5-21.

33. Jeong, H.K., et al., *Inflammatory responses are not sufficient to cause delayed neuronal death in ATP-induced acute brain injury.* PLoS One, 2010. **5**(10): p. e13756.

34. Jeong, H.K., et al., *Brain inflammation and microglia: facts and misconceptions.* Exp Neurobiol, 2013. **22**(2): p. 59-67.

35. Huang, H., et al., *Physiological levels of ATP negatively regulate proteasome function.* Cell Res, 2010. **20**(12): p. 1372-85.

36. Hladky, S.B. and M.A. Barrand, *Mechanisms of fluid movement into, through and out of the brain: evaluation of the evidence.* Fluids Barriers CNS, 2014. **11**(1): p. 26.

37. Khasawneh, A.H., R.J. Garling, and C.A. Harris, *Cerebrospinal fluid circulation: What do we know and how do we know it?* Brain Circ, 2018. **4**(1): p. 14-18.

38. Hausser, M., *The Hodgkin-Huxley theory of the action potential.* Nat Neurosci, 2000. **3 Suppl**: p. 1165.

39. Penna, E., et al., *Development of the Neuro-Immune-Vascular Plexus in the Ventricular Zone of the Prenatal Rat Neocortex.* Cereb Cortex, 2021. **31**(4): p. 2139-2155.

40. Davies, D.S., et al., *Microglia show altered morphology and reduced arborization in human brain during aging and Alzheimer's disease.* Brain Pathol, 2017. **27**(6): p. 795-808.

41. Nedergaard, M. and S.A. Goldman, *Glymphatic failure as a final common pathway to dementia.* Science, 2020. **370**(6512): p. 50-56.

42. Bich, L., T. Pradeu, and J.F. Moreau, *Understanding Multicellularity: The Functional Organization of the Intercellular Space.* Front Physiol, 2019. **10**: p. 1170.

43. Sakka, L., G. Coll, and J. Chazal, *Anatomy and physiology of cerebrospinal fluid.* Eur Ann Otorhinolaryngol Head Neck Dis, 2011. **128**(6): p. 309-16.

44. Pollay, M., *The function and structure of the cerebrospinal fluid outflow system.* Cerebrospinal Fluid Res, 2010. **7**: p. 9.

45. Oreskovic, D. and M. Klarica, *The formation of cerebrospinal fluid: nearly a hundred years of interpretations and misinterpretations.* Brain Res Rev, 2010. **64**(2): p. 241-62.

46. Brown, A., *The Hodgkin and Huxley papers: still inspiring after all these years.* J Physiol, 2022. **600**(2): p. 173-174.

47. El Hady, A. and B.B. Machta, *Mechanical surface waves accompany action potential propagation.* Nat Commun, 2015. **6**: p. 6697.

48. French, C.R., et al., *A voltage-dependent persistent sodium current in mammalian hippocampal neurons.* J Gen Physiol, 1990. **95**(6): p. 1139-57.

49. Sloviter, R.S. and T. Lomo, *Updating the lamellar hypothesis of hippocampal organization.* Front Neural Circuits, 2012. **6**: p. 102.

50. Bolmont, T., et al., *Dynamics of the microglial/amyloid interaction indicate a role in plaque maintenance.* J Neurosci, 2008. **28**(16): p. 4283-92.

51. Plog, B.A. and M. Nedergaard, *The Glymphatic System in Central Nervous System Health and Disease: Past, Present, and Future.* Annu Rev Pathol, 2018. **13**: p. 379-394.

52. Csaszar, E., et al., *Microglia modulate blood flow, neurovascular coupling, and hypoperfusion via purinergic actions.* J Exp Med, 2022. **219**(3).

Vita

Name	*Jesus Antonio Trejos*
Baccalaureate Degree	*Bachelor of Science,* *St. John's University* *Jamaica, New York* *Major: Toxicology*
Date Graduated	*May, 2002*
Baccalaureate Degree	*Master of Science,* *St. John's University,* *Jamaica, New York* *Major: Toxicology*
Date Graduated	*May, 2004*